Pipeline leak detection using in-situ soil temperature and strain measurements

S. I. JAHNKE

Pipeline leak detection using soil temperature and strain measurements

Sebastian Ingo Jahnke

A dissertation submitted in partial fulfilment of the requirements for the degree of

MASTER OF ENGINEERING (WATER RESOURCES ENGINEERING)

in the

FACULTY OF ENGINEERING, BUILT-ENVIRONMENT AND INFORMATION TECHNOLOGY

University of Pretoria

January 2018

SUMMARY

Pipeline leak detection using in-situ soil temperature and strain measurements

Sebastian Ingo Jahnke

Supervisor: Professor S. W. Jacobsz
Co-Supervisor: Mr. M. van Dijk
Department: Civil Engineering
University: University of Pretoria
Degree: Master of Engineering (Water Resources Engineering)

This project investigated whether by measuring temperature and strain changes in the ground around a pipeline a leak can be detected using fibre optic instrumentation. The concept entails installation of an optic fibre along the length of the pipeline in the pipe trench when a new pipe is installed. Alternatively, the possibility also exists to retrofit such a leakage detection system by burying it near (above) existing pipes, although this has not been investigated in this project. The success of such a leakage detection system is based on the hypothesis that the temperature differential between the water in a pipeline and the ground around the pipe will result in a detectable temperature change in the ground when a leak occurs. Softening of the pipe support due to leaking water should result in strain changes in the soil immediately around the pipe and in the pipe itself, both of which should be detectable. All three of these quantities, i.e. ground temperature, ground strain and pipe strain can be measured using fibre optic technology. This study is based on detecting temperature and strain changes using fibre Bragg grating sensors (FBGS) at discrete locations along the length of a pipe.

The success of a system based on temperature measurement implies that temperature changes caused by a leak should be distinguishable from naturally occurring temperature cycles. Installations were therefore conducted to measure ground temperature changes to a depth of 3m over the course of a year and comparing those to temperature changes measured in active water mains over the same period in Pretoria. A temperature differential that always exceeded 2°C was recorded, indicating that the system has potential to provide a means of leak detection.

A laboratory study was carried out to observe temperature changes associated with an advancing wetting plume caused by a simulated leak using thermistors buried in fine sand. Depending on the magnitude of the soil-water temperature differential, a rapid drop in temperature was observed at monitoring locations during the progression of the wetting plume (the water temperature is typically lower than the soil temperature). However, an initial short-duration increase (spike) in temperature was consistently observed at measurement locations upon first passage of the wetting front. It is hypothesised that this spike is caused by the release of free surface energy upon wetting of the soil. As expected, immediately following this spike after the passage of the wetting front, a significant and rapid change in temperature was noted during the tests. The temperature reduction is dependent on the temperature differential between the water and the surrounding soil and illustrated the potential of the proposed method of leak detection (i.e. detecting leaks by observing a reduction in ground temperature).

After the laboratory phase, a field study was conducted during which a 110 mm diameter 12 m long uPVC pipe was installed with sensor arrays consisting of both temperature and total strain FBGS. Thermistors were used as temperature sensors as in the case of the laboratory investigation. Strain sensors used were discrete optical strain gauges or fibre Bragg grating sensors (FBGS). Fifty percent of the FBGS were epoxied to the pipe to measure pipe strains, while the remaining 50% were free-floating, situated in a thin oil-filled plastic tube buried in the corner of the pipe trench. The purpose of the epoxied FBGS was to measure pipe strain changes, while the purpose of the free-floating FGBS was to detect temperature-induce strain changes. During a leak, strain changes were recorded in the free-floating FBGS several times exceeding the values expected based on the temperature changes measured by the thermistors. In addition, very significant pipe strain changes were observed. These observations indicate that significant ground and pipe strains occur due to wetting and subsequent softening of the soil caused by the leak. The change in total strain and temperature observed during a leakage event provided strong evidence that both parameters can be used to effectively indicate the presence of a leakage event.

A complication identified in the study is that network pressure fluctuations result in significant pipe strains which would complicate leak identification. It is therefore recommended that the leakage detection system should comprise of an optic fibre separated from, but in close proximity to the pipe. This study should be followed up to investigate the performance of a leakage detection system based on distributed strain measurement and the potential of retrofitting the proposed detection system to existing pipelines.

DECLARATION

I, the undersigned hereby declare that:

- I understand what plagiarism is and I am aware of the University's policy in this regard;
- The work contained in this thesis is my own original work;
- I did not refer to work of current or previous students, lecture notes, handbooks or any other study material without proper referencing;
- Where other people's work has been used this has been properly acknowledged and referenced;
- I have not allowed anyone to copy any part of my thesis;
- I have not previously in its entirety or in part submitted this thesis at any university for a degree.

Signature of student: 

Name of student: Sebastian Ingo Jahnke

Student number: 10687930

Date: 14 February 2018

ACKNOWLEDGEMENTS

I wish to express my appreciation to the following organisations and persons who made this dissertation possible:

a) The Water Research Commission for their financial support.

b) The following persons are gratefully acknowledged for their assistance, support and guidance during the study:

   i. Professor S. W. Jacobsz (supervisor)
   ii. Mr. M. van Dijk (co-supervisor)

c) My wife, Veronica, and family for their encouragement and support during the study.

TABLE OF CONTENTS

LIST OF FIGURES

LIST OF FIGURES

LIST OF SYMBOLS

%	Percentage
bar	pressure
km	kilometers (distance)
K	Kelvin (Temperature)
kPa	kilopascal (pressure)
l/min	litres per minute (volumetric flow rate)
m	meters (distance or meters of head)
m^2	square meter (area)
m^3/s	cubic meters per second (volumetric flow rate)
nm	nanometre (distance or wavelength)

LIST OF ABBREVIATIONS

ASSHTO	American Association of State Highway and Transportation Officials
AWWA	American Water Works Association
BFW	Basic Free Water
CARL	Current Annual Real Losses
DSTS	Distributed Strain and Temperature Sensor
EPA	Environmental Protection Agency
FBGS	Fibre Bragg Grating Sensor
FOS	Fibre Optic Sensors or Factor of Safety (look at context)
GIS	Geographical Information System
IAM	Integrated Asset Management
ILI	International Leakage Index
IWA	International Water Association
KPI	Key performance indicator
NRW	Non - Revenue Water
OMC	Optimum Moisture Content
PU	Polyurethane
RTD	Resistance Temperature Detector
SABS	South African Bureau of Standards
SANS	South African National Standards
SCADA	Supervisory Control and Data Acquisition
TLB	Tractor loader backhoe
TMH	Technical Methods for Highways
UARL	Unavoidable Annual Real Losses
WDM	Water Demand Management
WSDP	Water Services Development Planning
ZMA	Zone Meter Areas

1. INTRODUCTION AND OBJECTIVES

1.1 Background

South Africa is a water scarce country which has a limited supply potential, therefore Water Demand Management (WDM) has to be prioritised. Continuous monitoring of water supply schemes and reticulation networks has great potential to create a working infrastructure archive to proactively repair, detect leaks and to anticipate catastrophic failures (McKenzie & Bhagwan, 2003).

Up to 30% of the total potable water introduced into water networks is unaccounted for in South Africa (McKenzie et al., 2012). Unaccounted and unbilled water due to leakage, illegal connection, Basic Free Water (BFW) allocations and other factors are termed Non-Revenue Water (NRW). It describes the portion of water which is not sold, and the cost has to be recovered or added to the portion of water sold. Table 1-1 below indicates the standard water balance prescribed by the International Water Association (IWA). NRW, specifically Real Losses, is recognised as a major portion of the total input volume which can actively be reduced by locating and repairing leaks. This study's focus area is in light grey in Table 1-1 below, i.e. "leakage on transmission and distribution mains". The reduction in real losses will add to the overall distribution efficiency, enabling the added capacity to supplement the growing demand (McKenzie et al., 2012).

Table 1-1: IWA best practice standard water balance (McKenzie & Bhagwan, 2003)

<table>
<tr><td rowspan="10">System Input Volume</td><td rowspan="4">Authorised Consumption</td><td rowspan="3">Billed Authorised Consumption</td><td>Billed Water Exported</td><td rowspan="3">Revenue Water</td></tr>
<tr><td>Billed Metered Consumption</td></tr>
<tr><td>Billed Unmetered Consumption</td></tr>
<tr><td rowspan="2">Unbilled Authorised Consumption</td><td>Unbilled Metered Consumption</td><td rowspan="6">Non-Revenue Water</td></tr>
<tr><td>Unbilled Unmetered Consumption</td></tr>
<tr><td rowspan="6">Water Losses</td><td rowspan="2">Apparent Losses</td><td>Unauthorised Consumption</td></tr>
<tr><td>Customer Meter Inaccuracies</td></tr>
<tr><td rowspan="4">Real Losses</td><td>Leakage on Transmission and Distribution Mains</td></tr>
<tr><td>Leakage and Overflow at Storage Tanks</td></tr>
<tr><td>Leakage on Service Connection up to point of Customer Meter</td></tr>
</table>

The focus of this study is to determine the effect of potable water pipe leaks on the temperature distribution in the surrounding soil and to assess whether, by monitoring temperature of the soil near a pipeline, leaks can be detected. Furthermore, strain development in the pipe base is investigated as well as possible changes in pipe support conditions due to wetting.

Fibre optic strain measurement is available as a means to measure both mechanical and thermal strain with unprecedented resolution and accuracy. Fibre optic sensing technology has many advantages over conventional strain and temperature measurement technology as it is more cost effective over longer distances, is not affected by electromagnetic disturbances and is resistant to corrosion attack (Kreuzer, 2013). Furthermore, continuous monitoring of pipelines allow authorities to monitor the performance of their pipeline infrastructure in real time and address possible problems in good time. Fibre optic strain and temperature measuring technology is currently used for oil, gas and other potentially hazardous pipeline monitoring applications. The cost of distributed fibre optic readout equipment and suitably armoured fibre optic cable is currently expensive (Inaudi and Glisic, 2010), but is expected to reduce rapidly in years to come, rendering this technology available as a means of leakage detection on pipelines. This study is used to give an indication on the effectiveness of each parameter as leakage detection method for potable water pipelines.

1.2 Objective

The objective of the study is to investigate the use of fibre optic sensors as a water pipeline leak detection method, by observing temperature and strain changes in soil surrounding a pipeline. The hypothesis of this research project is the following: “Leak-induced temperature and strain changes in the ground near a pipeline can be distinguished from natural temperature variation, thereby serving as a leak detection method.”

1.3 Scope

This study presents an investigation into the possibility of using temperature monitoring in the ground near a pipeline and its deformation as a means of leakage detection. Exploratory tests comprising leakage tests in the laboratory were carried out, first in clean silica sand and then in a natural transported soil. After the laboratory phase, a large scale installation was implemented to test the hypothesis under conditions in the field where natural temperature variation occurs. Temperatures in the laboratory models were monitored using thermistors.

The field installation included both thermistors and fibre optic strain measurement. In terms of fibre optic instrumentation, FBGS were used to measure temperatures and strain at selected

points. Provision was made to install fibre optics that will support distributed strain measurement once the necessary readout equipment becomes available.

Natural temperature variation in soil with depth and in a typical distribution pipeline was measured at two locations to provide temperature data against which to interpret leakage-induced temperature variation.

1.4 Methodology

The initial testing includes the determination of the natural soil depth temperature distribution around and water temperature in a buried pipeline by inducing a controlled leakage scenario with various leakage rates and thermistor sensor depths.

Thermistors were placed into the natural ground up to a depth of 3 meters in specific increments on the experimental farm to determine a baseline temperature behaviour of in-situ soils.

A small-scale laboratory leakage test was conducted in homogenous sand and potable water from a municipal connection. The test was carried out in a temperature controlled box to eliminate ambient air temperature effect on the soil. The soil was heated up to indicate a significant temperature differential.

A full-scale field installation was planned, where potable water was circulated in a buried pipe and various leak locations were opened to determine if a temperature differential can be noted due to a leak. Fibre Bragg grating sensors (FBGS) were installed to investigate sensitivity factors, such as the minimum amount of leakage that can be measured. Effect of seasonal, daily temperature variation and soil moisture content on the effectiveness of the proposed leakage detection method was investigated.

The typical installation specifications for medium pressure buried pipelines (SABS 1200 LB-1983) and earthworks (SABS 1200 DB-1989) was used to ensure that the experimental setup was realistic. Mass balance principles will be applied to determine the amount of water being added to the system and therefore released into the surrounding soil at the controlled leakage.

Summary of main experiments:

- Baseline in-situ soil temperature distribution was observed at the University of Pretoria experimental farm with thermistors placed at various depth increments into the ground.
- Average water temperature variation was measured at a typical water distribution network access point with a resistance temperature device (RTD), the site selection is crucial to ensure that the water was not stagnant.
- A small-scale laboratory leakage test was used to determine temperature changes in soil due to a simulated leakage rate and differential temperature.
- A field installation with controlled leak locations was monitored with thermistors and FBGS.

The temperature differential between soil surrounding a pipeline and a potable water pipeline leak was determined. The effect of ambient air temperature, cyclic daily and seasonal effects were investigated. Thereafter a field installation with controlled leaks was investigated, with both thermistors and fibre optic sensors.

1.5 Report structure

The report has the following chapters:

- Chapter 1 serves as an introduction, overview of the experimental work and motivation for the study.
- Chapter 2 is a literature study, focusing on demand management, various leak detection methods, fibre optic strain and temperature sensors, measuring techniques, a discussion on international fibre optic leak detection case studies and typical soil parameters.
- Chapter 3 describes the experimental procedures.
- Chapter 4 contains a summary of the data analysis and experimental results.
- Chapter 5 comprises of recommendations and conclusions, to stimulate further research into the field.
- Appendices consist of summaries containing selected experimental data, analysis methodology and output, and other important details which were not covered in the report.

2. LITERATURE STUDY

2.1 Introduction to literature review

The project commenced with a literature study on conventional and new techniques employed to monitor the integrity and performance of pipelines and the application of fibre optic monitoring to observe the behaviour/performance of structures. This literature study contains an overview of buried water pipeline installation requirements for different pipe materials, current leak detection techniques and statistics regarding water leaks. Literature that supports the theory that rapid changes in soil temperature can be used as a method to detect water leaks is presented. Various options in terms of existing leak detection methods, their advantages and disadvantages are investigated, as well as the use of fibre optic techniques. South African soil conditions and buried water pipe installation details are examined to determine the applicability and the prospects for success of using measured temperature changes as a leak detection method. Temperature measuring devices are discussed and terminology is clarified.

2.2 Potable water pipe leaks

Water pipe leaks in distribution networks and water supply schemes is a major concern to water authorities and suppliers due to incurred financial losses, environmental implications, loss of supply potential and health and safety aspects. Financial losses are incurred when treated water cannot be sold against a possible income. Raw water abstraction, treatment and distribution forms part of the economic cycle involved in supplying water and for which municipalities pay suppliers. The income generated by the sale of water is used to improve the supply system, conduct maintenance and expand supply potential. Potable water is pumped from water treatment works to reservoirs or high points acting as distribution points and then gravity driven to consumers. Therefore the pumping of treated water to high points can be specified as a key cost component of potable water after the treatment process, depending on the conveyance distance between treatment works and consumer (McKenzie, 2001a).

In South Africa it is estimated that NRW amounts to 36% which falls between developed countries such as Australia, with as little as 7% NRW and developing countries such as Armenia, with up to 83%, and Albania with 70% (McKenzie et al., 2012) (see Figure 2-1 below).

It should however be noted that data quality concerns with regard to current NRW statistics have been raised as some of the data is estimated from historic trends due to equipment malfunction, limited maintenance and inadequate data capturing. The size and extent of water distribution networks and bulk supply schemes is a major hurdle to overcome. The complexity further intensifies as to decide on a maintenance regime that takes into account the age, materials and operating regimes of the various network zones and the subsequent intervention periods to conduct leak surveys and condition assessments (Henrie et al., 2016).

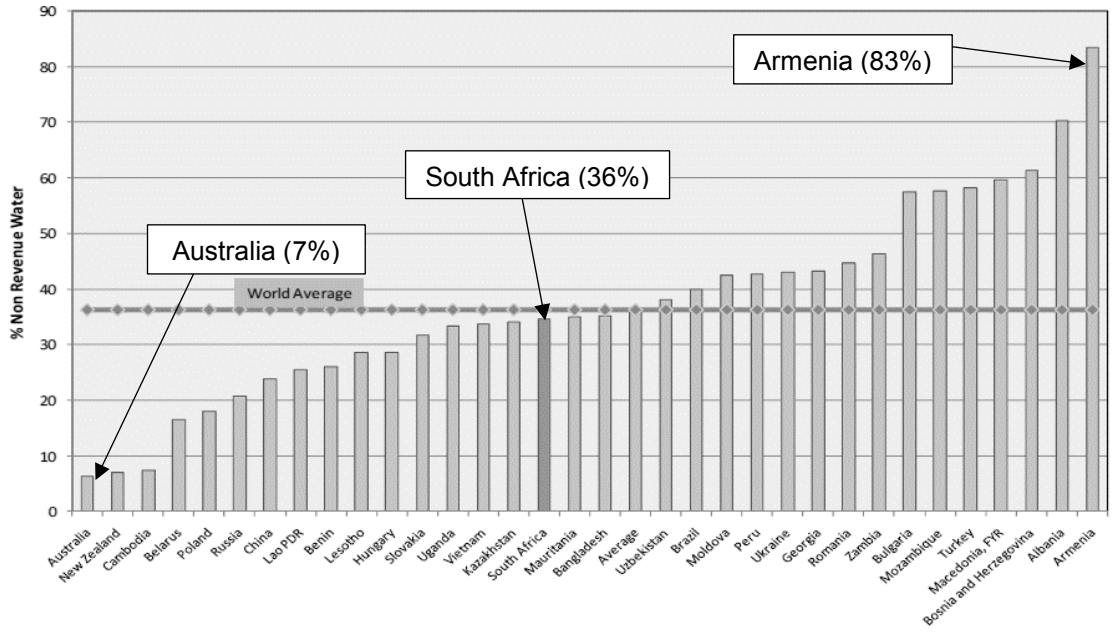

Figure 2-1: NRW international statistics (McKenzie et al., 2012)

A metric known as the Infrastructure Leakage Index (ILI) is commonly used to indicate the amount of water leaked from a system due to actual leaks. It is calculated by taking the ratio of the Current Annual Real Losses (CARL) to the Unavoidable Annual Real Losses (UARL). CARL is defined as the total sum of water losses from a system, even those resulting from operator errors such as when reservoir overflows. This metric is found by compiling a water balance, considering water input minus water output from the system. UARL is defined as being the minimum technically possible amount of water lost due to leaks, which is a function of network pipeline length, number of household connections, length of service connection (through private property) and the average pressure value in the system, see Equation 2-1 for details (McKenzie et al., 2012).

$$UARL = (18 \times L_m + 0.8\ N_C + 25 \times L_p) \times P \quad \text{Equation 2-1}$$

UARL	=	Unavoidable Annual Real Losses (litres/day)
L_m	=	pipeline network length (km)
N_C	=	total no. of connections in system
L_P	=	total length of service connection pipes passing through private property
P	=	average pressure value in the system

To establish a technically correct ILI, a water balance has to be obtained from the investigated water network. A water balance is essentially the difference between the water entering an isolated network (one inflow or isolated zone) and water being consumed. The difference between the supply and demand can then be specified as NRW with a small percentage subtracted as UARL (McKenzie et al., 2002).

Studies have been conducted in major municipalities in South Africa to determine the amount of NRW, most major municipalities within South Africa compile there NRW statistics periodically. The NRW then serves as key performance indicator (KPI). These studies were used to create and calibrate leakage models such as BENCHLEAK, ECONOLEAK, PRESMAC and SANFLOW. All of the models mentioned above deal with certain aspects of potable water leaks, such as pressure management, creating working knowledge of water balance and economic implications of leaks and standardizing procedure to classify bursts and background losses (McKenzie et al., 2002).

A number of documents listed below discuss the historic and current potable water loss situation in South Africa and summaries of case studies conducted:

- Metropolitan Municipality Non-Revenue / Water Loss Assessment (Wegelin and McKenzie, 2013)

- Benchmarking of Leakage from Water Reticulation Systems in South Africa (McKenzie et al., 2002)

- LEAKAGE MANAGEMENT - Introduction to WRC Tools to Manage Non-Revenue Water (McKenzie and Bhagwan, 2003)

- The State of Non-Revenue Water in South Africa (2012) (McKenzie et al., 2012)

Buried pipeline leaks are categorised in three main groups, being background, unreported and reported leakage, as shown in Figure 2-2 below. Background and unreported leaks are the biggest concern as they are undetected for many years or decades, depending on the amount of pipeline surveys conducted and the available maintenance budget.

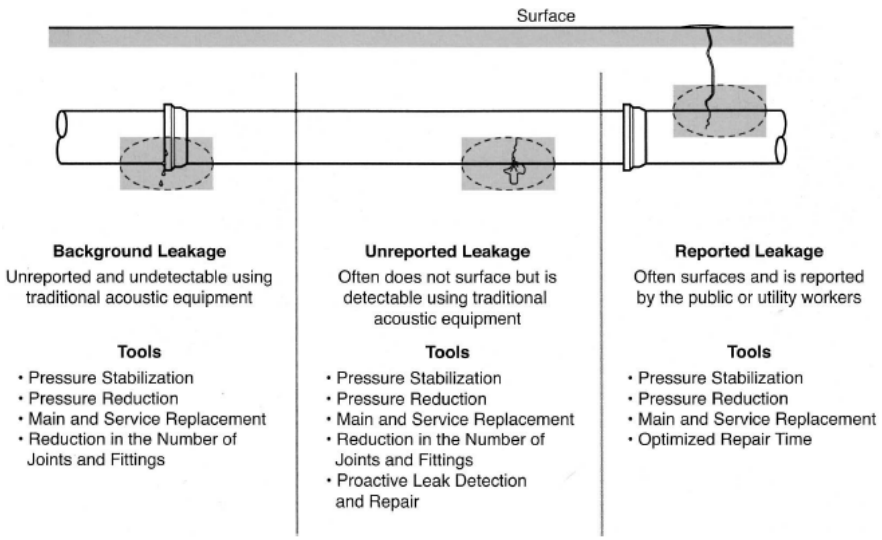

Figure 2-2: AWWA M36 leak classification and intervention methods (AWWA, 2009)

Background leaks commonly occur at joints or couplings they are minute leaks and therefore not easily detectable by traditional acoustic equipment. Unreported leaks are categorised as leaks occurring throughout a pipeline due to lacking support conditions, excessive bending or other mechanical failures, these leaks commonly have higher flow rates compared to backgrounds leaks. Reported leaks tend to have excessive flow rates which surface, are therefore reported and subsequently can be repaired (AWWA, 2009).

Lost water has many other implications besides supply reduction. There is a major financial aspect related to cost recovery, which has to be added to the revenue water portion. The amount of electricity used to abstract, treat and distribute water also has to be taken into account. Large amounts of electricity are used to transfer water from rural areas to high density areas, where it is treated and stored to meet consumer demands (AWWA, 2009).

In South Africa externally visible leaks are referred to as bursts, while small leaks, which are more difficult to detect, are referred to as background leaks. The threshold between background leaks and bursts is defined at 250l/hr. If the leak exceeds 250l/hr it is classified as a burst and if it is less than 250l/hr is classified as a background leak (McKenzie et al., 2006). To put the threshold flow rate into perspective, a flow rate of 250l/hr is 0.0694l/s or

4.2l/min which is a third of the maximum flow rate typically to be expected at a household connection.

The life cycle of a typical buried water distribution pipeline can be described with the life cycle “bathtub” curve as shown in Figure 2-3 below. Three phases can be used to describe the life cycle, the first being the “burn-in phase”, which is used to descibe the time just after installation, where leaks or failures are mainly caused due to installation defects or pipe deffects. The second phase is the “in-use phase”, where limited numbers of failures should occur after the pipe had settled. Failure typically occurs due to external interference such as overloading. The third and final phase is the wear out phase, where the pipeline reaches its design life and the pipe corrodes extensively, both internally and externally. The life cycle principle is applicable for all pipeline materials, environments and other important factors. However, the slope of the curve will change accordingly (Rajani and Tesfamariam, 2004).

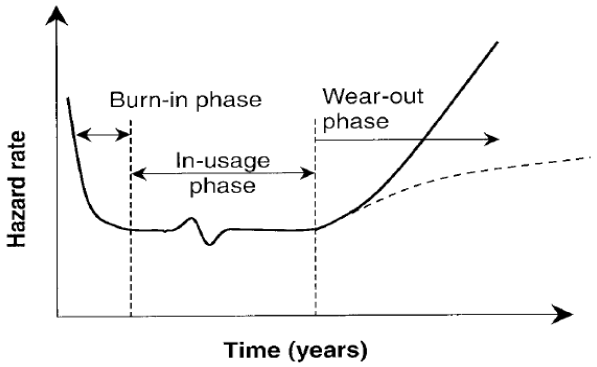

Figure 2-3: Lifecycle for a buried pipe (Rajani and Tesfamariam, 2004)

Figure 2-4 indicates the Factor of safety (FOS) of the pipeline over time. If the pipe is defect free and is installed according to good practice, avoiding damage to the pipe, the FOS will initially be far above 1. After a certain period in the ground, the pipe starts to deteriorate and corrode, due to a corrosive environment, poor water quality or natural deterioration. Once the initial break has occurred the pipe can start to leak and scour the supporting soil structure, which will eventually lead to failure with the FOS being just over or under 1. Over one would indicate near failure and under one would indicate a failure has occurred (Rajani and Tesfamariam, 2004).

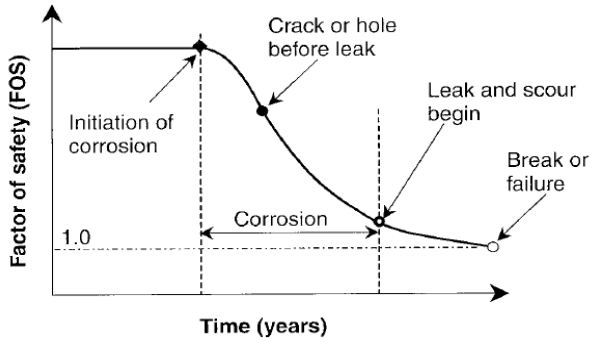

Figure 2-4: Factor of safety decrease over time (Rajani and Tesfamariam, 2004)

Pipe leaks are governed by the following factors: leak hydraulics, pipe material behaviour, soil hydraulics and water demand (Van Zyl, 2014b). Leakage hydraulics are described by the orifice equation below and the orifice or leakage coefficient is defined as 0.5 for turbulent flow, where the Reynolds number is greater than 4000 – 5000. For laminar flow, where the Reynolds number is less than 10, the orifice coefficient changes dramatically and can become large. It was however shown that a laminar flow condition is rare due to the prescribed pressure and flow requirements in pipelines. Equation 2-2 indicates the typical leakage/orifice equation (Van Zyl, 2014b).

$$Q = C_d A \sqrt{2gh} \quad \text{Equation 2-2}$$

Q = Flow rate (m^3/s)
C_d = Orifice or leakage coefficient (dimensionless)
A = Leakage area (m^2)
g = gravitational acceleration (9.81 m/s^2)
h = Available pressure head (m)

Pipe material behaviour is commonly based on the FAVAD model, which differentiates between rigid and elastic leaks (Van Zyl, 2014b). Elastic pipe leak cross section areas vary linearly with pressure, whereas rigid pipe leaks are fairly independent of pressure. This behaviour has been modelled with finite element software for different pipe materials. For elastic leaks a head-area slope term is defined, which incorporates the shape of the leak, pipe materials and section properties. Equation 2-3 below indicates the change in area due to change in pressure for elastic leaks. The value of coefficient m is small for round holes, while for other types of openings the value of m have been approximated using Computational Fluid Dynamics (CFD) (Van Zyl, 2014b).

$A = A_0 + m\,h$……..... Equation 2-3

A = Area at specific pressure (m^2)

A_0 = Initial area (m^2)

m = head-area slope term

h = head term

The two equations above are combined and shown in Equation 2-4 below (Van Zyl, 2014).

$Q = C_d\,(A_0 + m\,h)\,\sqrt{2gh}$……..... Equation 2-4

2.2.1 Soil hydraulics

Soil hydraulics are often described in terms of the Darcy flow equation, however high flows present at a leak location invalidate the use of the Darcy equation. The flow mechanism should rather be described as piping or hydraulic fracturing (Van Zyl, 2014b). The soil in close proximity to the pipe has been observed to act as an energy dissipations zone, but the high water pressures present in a reticulation network indicate that the soil surrounding a pipe does not have a major effect on pressure response of a leak. The area in close proximity to the leak can act as a fluid, therefore being described as soil fluidisation (Van Zyl, 2014b).

Soil fluidisation occurs in granular material when soil particles are free to move with pore fluid and the inter-particle forces become negligible (Van Zyl et al., 2013). This phenomenon can also occur under confined conditions, for example in a pipe trench, depending on the support conditions. A two-dimensional fluidisation experiment was carried out with various homogenous glass beads sizes (small balls or beads), depths and orifice sizes to replicate the fluidisation mechanism. It was found that each flow rate reached a specific stable fluidisation area and that the smallest hole produced the biggest pressure loss, between the internal pipe pressure and the external soil interface. The homogeneity of the experimental material does however not replicate in-situ backfill material and the variability thereof (Van Zyl et al., 2013).

2.2.2 Additional impacts of water leaks

In addition to a loss of potable water and the associated expense, distribution pipeline leaks in dolomitic areas can cause catastrophic surface failures known as sinkholes (see Figure 2-5 for details), which can also be formed naturally due to surface water ingress. Weathering of dolomitic rock occurs when rain water absorbs carbon dioxide, forming a weak carbonic acid. The slightly acidic groundwater enters tension fractures, faults and joints within dolomitic rock formations, which causes leaching of carbonate known as a dissolution process. The weathered dolomitic rock is usually overlain by much younger rock and soil cover which is highly variable, but typically less than 10 meters thick. These mechanisms cause the soil cover to erode or slump, losing support and exposing a cavity which leads to the formation of a hole as shown in Figure 2-6 and Figure 2-7. The process of dolomitic dissolution is slow and takes place over geological time (Oosthuizen and Richardson, 2011).

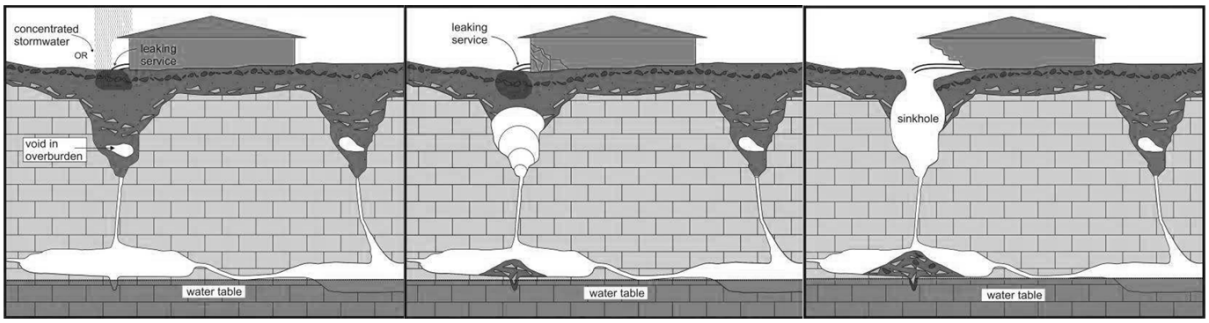

A: INGRESS OF WATER
Concentrated ingress of water from leaking services or surface water infiltration occurs. Cavities/ Receptacles exist within bedrock or overburden, which are in state of equilibrium

B: ACTIVE SUBSURFACE EROSION
Active subsurface erosion, caused by concentrated ingress water, resulting in transportation of materials down the nearest slot.

C: MATERIAL COLLAPSE
Sinkhole formation is thereby triggered.

Figure 2-5: Leaking service pipe causing sinkhole (Oosthuizen and Richardson, 2011)

Figure 2-6: Damage to houses in Pretoria due to a sinkhole (Oosthuizen and Richardson, 2011)

Figure 2-7: Leaking water pipe caused a sinkhole to form Pretoria (Oosthuizen and Richardson, 2011)

Being able to detect small settlements around a service pipe caused by subsurface failure can indicate a leaking service pipe and possibly lead to saving lives and limiting excessive damage to infrastructure caused by sinkholes.

Construction on dolomitic areas is governed by the South African Bureau of Standards (SABS) national standard SANS 1936 (2012). The document covers the following aspects of development on areas underlain by dolomitic areas:

- General Principles and Requirements
- Geotechnical Investigation and Determinations
- Design and Construction of Buildings and Structures
- Risk Management

2.3 Leak detection and management methods

Different methods can be used to detect potable water leaks, being either at a localised scale, looking at small portions of pipelines or at a network scale. There are internal as well as external leak detection systems (LDS). So-called “water audits” are typically done by municipalities to determine inflows (supply) and outflows (demand) of a subdivided section of a water distribution network. A major water distribution network is split into smaller constituencies, which are evaluated individually by isolating the system with valves or by using flow meters at strategic positions (du Plessis and Hoffmann, 2015).

The demand (consumption) and supply of water is determined according to flow meter readings taken each month by municipal workers, homeowners or from estimation, depending

on the location of the flow meter and the availability of staff to conduct water meter readings. Municipal and domestic water meter accuracy is a controversial topic as it is specified by a supplier for a particular inlet and outlet pipe diameter, operating regime (pressure and flow rate), water quality and environmental condition. Water meters are not commonly recalibrated in South Africa or installed according to international best practice with regard to placement of bends and other components. Depending on the size of the installation, the water meter should be installed with a straight upstream and downstream connection pipe to eliminate the effects of eddy currents or turbulence on the water meter readings (du Plessis and Hoffmann, 2015).

Domestic water meter performance testing is governed by South African National Standards SANS 1529 (2006) guidelines, which allows for clear set target flow rate deviations, depending on the class of meter tested. There are class A to D meters where a class D meter is supposed to be the most accurate. A lower permissible relative error of 5% and an upper zone of 2% is prescribed in the standard. Pressure tests are performed on new domestic water meters with a test pressure which is three times greater than “normal” working pressure (1,600 kPa or 16 bar) and between 4,000 to 6,000 kPa. Figure 2-8 below indicates the lower and upper accuracy specification zones for specified flow rates of water meters ($q_{min,}$ $q_{t,}$ q_p and q_s) and different flow meter classes (a, b, c and d). The values are given within the SANS 1529 specifications and are not further discussed in this literature study.

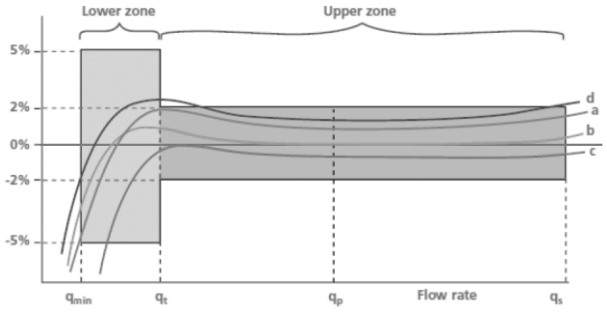

Figure 2-8: SANS 1529 water meter accuracy (du Plessis and Hoffmann, 2015)

A water meter audit was conducted on a minor water network portion in Cape Town to determine the accuracy of domestic water meters. The age of the water meters were in excess of 20 years and the cost of replacement had to be compared to the amount of water not billed to the consumer by meter reading errors. The study concluded that the water meter accuracy is acceptable after the long operational life of the water meters. However, it is difficult to obtain an absolute accuracy as certain flow meters might be more applicable to specific operating

flow regimes and installation detail. It was indicated that extremely low and extremely high flows are either being over or underestimated (du Plessis and Hoffmann, 2015).

Night flow principles (assumption of no or limited flow) and typically high pressure can be used to determine leaks in a pipeline network, as the assumption is made that water is typically not used throughout the night in residential areas. If high flows occur in an isolated network, a leak might be present. This method is labour intensive and has to be performed in a small time frame, not to affect consumers. Isolating valves in reticulation networks are often in a poor state, as they have not been exercised for a long time period or have been operated incorrectly (McKenzie and Bhagwan, 2003).

Other leak detection methods are listed below and might be used in combination with the above methods, where a mass balance or a water audit is the most common starting point:

- *Acoustic techniques* make use of a sensitive electronic or mechanical listening devices, which can detect vibrations caused by leaks exiting the pipe. The success of these methods rely heavily on the experience of the operator, pipe material, diameter, soil type, natural surrounding water table depth, interference signals, type of leak, size of leak and pressure. It was found that pipes having an internal pressure of less than 1 bar absolute pressure, acoustic methods are not effective, as background noise might exceed leakage noise (Van Zyl, 2014a). An increase in internal pressure will lead to an increase in leak detection effectiveness due to greater vibration. More sophisticated leak noise correlators with advances micro-processing can be used to accurately determine the location and size of a leak (EPA, 2010).

- *Tracer gas techniques* introduces gases such as helium or hydrogen into an isolated section of a pipeline. The gas is lighter than water and will therefore eventually permeate to the surface where it can be detected. The pipeline route is scanned directly above the surface with a sensitive gas detector, which will indicate the location of a leak (EPA, 2010).

- *Thermography* uses the principle of infrared imaging which detects long range infrared radiation with a range of up to 14,000 nm. A change in temperature or a hotspot will then indicate a leak. Infrared cameras can subsequently be used to locate these thermal radiation anomalies (EPA, 2010).

- *Ground penetrating radar* (GPR) can be used to detect voids caused by leaks or an increase in saturation levels. An increase in saturation levels increases the dielectric properties of soil, creating a discontinuity on the readout. The lag time from the transmitted to the reflected radar waves indicate the depth of a discontinuity, therefore indicating a possible leak or other buried services (EPA, 2010).

- *Remote water network sensing* is defined as small wired or wireless sensors embedded in a water distribution network which can measure flow, pressure and vibration. They are connected to a central control unit to monitor and indicate operational issues and leaks. These sensors are currently expensive and their lifespan might not be sufficiently long. However, they are improving rapidly and might become a good alternative to conventional measuring devices (EPA, 2010).

- *Satellite based radar technology* which uses spectral satellite imaging to detect the spectral signature of potable water in soil. The satellite imagery is superimposed onto the GIS water network to approximate leaks. Algorithms and filters are used to isolate background noise such as open water bodies, irrigation and other interferences. The leaks are then verified with alternative leak detection techniques and site visits (Utilis Israel Ltd., 2017).

South African models to quantify and mitigate leaks have been developed and the following guideline documents have been set up:

- PRESMAC - Pressure Management Program
  Pressure management incorporates the use of pressure management tools to minimise leaks as an increase in pressure will result in an increase in leaks. During high flow periods (high demand) the frictional losses will be high, resulting in lower pressures throughout a water network the inverse principle applies to low flow scenarios causing a high pressure. To avoid such spikes in a system, certain methods can be used to alleviate high pressures (McKenzie, 2001).

- ECONOLEAK – Economic Model for Leakage Management for Water Suppliers in South Africa (McKenzie and Lambert, 2002)

  Evaluating the most appropriate time for addressing possible leaks is covered by the ECONOLEAK guidelines. The method should however be used in conjunction with SANFLOW, PRESMAC and BENCHLEAK.

- SANFLOW- Development of a standardised approach to evaluate burst and background losses in water distribution systems in South Africa (McKenzie, 1999)

  The leak and burst evaluation guidelines are set out to determine the actual losses in zone meter areas (ZMA) and to further priorities areas with unacceptable high losses.

- BENCHLEAK - Benchmarking of Leakage for Water Suppliers in South Africa (McKenzie et al., 2002)

The tools were developed to standardise definitions and to simplify water balances for municipalities and water authorities. The model consist of three main inputs being, the Length of Mains, Number of Service Connections and Average Operating Pressure. Disturbance caused by repair actions can introduce new leaks or support failures in a water network.

Most major municipalities in South Africa and internationally make use of integrated asset management software. The use of such software enables decision makers not only to predict infrastructure demand and expansion, but to make informed decisions about existing infrastructure. IMQS for example is a South African company that provides integrated asset management (IAM) solutions for various infrastructure components. The addition of Geographical Information Systems (GIS) into asset management provides a spatial overview for network infrastructure such as water pipelines, electricity grids, roads and many more. Supervisory Control and Data Acquisition (SCADA) systems are used to obtain data from various network components and relay the data to central control centres. Commonly point sensors are used to collect data, compared to a distributed approach, which is a possibility with distributed fibre optic sensors (Gumbo et al., 2003).

Two key words are often used in conjunction with water infrastructure planning, namely water demand management (WDM) and water services development planning (WSDP). A number of aspects cumulatively form these terms, which are, pipeline and water meter replacement, pressure management and zoning, leak detection and repair, stepped water tariffs according to demand, public awareness campaigns and the continuous update of information management tools (Van Zyl, 2014a).

2.3.1 Effect of pressure in pipeline on leak

Leakage management is a universal term used to describe actions taken to reduce losses in a potable water pipeline. It is generally understood that leakage rates and system pressures are directly related. Saint-Venant's principle is often used to describe the shortening of a pipe due to an increase in diameter caused by internal pressure. The shortening effect can cause couplings or joints to leak due to a small pull out effect (AWWA, 2009).

The international leakage index parameter identifies system pressure as one of the main contributors to high leakage rates. It is therefore important to design and operate a system with various pressure divisions or zones to limit excessive pressure in certain areas of a network. Water supply networks are designed to supply a minimum allowable pressure at the furthest, highest or a combination of both in a system during high flow periods. These low pressure scenarios however only occur at high flow periods in the day such as in the early mornings or late afternoon/evenings. During low flow rate periods of the day high pressures can occur which can lead to elevated leakage rates (McKenzie, 1999).

2.4 Pipe materials

Various pipe materials are available and their selection depends on environmental aspects, pressure, diameter, stiffness and corrosive resistance requirements. Pipe materials range from thermoplastics such as polyvinylchloride (PVC) and polyethylene (PE), to metals such as ductile cast iron (DCI) and steel. Metal pipes are typically used for high pressure application, whereas plastic pipes are used in reticulation networks or harsh environments. There are different types of PVC pipes on the market such as un-plasticised or uPVC and modified or mPVC pipes (Van Zyl, 2014a). Composite pipes such as glass reinforced plastic (GRP) pipes are available, which are plastic fibres sandwiched between resin layers and cured to produce a solid pipe. Figure 2-9 below indicates different pipe materials with respect to the available diameters and pressure classes (Van Dijk, 2016).

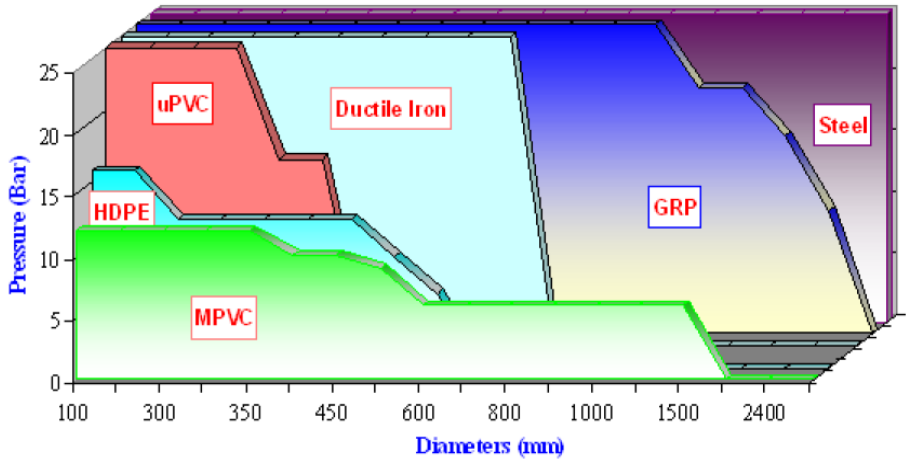

Figure 2-9: Pipe materials - pressure vs. diameter (Van Dijk, 2016)

Summary of pipe materials available:

- Thermoplastics
  - HDPE (high density polyethylene)
  - LDPE (low density polyethylene)
  - mPVC (modified polyvinylchloride)
  - oPVC (oriented polyvinylchloride)
  - uPVC (un-plasticised polyvinylchloride)
- Metal
  - DCI (ductile cast iron)
  - Copper (small diameter)
  - Stainless steel pipes (corrosive processes in industrial plants)
  - Steel (spiral or longitudinal weld)
- Composite
  - Asbestos cement (AC)
  - Fibre cement (FC)
  - GRP (glass reinforced plastic)
  - Pre-stressed concrete pipes

Thermoplastic pipes are commonly used in municipal reticulation networks as they are durable, lightweight and repair collars are inexpensive. Metal pipes such as steel and DCI are used for bulk water transfer schemes, where large diameter pipelines are required, which are able to cope with greater pressures. Composite pipes such as GRP have to be handled with care to avoid stress fractures, delamination and extensive ultraviolet exposure (Van Zyl, 2014a).

2.5 Pipeline construction details

South African Bureau of Standards (SABS) 1200 series is used to specify design details for medium pressure buried pipelines in South Africa. Pipe trenches are designed, constructed and payment is made in accordance with SABS 1200 DB (1989), which provide details pertaining the dimensions of the trenches, backfilling material specifications and compaction details. The pipe trench should be excavated as vertical as possible for at least the height of the bedding to limit excessive excavation. If the in-situ trench bottom has been disturbed below the specified invert level, the backfill material has to be compacted to 90% of Modified American Association of State Highway and Transportation Officials (AASHTO) density at specified moisture content (SABS, 1989).

According to Technical Methods for Highways (TMH) 1 method A7, the maximum dry density and optimum moisture content (OMC) determination procedure is defined in terms of establishing a moisture – density relationship when compacted according to Modified AASHTO compaction efforts. The maximum density is defined as the highest density that can be obtainable at various moisture contents. The OMC is defined as the moisture content at which the maximum density can be obtained according to TMH 1 method A7 (CSIR, 1986).

Pipe bedding is specified in SABS 1200 LB, for both rigid (Figure 2-10) and flexible pipes (Figure 2-11) with and without joints and couplings. Bedding types and trench dimensions are categorised in various classes, depending on the pipe material and in-situ soil type (SABS, 1983). Requirements for backfill materials are given.

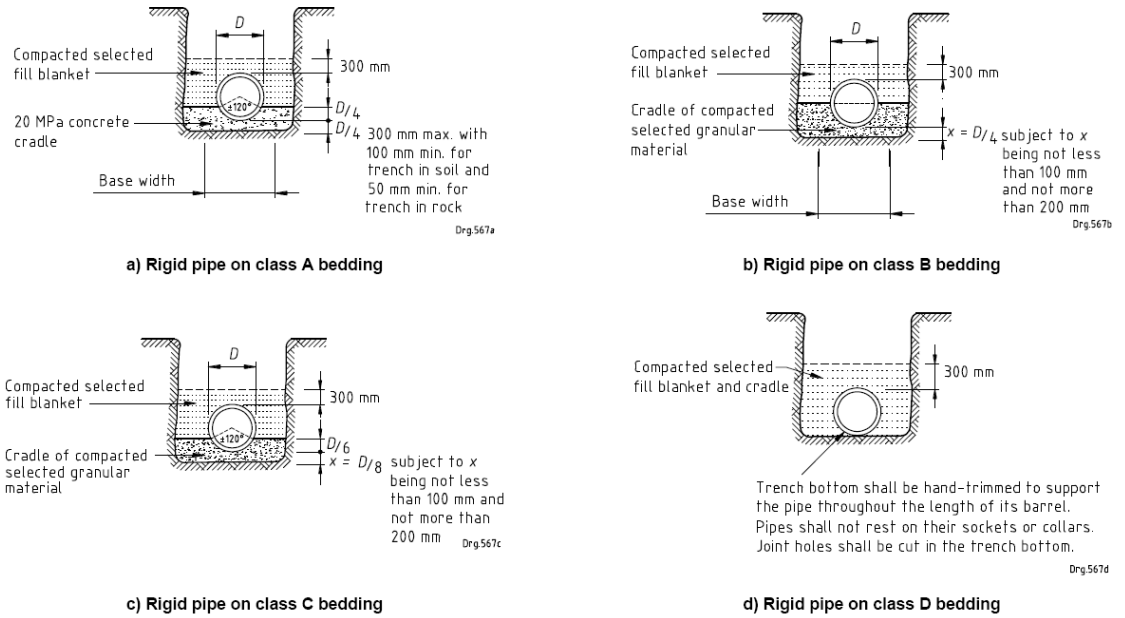

Figure 2-10: Rigid PIPE trench specification

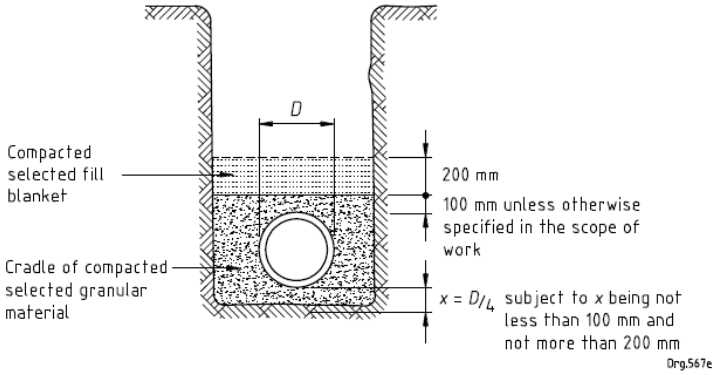

Figure 2-11: Flexible pipe trench specification

2.6 Pipe-soil support

The first phase of this study entails an investigation into the use of temperature measurement as a means of leak detection on pipelines. After prolonged leakage it is likely that pipe support offered by the bedding will deteriorate, possibly resulting in deformation and hence strains on the pipe. The detection of such strains can hypothetically serve as a secondary indicator of leaks, reflecting the degree of structural distress on the pipeline and will be the focus of the second part of the study. Pipe-soil interaction is therefore briefly discussed.

Pipe-soil interaction is a complex topic especially with regard to the support function offered by the surrounding soil to a pipe. It is often difficult to compact around the base of a pipe, as this region cannot easily be accessed. Therefore the contractor has to ensure that the bedding cradle is adequately compacted before placing the pipe (SABS, 2008).

The soil-pipe stiffness interaction can either be classified as rigid or flexible depending on the pipe material, pipe dimensions and soil properties. A number of studies have been conducted on the effect of tunnelling on pipe deflection, characterising pipe and soil stiffness parameters. Similar behaviour experienced by tunnelling underneath pipelines should be expected for sinkhole formation and other type of support failures in buried pipelines (Vorster et al., 2005).

Pipes used in water distribution networks typically have spigot and socket connection with lengths of 6m. In dolomitic areas continuously welded (fused) HDPE pipes are used to eliminate potential leakage at joints. The spigot and socket connections are allowed to rotate between 3º to 4^0 to allow for movement of the soil bedding and to follow the natural profile. However, over time this amount of rotation might not be possible due to aging of the rubber seal between two pipes. The design of pipelines to date also does not necessarily take into account aging of the pipe due to physical deterioration. However, the roughness factors are increased to allow for end of life hydraulic supply performance. The design also takes into account the resistance against circumferential stresses, such as overburden loads, live loads (traffic) and internal pressure. Loss of support from soil bedding and temperature dependant loads are not typically analysed in design. This could, however, be important in certain conditions where ground frost or high temperatures are experienced. It was shown that excessive temperature differentials between water and soil can also lead premature pipeline failure (Rajani and Tesfamariam, 2004).

2.7 Fibre optic sensors (FOS)

Fibre optics technology was developed as a telecommunication transmitting medium since the 1960s. The development and deployment of the technology over long distances decreased the component cost and improved the cable quality, reducing overall transmission losses or attenuation. The principle of fibre optic transmission makes use of propagating light wave properties such as the intensity, phase, polarisation and frequency. The most simplistic fibre

optic sensor comprises of a light source (pump), fibre optic cable, sensing element and interrogator or readout equipment (National Instruments, 2011).

Over the past two decades, the quality, sensitivity and resolution of FOS and interrogators improved significantly. There are various types of FOS available, depending on the intended application. Interrogators are optical instruments that emit a light pulse into the fibre optic sensor cable and analyse the return signal for changes in backscatter light amplitude and shifts in frequency (Kreuzer, 2013).

Fibre optic sensors (FOS) have many advantages over conventional sensor methods as they are not affected by electromagnetic interference, are nonconductive, electrically passive, and lightweight. Initially, fibre optic cables contained too many impurities causing a high degree of damping (losses), up to 100 dB/km, which has since been reduced to less than 0.2 dB/km due to improved manufacturing processes. Only recently have fibre optic sensors been incorporated as structural health monitoring devices for infrastructure assets such as, bridges, buildings and pipelines (Kreuzer, 2013).

Fibre optic cables comprise of a number of layers, such as the core, cladding, buffer coating and jacket as shown in Figure 2-12 below. The core consist of a fine strand of glass which transmits light (n1), the cladding (n2) surrounds the core and reflects stray light into the core. This is achieved by having a core with a higher refractive index compared to the cladding, therefore reflecting the light within the cable. The buffer coating protects the cladding and the core from external influences and damage. The jacket further ruggedises the cable adding more protection to the cable and limiting the bend radius (National Instruments, 2011). More complex ruggedized variations are available, depending on the intended application. Steel cables as well as tougher plastics are used to increase the cable strength and robustness

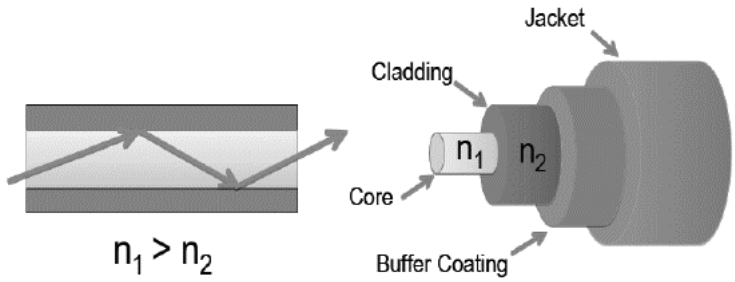

Figure 2-12: Optical Fibre Schematic (National Instruments, 2011)

A summary of the basic structure of a fibre optic cable is listed below:

- Core: Consists of pure silicon dioxide (SiO_2 or glass).
- Cladding: Fused from SiO_2, has different level of impurities than core to adjust refractive index.
- Buffer coating: protective layer of ultraviolet cured acrylate or polyamide.
- Jacket: Mechanical protection consisting of polyethylene or other thermoplastic. Kevlar layer typically wedged between cladding and jacket.

2.6.1 Type of sensors

There are various fibre optic sensors (FOS) available on the market, which are classified as single-point, multi-point and distributed. A single-point sensor is typically located at the tip of the fibre optic cable, while a multi-point sensor has many discrete measuring points along the length of the fibre optic cable with spacing options to match user and application requirements. Distributed sensors makes use of the entire cable length to measure changes in strain, temperature or vibration (National Instruments, 2011).

The focus of this literature study is to investigate Fibre Bragg Grating Sensors (FBGS) and Distributed Strain and Temperature Sensors (DSTS) shown in Table 2-1. Both sensors types are discussed below. There are however other sensor types such as intensity, interferometric, resonant and polarimetric type sensors which are not discussed in this literature study.

Table 2-1: Comparison of different fibre optic sensors (National Instruments, 2011)

Technology	Topology	Range (km)	Parameter			
			Temperature	Strain	Pressure	Vibration
FBGS	Multi- or Single-point	< 50	Yes	Yes	Yes	Yes
DSTS – Rayleigh	Distributed	< 0.07	Yes	Yes	No	No
DSTS – Raman	Distributed	< 20	Yes	No	No	No
DSTS – Brillouin	Distributed	< 50	Yes	Yes	No	No

FBGS are sensitive to temperature, strain, pressure and vibration. However it is difficult to disseminate between temperature and mechanically induced strain components. A temperature compensation technique has to be used, where a Bragg grating is isolated from mechanical strain and used to back calculate only temperature effects from the total strain. The distributed sensors can either measure strain and temperature or, when making use of Raman scattering, only temperature is measured (National Instruments, 2011).

2.6.2 Fibre Bragg Grating Sensors (FBGS)

FBGS or optical strain gauges are made with single-mode glass fibre strands which consist of a core of between 4µm - 9µm in diameter and an outer cladding of 125µm diameter (National Instruments, 2011). The outer core has a lower refractive index compared to the inner core allowing light to travel inside of the inner core. By doping the inner core with Germanium or other photosensitive materials, the core can then be exposed to a UV light source or laser creating narrowly spaced mirrors acting as optical strain gauges. A shift in frequency can be detected as the FBGS responds to any mechanical or thermal strain. The glass fibre core is coated with acrylate, polyimide or organic modulated ceramic (ORMOCER) to increase mechanical stability and limit attack of hydrogen and water. The fibre Bragg grating are written onto the core by dismantling the coating and using either a phase mask process or a superimposing laser light source to imprint imperfections (reflective fringes) at a desired wavelength (see Figure 2-13). The coating is later reapplied after the fibre grating has been written to the core. This process has to be completed to a high standard of workmanship to preserve the mechanical stability and resistance of the cable. Three parameters govern FBGS properties, i.e. the grating mechanical strength, grating length and grating wavelength (Rao,1997).

There are six different grating structure available, i.e. uniform positive-only index change, Gaussian apodised, raised cosine apodised, chirped, discrete phase shift and superstructure (Rao,1997). These terms define the shape of the grating structure and are defined as the optical filtering technique to improve the optical peak shape. There are five different types of gratings available being, type 1 grating, type 1A grating, type 2A grating, regenerated gratings and type 2 gratings. The type of grating relates to the processed used to produce the fibre. This summary is intended to indicate the variety of Bragg gratings available, but details are outside the scope of this research topic. FBGS is typically created (“written”) with a grating wavelength of between 1500nm and 1600nm, which is the range in which most FBGS interrogators can capture reflected light signals (Kreuzer, 2013).

The FBGS or strain sensors are typically fixed to an object such as a bridge or a pipe by glueing or embedding the sensor in, for example, concrete. If an FBGS is stretched, a change in the wavelength of the reflected ultraviolet (UV) light can be detected. Each fringe will reflect a small amount of the incoming wavelength (Figure 2-13), depending on the amount of energy used to write the Bragg grating and the amount of Germanium used to dope the cable. The reflective factor per fringe varies between 0.001% and 0.1% of the total incoming light (Kreuzer, 2013). By writing Bragg gratings with incrementally different wavelengths (say 5 nm) onto a single fibre optic strand, a multi-point sensor can be created that can be interrogated with a single readout unit.

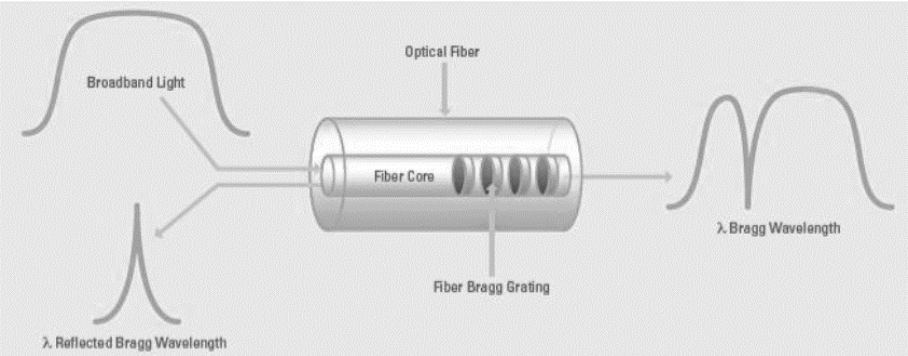

Figure 2-13: FBGS operating principle (National Instruments, 2011)

The wavelength of an FBGS changes with mechanical and thermal strain as shown in (Equation 2-5). Mechanical strain can be calculated with Equation 2-6, and thermal strain can be calculated with Equation 2-7.

$$\frac{\Delta l}{l_o} = k \times \varepsilon + \alpha_\delta \times \Delta T \qquad \text{Equation 2-5}$$

where

Δl = change in wavelength (nm)

l_o = base wavelength at test start (nm)

k = gauge factor (0.78)

ε = strain

α_δ = change of the refractive index (5-8 * 10^{-6} / K)

ΔT = change in temperature (K)

$$\varepsilon_m = \frac{1}{k} \times \frac{l_o}{\Delta l} - \left(\alpha_{sp} + \frac{\alpha_\delta}{k}\right) \times \Delta T \quad \text{Equation 2-6}$$

ε_m = mechanical strain

α_{sp} = refractive index of specimen

$$\Delta T = \frac{\Delta l}{l_0} \times \frac{1}{k \times \alpha_{glass} + \alpha_\delta} \quad \text{Equation 2-7}$$

α_{glass} = refractive index of glass (0.55 * 10^{-6} per Kelvin)

Draw Tower Gratings (DTG) FBGS have developed their own approximation formula as shown in Equation 2-8 below. The coefficient of thermal expansion given by DTG for the SWM-01 strain sensor is 0.5 micro strain per degree Celsius change in temperature.

$$\ln \frac{l}{l_0} = S_1 \times (T_1 - T_0) + S_2 \times (T_1 - T_0)^2 + k \times \varepsilon \quad \text{Equation 2-8}$$

l = wavelength (nm)

l_0 = base wavelength at test start (nm)

k = gauge factor (0.772 for DTG FBGS SWM-01 sensors)

T_0 = base temperature at time t0 in Kelvin

T_1 = temperature at time t1 in Kelvin

S_1 = temperature coefficient 1 6.37 x 10^{-6}

S_1 = temperature coefficient 2 7.46 x 10^{-9}

ε = Strain

A summary of FBGS advantages is presented below:

- High strains can be measured (>10 mε), depending on the elasticity of the fibre optic cable.
- Sensors are small and lightweight
- Passive sensors, can be placed in high voltage, explosive environments and do not need an external power source
- Signal is not distance dependant, can be used for distances exceeding 50 km
- Many FBG sensors can be used in series, creating multi-point sensor
- Long term stable, corrosion resistant and high temperature applications
- Low magnetic field interaction
- A typical sensor accuracy of 7.8 x 10^{-6} $\mu\varepsilon^{-1}$

A summary of FBGS disadvantages is presented below:

- FBGS are temperature-sensitive. Therefore a temperature compensation techniques must be used if measuring only mechanical strain
- High sensitivity to lateral forces or pressure causing birefringence. Optical material property causing a refractive index depending on the polarisation and light propagation direction.
- FBGS have greater stiffness compared to other types of strain gauges
- Interrogator equipment is costly
- The installation of FBGS can require more surface area compared to conventional foil type strain gauges, due to minimum fibre bend radius of 100mm

Fibre Bragg grating sensors have many advantages over traditional electro-mechanical sensors as shown above. Unfortunately no FBGS are manufactured locally in South Africa for industry use, which makes it currently an expensive alternative to consider. The University of Pretoria has used Bragg gratings manufacture by HBM and Draw Tower Grating (DTG) FBGS.

2.6.3 Distributed strain and temperature sensors (DSTS)

Distributed fibre optic sensors can detect temperature changes with a resolution up to 0.05°C and spatial resolution of 1m over 10km if a specific fibre optic cable is used (Mishra, 2011). The quality of fibre optic cables is commonly tested using optical time-domain reflectometer (OTDR), which sends out a pulse of light and measuring the resulting amount of backscatter. The amount of backscatter and absorption will indicate the quality of the cable and the total losses due to impurities. Exactly the same backscattering principle can be used for optical sensing techniques. DSTS makes use of the full length of cable as sensor to measure various parameters, such as strain, temperature, vibration and pressure. Three main categories of scattering or interrogator techniques are described, i.e. Rayleigh, Brillouin and Raman scatter (Inaudi and Glisic, 2010).

Figure 2-14 indicates the physical changes which are observed for the different types of backscatter mechanisms. As shown in the figure, Raman scatter is used to measure changes in temperature as the peak intensity of back-scattered light changes, while Brillouin scatter can be used for both thermal and mechanical strain as the wavelength of reflected light shifts

in response to strain. Rayleigh backscatter can be used to determine strains for short measurement distances.

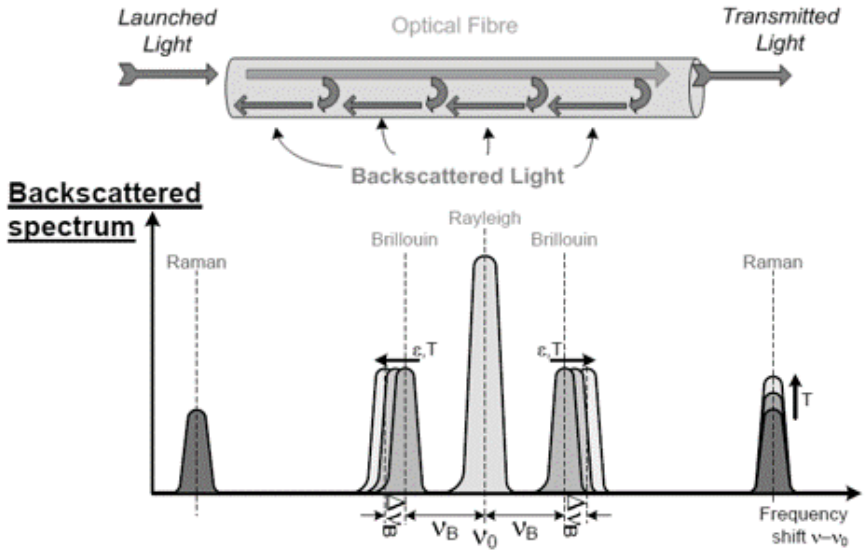

Figure 2-14: Distributed fibre optic methods (Soga, 2017)

The fundamental principle of DSTS is summarised briefly in the list below:

- Light pulse is sent through fibre optic cable
- Back scatter detected by optical interrogator
- Location of back scattering deducted by travel time interval, as speed of light is known
- The shift in frequency of back scatter light corresponds to change in strain
- The frequency shift can be converted to strain
- By repeating this process for all back scatter points a strain profile can be created for whole length of cable

These three different types of scatter principles and analysis methods available are described in detail below (Inaudi and Glisic, 2010):

Rayleigh method is the most dominant scattering and analysis method and depends on the density and composition fluctuation resulting from the manufacturing process. A narrow wave length light pulse is shone into the cable and impurities or variations cause back-scatter which are used to determine the locations. This backscattering technique is insensitive to temperature changes and is not recommended for distances greater than 70 meters (Inaudi and Glisic, 2010).

Raman scattering makes use of molecular vibrations of glass fibre which is stimulated by incident light. The final scatter has two components which are on both sides of the wavelength of the incident light. They are referred to as Stokes and anti-Stokes. The ratio between the Stoke and anti-Stoke represents the temperature sensitive component and is independent of strain influences. This type of scattering application is commonly used for oil and gas applications to monitor temperature (Inaudi and Glisic, 2010).

Brillouin scattering can also be used to detect acoustic vibration. Conservation of energy principle is used to determine the frequency shift between the Brillouin scattering and the incident light. The frequency shift is sensitive to both temperature and strain. It allows for the profiling of temperature and strain throughout the fibre optic cable. There is, however, some degree of difficulty involved in separating mechanical and purely temperature components. Therefore Brillouin is often used in combination with other sensors to disseminate the various components (Zou and Landolsi, 2014).

DSTS interrogator equipment is currently costly and therefore not yet widely used in water network management. Current applications are more common in the field of oil and gas pipelines. As the technology becomes more affordable, it is highly likely that it will find application in the field of water pipeline leak detection and monitoring. A typical interrogator is shown in Figure 2-15 below.

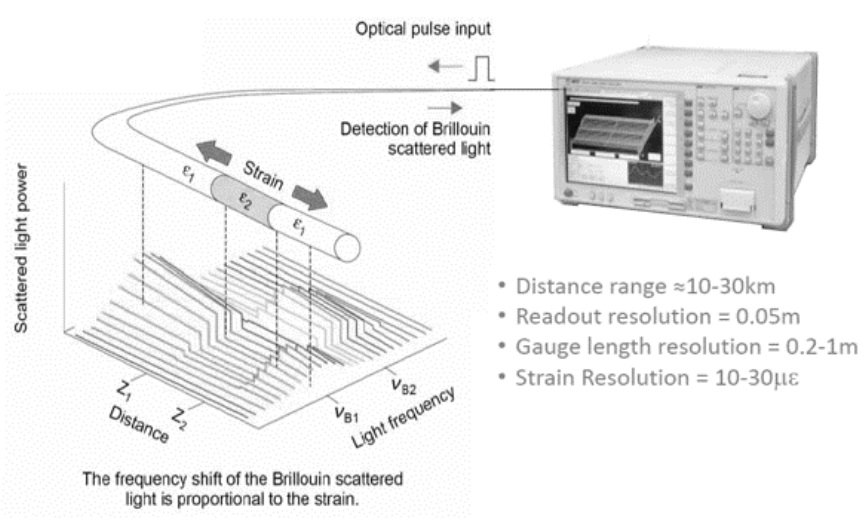

Figure 2-15: Typical Brillouin DSTS readout unit (Yokogawa, 2010)

2.6.4 Fibre optic leak detection

A variety of fibre optic leak detection technologies are available for external and internal applications and different conveyance media, such as gas, crude oil, water and other fluids. There are two different types of fibre optic sensors available for pipeline monitoring, i.e. distributed or multi-point, which measure depending on their configuration either strain, temperature or vibration.

Multi-point sensors or FBGS can be compared to mechanical foil strain gauges which are typically glued to the surface of the monitored specimen accompanied by a temperature compensating FBGS which is mechanically strain relieved and embedded in proximity to the main FBGS to measure only temperature effects. FBGS can however also be used to measure local temperature changes.

For buried gas pipelines the fibre optic cable is typically embedded above the pipeline and for liquid pipelines below the pipelines, as shown in Figure 2-16 below. This configuration has been chosen based on the physical properties of the transported media and the parameter to be observed. A gas such as liquefied petroleum gas typically rises as it expands out of the leak hole from its liquid form because it is lighter than air. The sudden expansion causes a cooling effect to occur referred to as Joule-Thompson effect. Third party interference such as nearby construction should also be detected by placing a fibre optic cable above the pipe, immediately informing the authorities of possible damage to the pipeline. Pipeline strain is complex to monitor as it is not known to which direction the pipe is moving as only the change in length over the total length can be deducted. Therefore three cables are attached at equal spaces around the pipe to obtain a strain profile around a pipe. Some liquid leaks such as oil are easily detected as they are typically transmitted at a much higher temperature compared to the surrounding soil. Water, for example, might be more difficult to detect as the temperature is not altered for transfer purposes, but authorities try to limit water temperature to less than 20ºC. The type of leak will also determine the effectiveness of the method as bigger leaks or bursts facing towards the surface will cause immediate upward piping with downward inundation only occurring as a secondary mechanism (Frings, 2011).

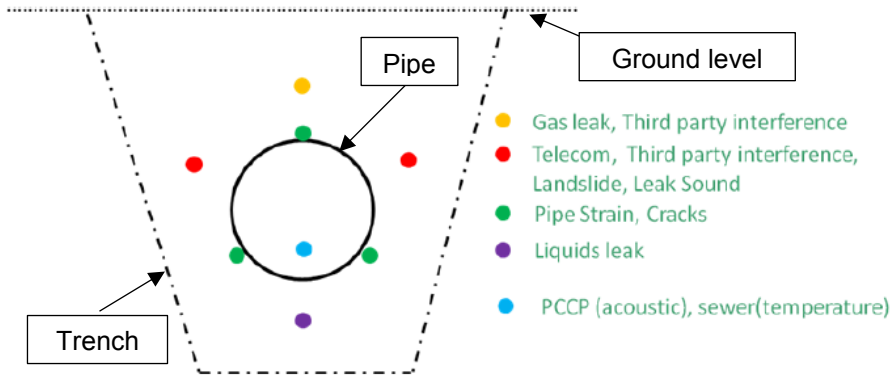

Figure 2-16: Fibre optic placement for different media and parameters (Frings , 2011)

Distributed fibre optic technology is the preferred technology used for monitoring pipelines in terms of strains, surrounding soil temperature and vibration. Using the full length of cable as measurement device compared to a multipoint sensor does create a better mechanistic understanding of pipeline behaviour.

They have been evaluated as a structural health monitoring tool for pipelines with regard to strains induced by earthquakes. An artificial shear fault was simulated in a shear-box setup with various strain sensor locations as shown in Figure 2-17 to validate the use of distributed sensors to detect damage to pipelines caused by ground movements. The study successfully indicated that fibre optic sensing can be an effective tool to determine possible pipeline failures by earthquakes and landslides (Glisic and Yao, 2012).

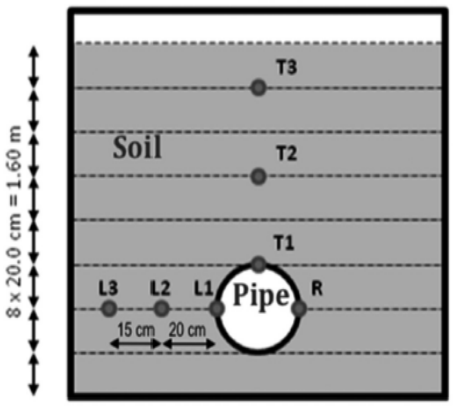

Figure 2-17: Fibre optic cable location to measure strain (Glisic and Yao, 2012)

Henrie et al. (2016) indicates that distributed fibre optic has been researched extensively as a method to detect leaks in water distribution systems. When using temperature as a means of

leak detection it is essential that the temperature differential between the water and soil has to be sufficiently large for the method to function successfully.

Various companies have developed long range pipeline monitoring instruments with DSTS as their basis. An example of such a product is the distributed temperature and strain monitoring system or DiTeSt by SMARTEC (see Figure 2-18), which is based on the Brillouin scattering principle. Normal fibre optic telecommunication cable can be used for a temperature range between 20ºC to 60º. This limitation is especially prevalent for Brillouin scattering as the mechanical strain component has to be isolated from thermal strain. This is typically done by having at least one cable bonded to allow for full or partial strain transfer and at least one cable in close proximity unbonded allowing for thermal expansion and contraction irrespective of mechanical strain. A number of sensing cables were developed to measure both temperature and strain either in close proximity to the pipeline or on the pipeline surface. The so called SMARTape is made up of a fused glass fibre reinforced thermoplastic, which can be glued onto a pipeline to measure strains. SMARTprofile is senor cable which can be used to measure both strain and temperature due to a bonded and unbonded approach as discussed earlier. A number of case studies were conducted by Inaudi and Glisic (2010) to showcase the efficiency of their products, which are briefly summarised below.

The measurement range for the DiTeSt device is 30km, which can be extended to 150km and 60 channels with intermediate optical amplifier modules. The spatial resolution is dependent on the length of the fibre optic sensing cable, number of splices and type of cable. A spatial resolution of 1m over 5km and 2m over 25km is given with a temperature resolution of 0.1ºC, the temperature range is dependent on the type of sensing cable used. The strain resolution is given as 0.002mm/m. The strain and temperature requisition time for the analyser is typically 2 minutes, depending on all of the parameters mentioned above.

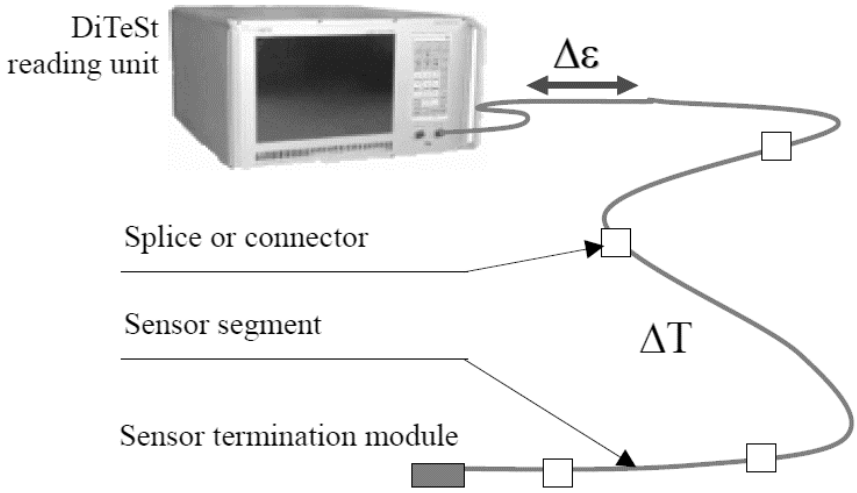

Figure 2-18: DiTeSt readout unit and fibre optic sensor cable (Inaudi and Glisic, 2010)

Case Studies

Brine pipeline leakage detection:

A 55km long brine pipeline in Berlin (Germany) was instrumented with a distributed fibre optic cable and DiTeSt analyser. Two analysers were used because high losses were experienced at splice points. The whole system is autonomous and obtains a temperature profile of the whole pipeline every 30 minutes, which is compared to previous temperature profiles. If anomalies are detected during the analyses period an alarm is raised, which alerts authorities to the location of a possible leak (Inaudi and Glisic, 2010).

Monitoring gas pipeline:

A 500m long and 35 year old gas pipeline situated in an unstable area in Italy was retrofitted with SMARTape and distributed temperature sensing cable in combination with a DiTeSt analyser. For retrofitting purposes the pipeline was excavated and exposed to allow for the sensors to be added to the pipeline. The distributed temperature measurement was placed on top of the pipeline crown used primarily as a temperature compensating device. The SMARTape strain sensors are placed on each side with a 120^0 offset from the vertical top axis position. This sensor layout allows for long term deflection monitoring and an instantaneous warning of excessive strains due to support failure and ground movement. A leak was

simulated using a CO_2 fire extinguisher, cooling the soil around the pipe and therefore simulating a gas leak. The study indicated promising results (Inaudi and Glisic, 2010).

SMARTPipe:

This is a reinforced thermoplastic pipe, which incorporates the use of distributed fibre optic sensing. The pipe is designed to be used in a trenchless rehabilitation option or a standalone option. The pipe is customisable to suit the application needs. The fibre optic senor cable is interwoven with reinforced plastic strings over a thermoplastic pipe, allowing for greater strength and robustness (Inaudi and Glisic, 2010).

Further case studies:

Temperature monitoring of water pipes are rare. Pipeline subsidence monitoring is available. The distributed fibre optic system developed by Sensornet consists of a Raman and Brillouin scattering unit which prevents costly use of secondary cables and combines a unique independent temperature and strain system which eliminates noisy signal.

Range – 24km
Strain resolution – 10με
Temperature resolution – 1°C

An early pipeline leak detection method based on distributed differential temperature sensors (DdTS) was investigated by Wang et al. (2016). A number of issues and limitations were found with existing fibre optic leak detection methods, such as the ability to detect small leaks and act as an early warning system. It is accepted internationally that leaks being less than 1% of total daily volumetric throughput are defined as small and that these leaks are especially difficult to detect with conventional leak detection methods. The proposed DdTS method not only use differential temperature as a leakage indicator but also an acoustic signature. This is especially useful if the background temperature of the soil surrounding the pipe is similar to that of the transported media. The technology used for the proposed DdTS method uses coherent optical domain reflectometry (C-OTDR) and is not only limited to a quasi-static measuring regime for strain and temperature but can also be used on dynamic acoustic signature. C-OTDR makes use of the phase shift principle of the backscatter light caused by strain changes which can be replicated by the shift in wavelength of the interrogator light signal. The temperature sensitivity is several orders of magnitude greater than similar Brillouin

and Raman based sensors, it is claimed that “temperature differential sensitivity” is 0.0005°C. A test setup with a cable length of 20 km was used, 100 m of the total length was installed inside of a temperature controlled oven. The temperature within the oven was increased in increments of 1°C, in addition point sensors were placed in close proximity to the cable, having an accuracy of 0.01°C. Various orifice leakage opening sizes were investigated to determine their acoustic signature. The spatial resolution of the sensor is however not yet optimised as a localised incident might not be recognised by the readout unit. The results from the study indicated that the proposed sensor is promising (Wang et al., 2016).

A number of case studies have been conducted on oil and gas pipelines due to the significant temperature differential present between the soil surrounding a pipe and the media transported within the pipe in those applications. Oil is typically heated, decreasing its viscosity and subsequently allowing easier transport due to lower friction in a pipeline. Gas expands rapidly at the outside of a pipe at the leak location allowing for an instantaneous cooling effect commonly referred to as Joule-Thompson effect. Water temperature in a distribution network is dependent on the flow rate, water source and soil characteristics, to name a few influencing factors.

Another key difference between water pipelines and oil/gas pipelines is that oil/gas leaking into the surrounding soil has detrimental environmental impacts, leading to contamination. Potable water as such has no apparent adverse environmental impacts, however could lead to erosion and sinkhole formation, as discussed in previous chapters. Potable water within the pipeline could also be contaminated from external pollutants entering the pipeline during certain operating regimes. The difference in cost of transported product is another driver for oil/gas pipelines to be more accepting and accommodating of new technology such as fibre optic monitoring.

2.6.5 Calibrating fibre optic strain and temperature sensors

Fibre optic sensor properties are described by their manufacturers. For distributed fibre sensing the amount of impurities present in the cable is important, more impurities would mean a greater measurement sensitivity, but less measuring distance can be covered. This is due to a greater attenuation or more light being backscattered therefore the signal strength is decreasing faster with distance. For FBGS the distance, length and intensity of the individual

Braggs are important, as well as intrinsic cable properties such as strain specific properties and thermal expansion coefficients (Kreuzer, 2013).

FBGS and DSTS are typically temperature calibrated by inserting the sensors into a temperature controlled calibration device which is set to simulate specific temperature changes at specific time intervals. Mechanical strain is measured in a temperature controlled environment where the sensors are stretched a known distance which is back-calculated to a change in wavelength. These methods are typically used to verify the manufacturer specifications (Kreuzer, 2013).

The gauge factor for FBGS is defined as the wavelength-normalisation wavelength change per mechanical strain (ε) according to Jülich et al. (2013) and it is said to be the most important FBGS parameter. A gauge factor value of 0.78 is typically given for an FBGS with a strain sensitivity of 1.2pm/με at a wavelength of approximately 1535nm. There are two main components that influence the gauge factor, which are the strain transfer ratio and effective strain-optic coefficient. The strain transfer ratio indicates how efficiently strains are transferred from a structure through an adhesive and the protective layers to the fibre optic cable. It is technically seen as ratio of the strain along the fibre optic cable axis and the strain parallel to fibre optic cable along the structure. The second factor is defined as change in refractive index due to change in strain. If an acceptable adhesive technique is used for surface bonding it can be assumed that the strain transfer ratio is greater than 0.99, which means that there is nearly full strain transfer (1). The physical properties of the cable such as the core radii, Young's moduli, doping materials and concentration have a greater effect on the gauge factor which is attributed to the effective stain –optic coefficient. It is important that the manufacturer provides a gauge factor for surface mounted FBGS to be used as standardised calibration factor (Jülich et al., 2013).

2.8 Selected thermal properties of soils

As the proposed research involves the measurement of soil temperatures, an overview of factors relevant to the thermal behaviour of soil is briefly presented.

2.7.1 Thermal conductivity of soil and rock

Leaks from buried pipelines are investigated which are surrounded by various soils along their length which differ in thermal properties. This section has been incorporated in the literature study as to understand how the thermal properties changes with different soils properties. Thermal conductivity of soil is a function of the soil moisture content, mineralogical composition, density and particle size distribution (Barry-Macaulay et al., 2013). In general, coarse grained soils are said to have a higher thermal conductivity at low saturation levels compared to fine grained soil. Thermal conductivity also increase with an increase in moisture content and dry density. Depending on the mineralogical composition the thermal conductivity differs, for example where moisture content might not change the thermal conductivity. Increasing moisture content increases the contact between particles. Similarly, an increase in dry density, causing a repacking of particles, allows for greater inter-particle contact, leading to an increase in thermal conductivity (Barry-Macaulay et al., 2013).

There are a number of methods available to measure thermal conductivity of soils, one method being a thermal needle probe and another being a divided bar apparatus. The thermal needle probe is based on the infinite line heat source theory, which uses heat dissipation calculations to determine a soil-specific thermal conductivity. A divided bar apparatus is used to test thermal conductivity of rock samples. However, the contact area between the needle probe and a drilled hole in the rock does not provide sufficient heat transfer capability. Thermal conductive grease is used in the cavity between the rock and the thermal needle probe (Barry-Macaulay et al., 2013).

To summarise the parameters that effect thermal conductivity of soil and rocks the following list is presented (Barry-Macaulay et al., 2013):

- Saturation: Fine and coarse soils are distinguished. For fine soils the thermal conductivity increases with an increase in saturation levels, whereas coarse soils show a great initial increase in thermal conductivity with low saturation levels with little increase at higher saturation levels. The mechanisms is driven by inter-particle contact points, coarse soils have much less contact point compared to finer soils.

- Mineralogy: Different minerals have different thermal conductivities, quartz typically has the highest thermal conductivity of 7.7W/mK compared to other soil minerals which have a far lower thermal conductivity of between 1.8 to 2.8W/mK. Fine grained soils typically

have a much lower quartz content, therefore having a lower thermal conductivity compared to coarse grained soils at low saturation levels.

- Density: A higher soil density indicates a greater thermal conductivity due to greater inter-particle contact points. The same trend can be observed when compacting soils increasing the density and the packing structure.

- Anisotropy: In some rock formations the direction of the stratification being either inclined, horizontal or vertical influences the thermal conductivity in various directions.

There are a number of parameters that influence the thermal conductivity of soils. A given pipeline often passes through varying soil types and densities which makes it difficult to predict the effectiveness of the heat transfer mechanisms with great accuracy (AWWA, 2009). Daily and seasonal soil temperature variation decreases with depth as the upper soil layers act as an insulating buffer zone compared to lower soil layers. From a certain depth below the natural ground level, little temperature variation can be observed, depending on the parameters mentioned above (Florides and Kalogirou, 2007). Given the mentioned factors a study to evaluate the use of temperature measurement as a means of leak detection is best carried out by means of a physical study rather than numerically.

2.7.2 Thermal conductivity of buried pipes

It is expected that media transported in a buried pipeline has a different temperature to its surrounding soil. Depending on the pipe material and its properties the temperature of the medium does not fluctuate a lot and the pipe will create a thermal barriers or lag between the surrounding soil and media. Heat transfer between the soil and a buried pipe occurs naturally as the transported media is introduced from an external source such as a reservoir into the underground pipeline. Depending on the temperature differential between the surrounding soil and the water transported in the pipe, heat transfer occurs between the soil and the fluid in the pipe or vice versa. This heat transfer is affected by the ambient atmospheric temperature, the flow rate in the pipe, the hydraulic conductivity in the soil and other factors (Conway, 2010).

In a study involving numerical modelling of heat transfer in a buried pipe, Conway (2010) describes the mechanisms and the mathematics needed to describe thermal heat exchange in underground pipes.

Heat flow in the ground is described by Fourier's law of heat conduction (Equation 2-8).

$$\vec{q} = -k \nabla T$$ ..... Equation 2-8

$\vec{q}$ = Heat flus (heat flow per unit area)
K = Thermal conductivity of the material
∇T = Temperature gradient

Water temperature in distribution networks should not exceed 20ºC as it will reduce the effectiveness of disinfectants (WHO, 2014). Even though there is little scientific evidence that an increase in water temperature is directly related to an increase in corrosion rates, secondary factors such as lower residual chlorine and chloramine are linked to elevated water distribution temperatures which indicate higher corrosion rates. Elevated water temperatures in distribution networks also indicate an increase in biological activity and growth, leading to higher corrosion rates of pipeline walls, referred to as micro-erosion or bio-corrosion (WHO, 2014).

Pipe-soil interaction in terms of heat transfer from the transported media to the surrounding soil (or vice versa) is often investigated with numerical models. Finite element models are commonly used to determine the interaction of ambient air/soil temperature and transported media temperature as shown in an example in Figure 2-19.The air temperature in this example is -10ºC and the transported crude oil temperature is 33ºC, the heat transfer surrounding the pipeline is significant compared to the surrounding soil temperature. The effects of seasonality, as well as daily temperature fluctuation on both the transported media and the surrounding soil have to be investigated to determine if possible blind periods can occur. Blind periods are referred to as time periods when the transported medium temperature and the surrounding soil temperature is similar, therefore it becomes difficult to detect a leak on the basis of temperature changes (Frings, 2011).

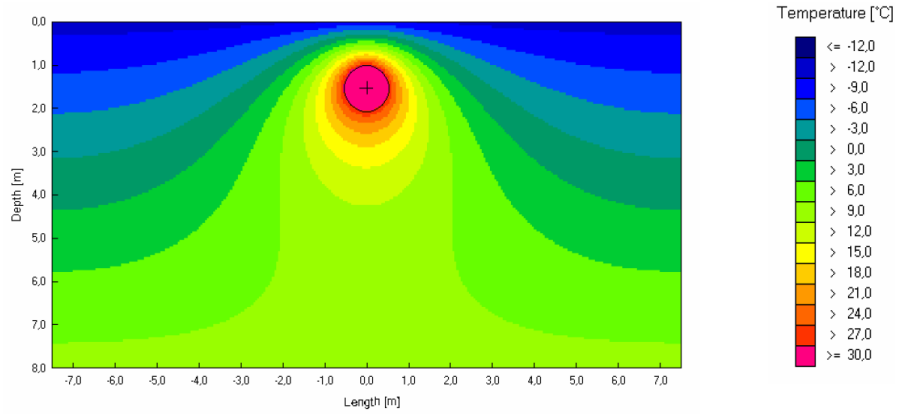

Figure 2-19: Steady state temperature distribution around a crude oil pipe (Frings, 2011)

Buried water pipes in a reticulation network can be described as thermal heat sinks or sources (depending of the relative soil-water temperature) affecting the temperature of the ground around them (Florides and Kalogirou, 2007). The detection of leaks by measuring temperature changes in the ground near a pipeline is dependent on the extent to which the presence of the pipe has affected the temperature of the surrounding ground.

2.9 Temperature measurement

2.9.1 Negative thermal coefficient thermistors

Negative thermal coefficient (NTC) thermistors are resistors that decrease in resistance as the surrounding temperature increases. They are made of different mixtures of metals, such as manganese, nickel, copper, cobalt and iron oxides depending on the desired properties (AVX, 2017). A carefully controlled mixing, pressing and metallisation[1] process ensures good quality, accuracy and precision. The size and the composition of the thermistor will determine the temperature coefficient and range. The nominal resistance of a thermistor is typically given at 25 degrees Celsius at low power, making the heating effect of the NTC resistor negligible. The resistance behaviour compared to temperature changes is expressed as temperature – resistance characteristics, where a temperature coefficient (α, Equation 2-9) and a sensitivity index (B, Equation 2-10) are given (AVX, 2017).

[1] Is the process of coating a metal surface with ceramic or other metal

$$\alpha = \frac{100}{R} \times \frac{dR}{dT} \quad \text{Equation 2-9}$$

α = temperature coefficient % per ºC

$\frac{dR}{dT}$ = Change is resistance over change in temperature (slope of resistance/temperature curve)

R = resistance value (Ω)

$$B(K) = \frac{1}{\left(\frac{1}{T_1} - \frac{1}{T_2}\right)} \times \ln\left(\frac{R_1}{R_2}\right) \quad \text{Equation 2-10}$$

B (K) = Sensitivity index

T_1 = Temperature value 1 (typically 25ºC)

T_2 = Temperature value 2 (controlled ºC)

R_1 = Resistance value 1 (typically 5 000Ω)

R_2 = Resistance value 2 (output Ω)

The α and B parameters specific to the thermistor or NTC resistor can then be used to create a resistance/ temperature approximation relationship. For the thermistor from AVX with a material Code MA 3960, the following formula was developed at 25 degrees Celsius the resistance is 5 kilo Ohm (Equation 2-11) (AVX, 2017).

$$T = \frac{1}{\left(2.5374 \times 10^{-4}\right) \times \ln(R) + \left(1.1958 \times 10^{-4}\right)} - 273.15 \quad \text{Equation 2-11}$$

T = Temperature value (ºC)

R = Resistance value (Ω)

The response time to temperature change is dependent on the substance that the thermistor is embedded in or surrounded with. If the thermal conductivity of the media surrounding the thermistor is low, the thermistor will react slowly compared to a fast change in resistance for a material with high thermal conductivity (AVX, 2017).

Alternatively a thermocouple could also be used to measure temperature, which are made by joining two different metals at one end. The voltage output from the thermocouple can be back calculated to a pre-calibrated temperature. Thermocouples are less sensitive, non-linear, have

low output voltage, unstable and measurements are difficult to repeat. Therefore thermistors were preferred for temperature measurement in the work presented here.

Thermistors from AVX and Vishay were used for the experiments, both with their respective calibration curves and conversion formulae.

2.10 Research focus and motivation

It is hypothesised that a leak will result in deviation in soil temperature from the normally observed soil temperature. This research aimed to gain an understanding of the daily and seasonal temperature differential between water in distribution pipes and the surrounding soil. This project initially focuses on the determination of the typical daily and seasonal temperature differential in the soil with depth, followed by investigating the temperature changes in the soil near a pipeline associated with a leak. This was initially done using thermistors as temperature measurement device, followed by the use of FBGS. The provision was made in the experimental arrangement to allow for continuous distributed strain/temperature measurement to be added to the current discrete experimental setup.

It can be deducted from the literature study that there are some research areas not yet fully covered. The use of FBGS as water pipeline leak detection sensors has not yet been widely researched, therefore this research will form a valuable contribution to the sensor base to detect leaks and monitor pipelines.

3. EXPERIMENTAL WORK

Experimental work was aimed at gaining an understanding of the temperature variation in the natural ground and potable water in distribution network in Pretoria. The effects of a leak in a buried pipeline on the surrounding ground temperature and pipe support conditions were investigated. This chapter contains a description of the experimental work carried out.

The experimental farm of the University of Pretoria, on which two of the four experiments were conducted, is located within the Pretoria geological Group and the Transvaal Supergroup which comprises of sedimentary rocks, mudstone and quartzites with some basalt of Archean-Vaalian age, which formed over a period of 2350 to 2100 million years ago (McCarthy and Rubidge, 2005). Locally the site is underlain by hillwash soil comprising of slightly moist, red-brown, slightly clayey silty sands of medium dense to dense consistency. The water table is deep and does not affect the site. Undisturbed soils on site are unsaturated. The site is relatively flat, sloping gently towards the North West with a mean elevation above sea level being approximate 1385m. The site coordinates are 28°15.220'E longitude and 25°45.229'S latitude.

The climate is typical of the South African Highveld conditions with daily average summer temperatures of between 18°C to 32°C and average winter temperature fluctuations between 12°C to 24°C. The mean annual rainfall is 685mm. These statistics were obtained from the South African Weather Services (SAWS) UNISA Pretoria weather station (SAWS number 513346).

3.1 Investigating natural temperature variation in the ground

The success of the monitoring system under investigation is based on the ability to distinguish leakage induced temperature changes from natural temperature changes in the field. In January 2017 a series of thermistors were installed at depth increments of 250mm in a test pit on the University of Pretoria's experimental farm to a depth of 3m as illustrated in Figure 3-1 to provide information on the normal daily and seasonal temperature variation in the ground. This information is necessary so that temperature changes due to leakage can be distinguished from the normal ambient changes. AVX M3950 NTC thermistors were used which indicate 5 kΩ at 25°C. The parameter conversion from resistance to temperature is given by the manufacturer.

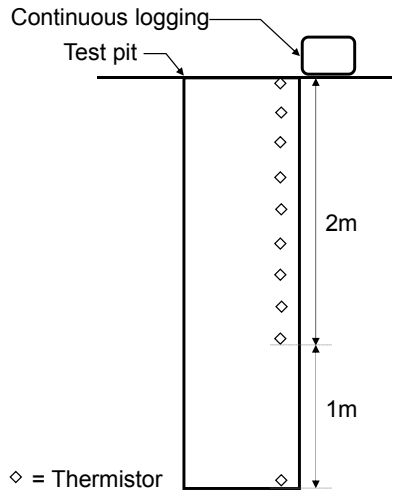

Figure 3-1: In-situ soil temperature distribution

A photograph of the test pit with the series of thermistors is presented in Figure 3-2. In-situ soil from the testpit was used for backfilling and the TLB bucket was used to light compact backfill layers in 150mm increments.

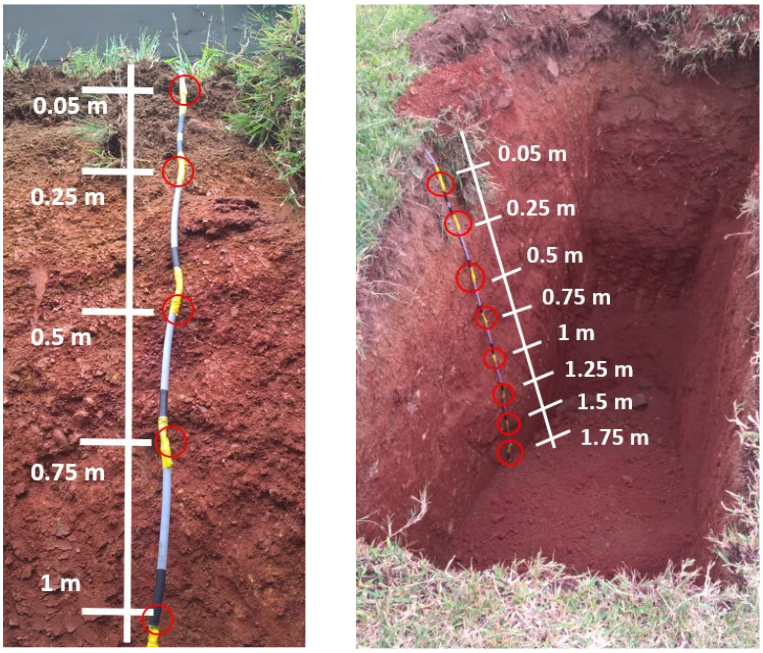

Figure 3-2: Thermistor placement in testpit on the experimental farm

Figure 3-3 shows a photograph of the data logger used to continuously record the resistance of the series of thermistors.

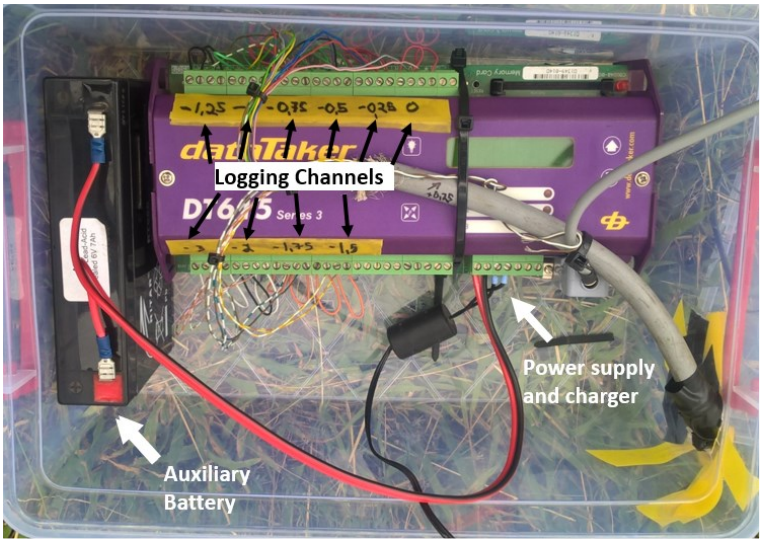

Figure 3-3: DataTaker DT615 with 10 channels

3.2 Temperature variation in water mains

It is important that temperature deviation induced by water leaking from a pipeline can be distinguished from natural temperature variation in the ground. This aspect is further complicated by the fact that the temperature of water in a distribution network also varies over time. A resistance temperature device (RTD) is used to continuously monitor water temperature upstream of the Pierre van Ryneveld Reservoir south of Pretoria in a valve chamber (for location see Figure 3-4). The water supply to the reservoir originates from a large diameter distribution pipe, nearby Rietvlei Dam water treatment works and from the Vaal Dam water supply scheme through Rand Water. This data is used to indicate daily and seasonal temperature trends in a typical water distribution network.

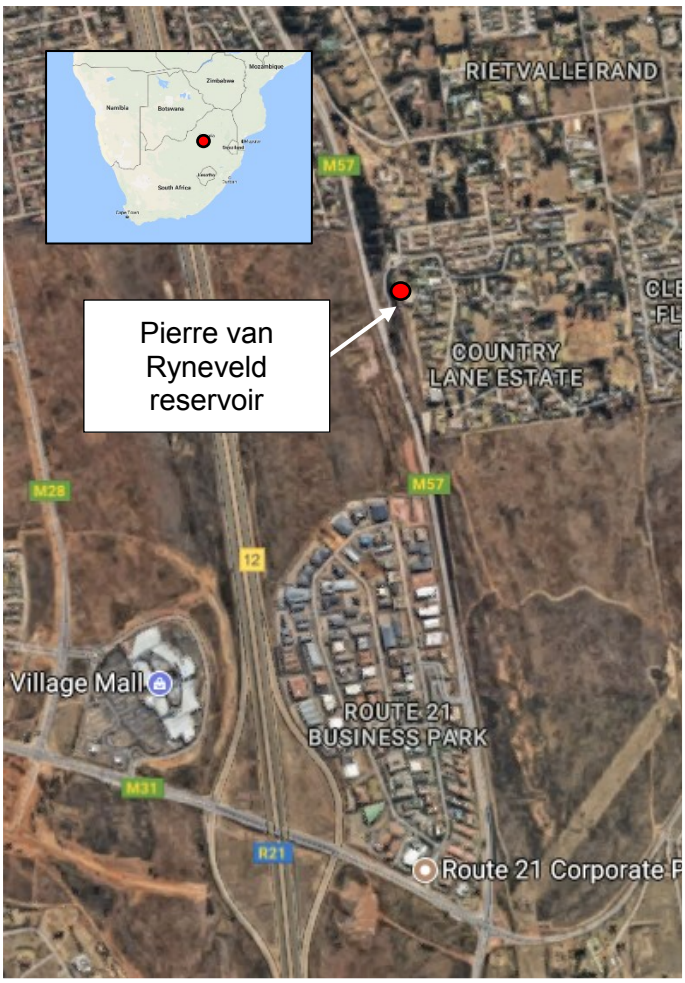

Figure 3-4: Pierre van Ryneveld reservoir location

The specific RTD used for the experiment is shown in Figure 3-5, a current output of 4mA – 20mA corresponds to a temperature of 0ºC – 100ºC. See Figure 3-6 for the installed RTD in the valve chamber. A data logger was used to capture the temperature data every hour.

Figure 3-5: RTD 4 - 20 mA corresponding to >0 – 100 ºC output

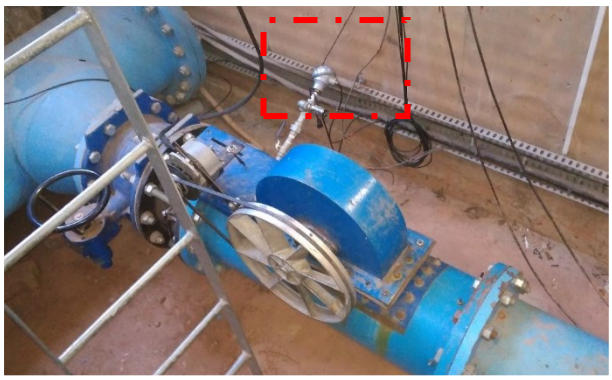

Figure 3-6: RTD installed at Pierre van Ryneveld reservoir

3.3 Investigating temperature changes caused by water leaks (laboratory phase)

Experiments were conducted in the laboratory in which water was allowed to leak under controlled conditions into a soil mass into which a number of thermistors were installed to investigate to what extent an advancing wetting front from a leaking pipeline results in a change in temperature in the ground. The tests were carried out in a semi-transparent plastic container measuring 790mm x 400mm x 590mm high to allow the advancing wetting front to be visually observed. Advancing wetting fronts resulting from a number of flow rates were investigated as slow flow rates might result in the water temperature equalising with the soil temperature, resulting in a difficulty to detect temperature variation associated with the arrival of a wetting front. The experiments were carried out in a temperature isolated enclosure where temperature was kept at a constant 25°C to eliminate environmental temperature fluctuation.

Figure 3-7 presents an elevation of the experimental setup, showing the model container, water introduction point and thermistor locations, with a photograph in Figure 3-8.

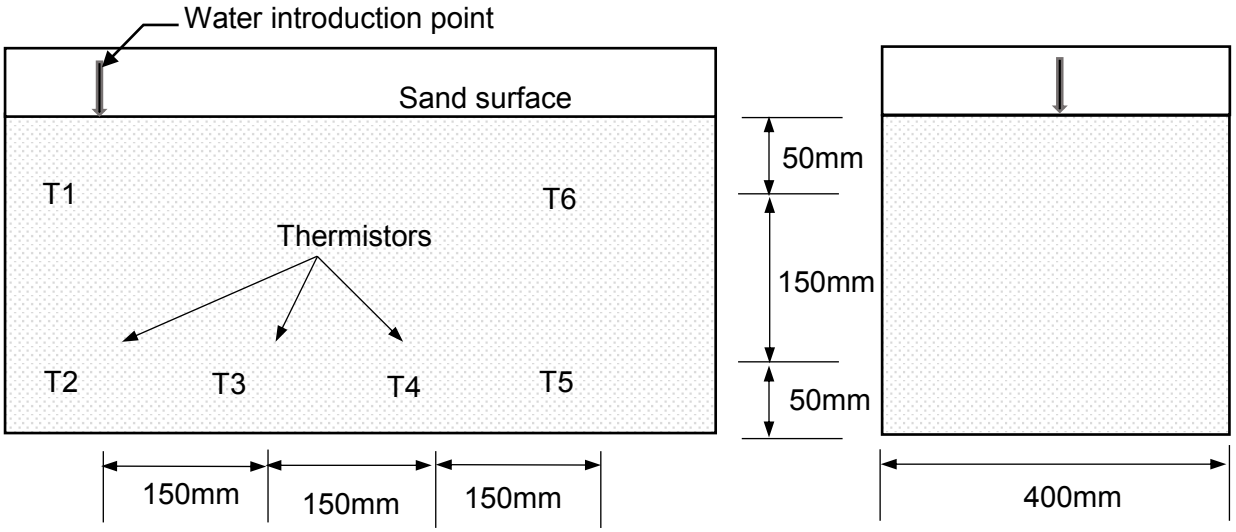

Figure 3-7: Experimental arrangement for laboratory leakage experiment.

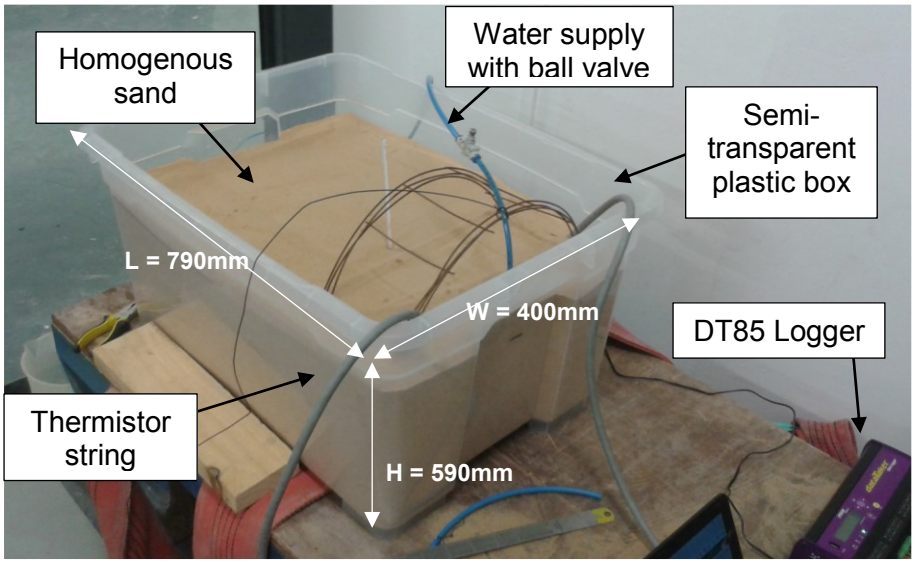

Figure 3-8: Photograph of the experimental arrangement for laboratory leakage experiment.

3.4 Investigating temperature changes caused by water leaks (field phase)

3.4.1 Introduction to field phase experiment

It was expected that temperature changes underneath a pipeline will provide the first indication of a leak occurring. Over time, leakage is likely to result in softening of the ground near the leak and this is likely to impose some strain on the pipe due to changes in the support conditions underneath the pipe. It is hypothesised that these strains can be detected using fibre optic strain measurement. How soon after detection of a temperature change a change in pipe strain becomes detectable may possibly also provide an indication of the severity of the leak. The detection of strain will be especially important in dolomitic ground because it may provide an indication that a sinkhole is forming which would be a trigger for urgent remedial action, a sinkhole or cavity would be registered as major strain occurrence. A short length of pipeline was therefore installed at the experimental farm of the University of Pretoria which was instrumented for both temperature and strain measurement to allow the abovementioned aspects to be investigated under controlled conditions.

It is believed that the correlation between pipe strain and ground movement will enable pipe owners to judge the urgency by which remedial action is required. For example: If a sudden temperature change is detected and no measureable strain, it would imply that the pipe is leaking but has not suffered significant structural damage yet. However, should significant strains be detected in addition to a temperature change, the pipe has suffered some deformation (possibly damage) and more urgent remedial action is required. The knowledge gained in term of this behaviour could assist in refining water distribution network maintenance plans.

A short pipeline section installed on the University of Pretoria's experimental farm is illustrated in Figure 3-9 (see Figure 3-10 for locality). It was instrumented with an array of FBGS and conventional thermistors. This was done to verify whether the proposed leakage detection system would be able to detect leakage from a pipeline in the field. This was necessary because the ambient temperature changes occurring in the field are different from those in the laboratory and it is necessary to observe whether temperature changes from leakage can be distinguished from the ambient. Furthermore, the effect of soil wetting in the pipe trench on the support condition around the pipe had to be investigated.

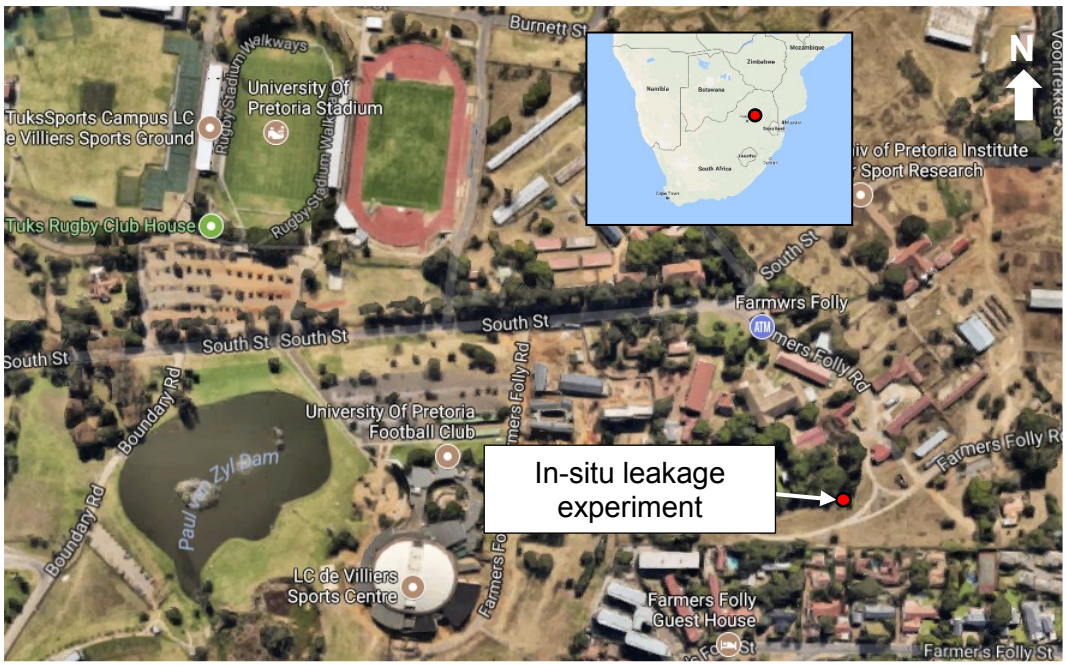

Figure 3-9: Location of in-situ pipe leakage experiment

Figure 3-10: View of the location of pipe leakage experiment

3.4.2 Experimental installation

The installation comprises of a 12m long 110mm diameter uPVC Class 9 pipe buried under backfill of 600mm to the pipe crown. Provision was made to allow water to be circulated through the pipe during testing. It was undesirable to leave stagnant water in the pipe during

testing as this water would soon take on the temperature of the surrounding soil, significantly reducing the temperature gradient. This scenario was investigated in the test-set up.

The pipe was equipped with three leak points installed at 2m intervals along the pipe length, with one leak point at the pipe invert, one at the pipe crown and one at the side of the pipe to allow leaks originating from different parts of the pipe to be studied. The leak points were operated via valves located on the ground surface and are fitted with flow restrictors to impose leakage at the desired rate.

A number of thermistors were installed in the ground and on the pipe around each leak point to allow the temperature changes associated with a leak to be observed in great detail. Vishay NTCLE305E4 thermistors were used which indicate 5kΩ resistance at 25°C. In addition, fibre optic cable with 16 FBGS were included in the installation. FBGS DTG SWM-01 strain sensors were used. They have excellent corrosive properties with an operational temperature range from -40°C to 120°C, an elastic modulus greater than 48GPa for the complete sensor cable, maximum tensile strain of 2.5mε and a maximum allowable longitudinal load of 0.95kN (FBGS, 2017). Eight of the 16 strain sensors were rigidly fixed (epoxied) over the length of the FBGS to the external pipe base to allow for strain measurement on the pipe. The pipe surface was cleaned before epoxying. The remaining Bragg sensors were placed within a 4mm polyurethane (PU) tube filled with low viscosity oil in the left trench corner looking into the downstream direction (see Figure 3-11c). The purpose of the free cable was to ensure that the 8 fibre Bragg gratings were mechanically isolated from any pipe strain with the intension that they would only be sensitive to temperature changes.

Two locations for the positioning of the fibre optic cables in the proposed leak detection system were investigated to determine the position for optimal leakage detection, i.e. fixed to the pipe and free-floating within a thin plastic tube filled with oil in the pipe trench.

A long section schematic of the pipeline is shown in Figure 3-11 (a) with a plan view shown Figure 3-11 (b). The instrument locations are indicated in these schematics. A detailed plan and section view of one leak location are indicated in Figure 3-11 (c). Each leak location had a thermistor string located 0.15m upstream, 0.15m downstream and at the leak location to allow temperature migration around a leak location to be studied. Each thermistor string consisted of 9 individual thermistors, giving a total of 27 thermistors per leak location. Their arrangement around the leak locations are indicated in Figure 3-11(c). The FBGS in the trench corner measure thermal strain changes and attached to the pipe measure mechanical and thermal strain.

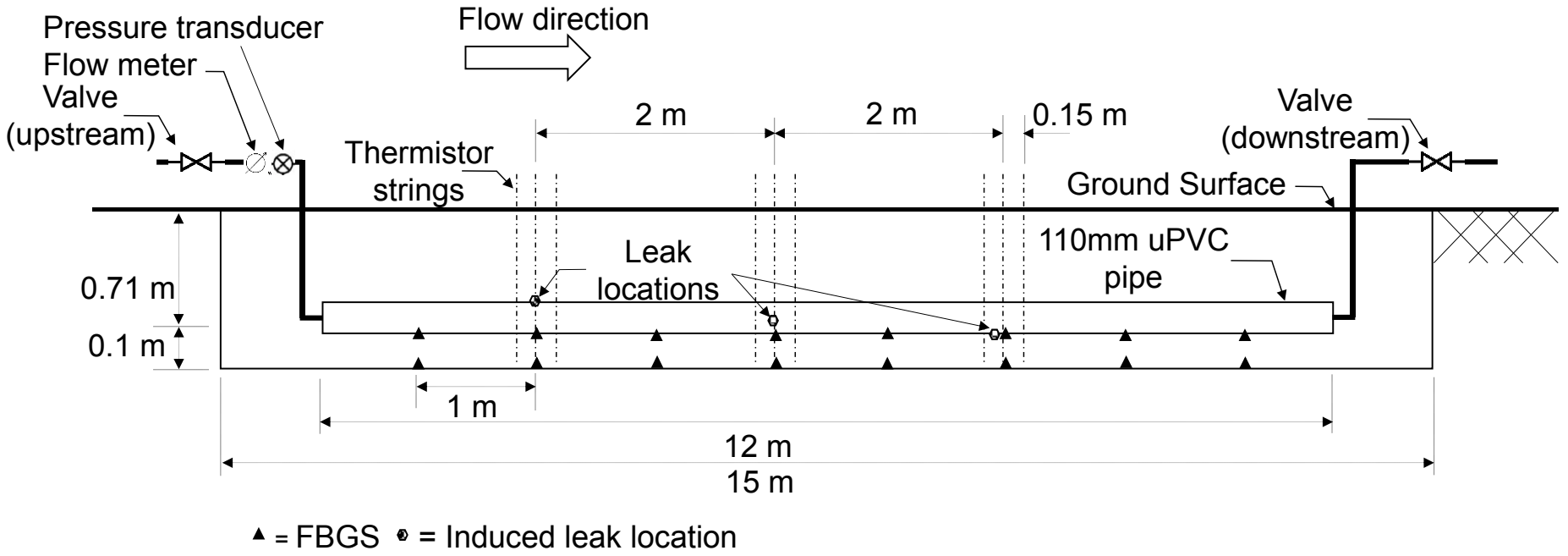

(a) Elevation of 110mm uPVC pipe field installation.

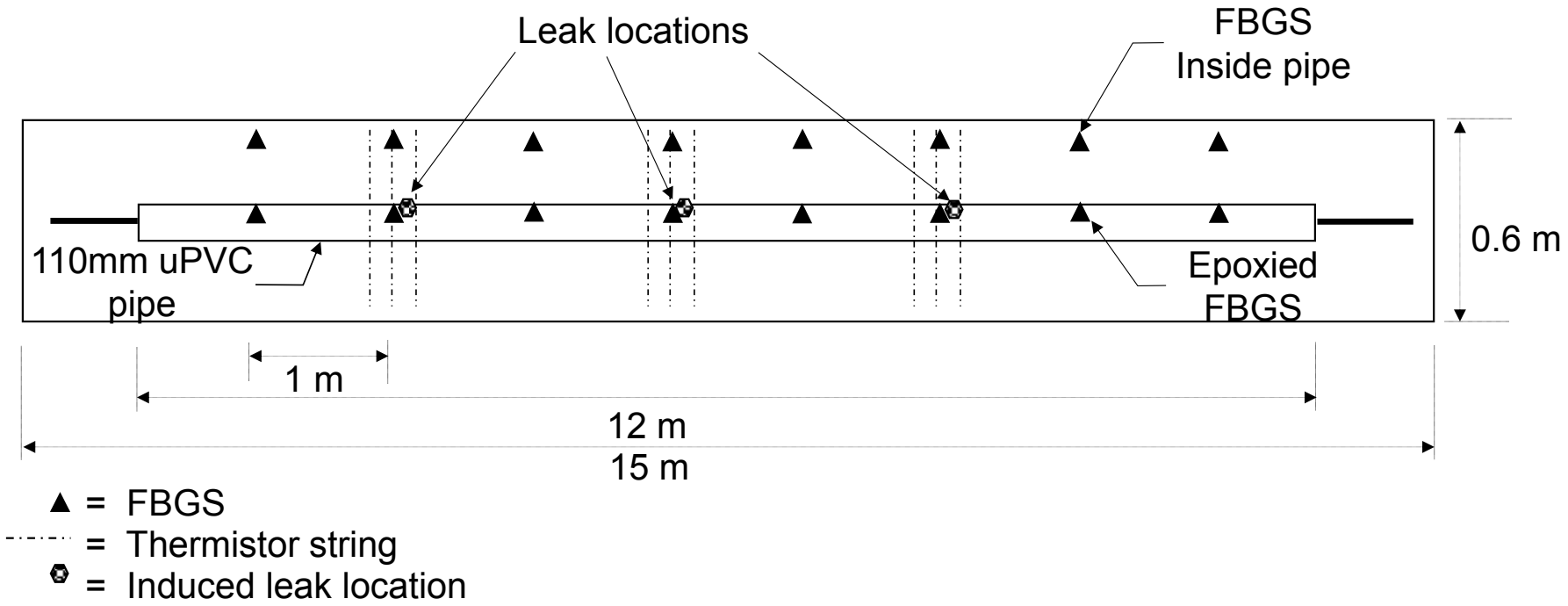

(b) Plan of field installation showing temperature and strain Bragg gratings and thermistor strings.

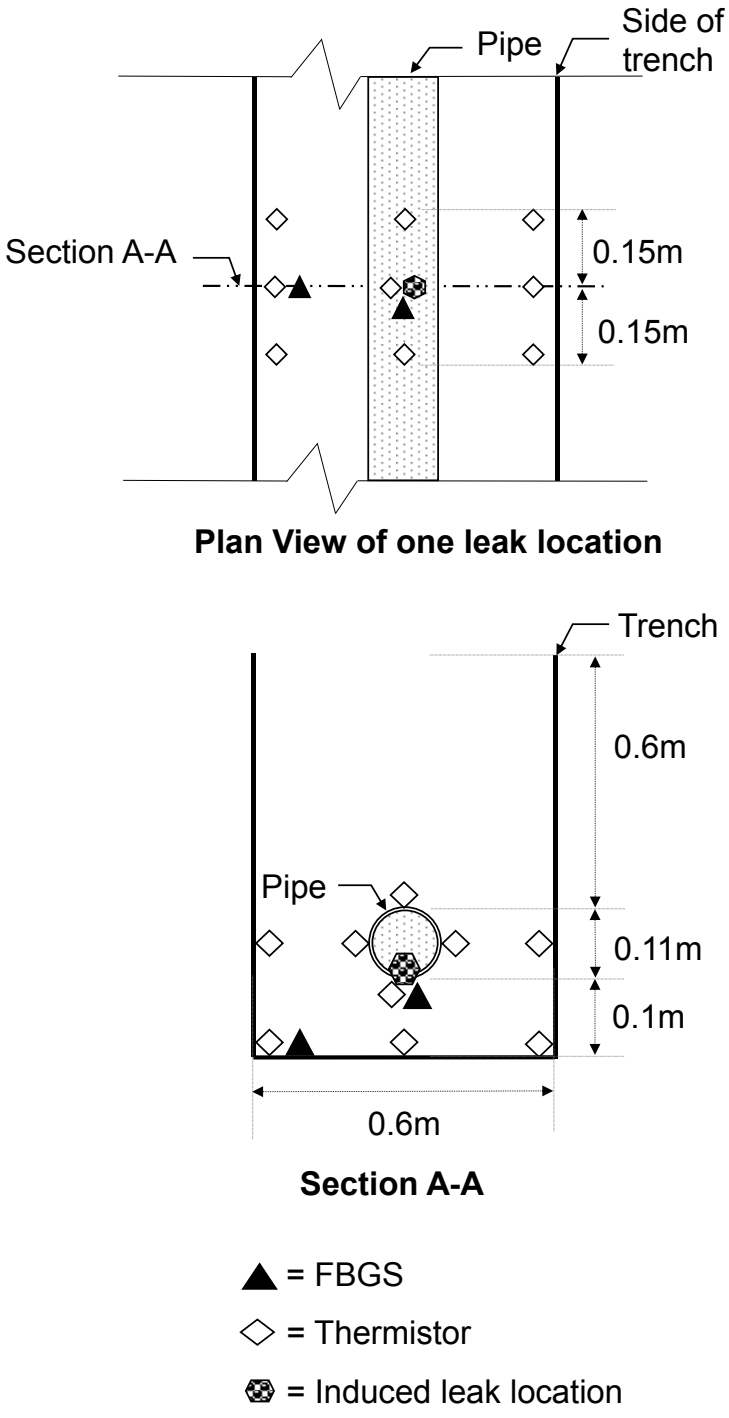

(c) Cross section view of field installation.

Figure 3-11: Layout of experimental arrangement installed on the experimental farm of the University of Pretoria

The installation process started with the trench excavation measuring 15m x 0.6m x 0.8m deep, see Figure 3-12 below. Before commencing trenching, test pits were excavated to ensure that no existing services will be damaged during the installation.

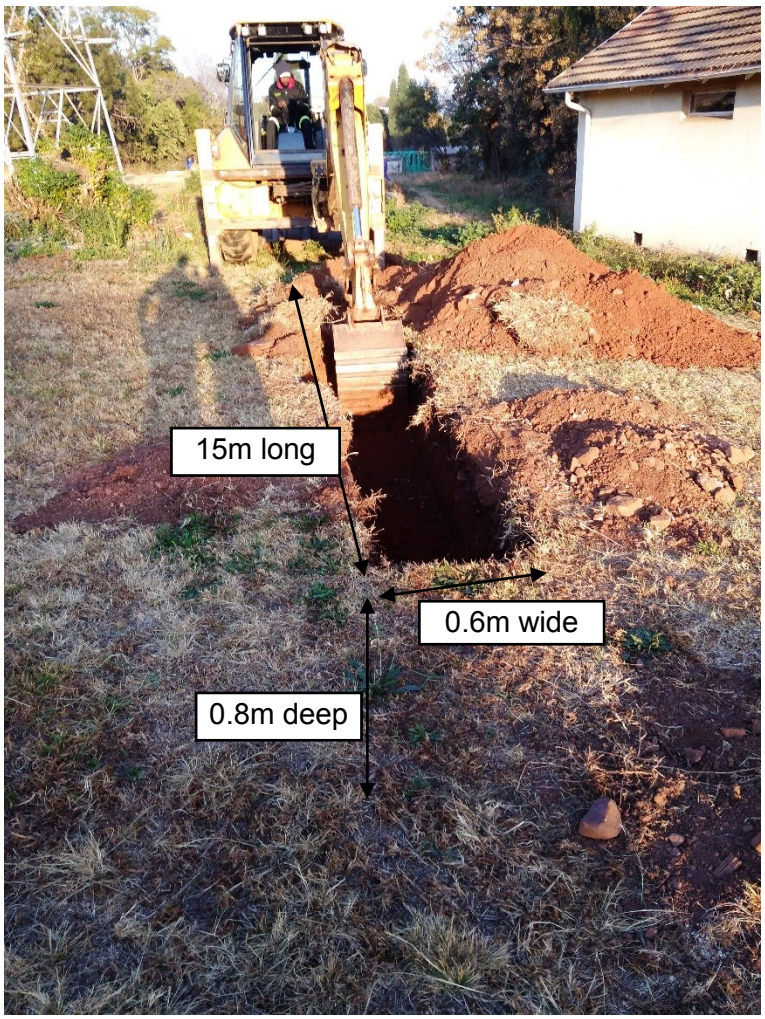

Figure 3-12: Excavation of trench

Following trenching, the sensors were laid out according to their planned installation location to the side of the trench. The base of the trench was levelled with reference to the undisturbed ground and the design invert depth of 800mm. A slope of 1:0.026 was created to aid the drainage process in the flow direction from the upstream municipal connection to the downstream drainage tanks used to hold the water circulated through the system. The slope amounts to a level drop of 400mm over the 15m long trench (see Figure 3-13).

Figure 3-13: Sensor layout and levelling bottom of trench

The thermistor strings were placed at the leak locations, as well as 150mm upstream and downstream of the leak location. The leak locations were spaced at 2m intervals, indicated in Figure 3-14. A 20mm sleeve (HDPE pipe) which is unperforated was installed in the right hand corner of the trench, looking downstream, to allow for future addition of distributed fibre optics or other sensors. In the left corner of the trench 8 FBGS were placed enclosed within a 4mm PU tube to allow for mechanically strain-isolated thermal movement. The remaining 8 FBGS were epoxied to the pipe to measure possible changes in strain due to the occurrence of the simulated leak and changes in network pressure (see Figure 3-15).

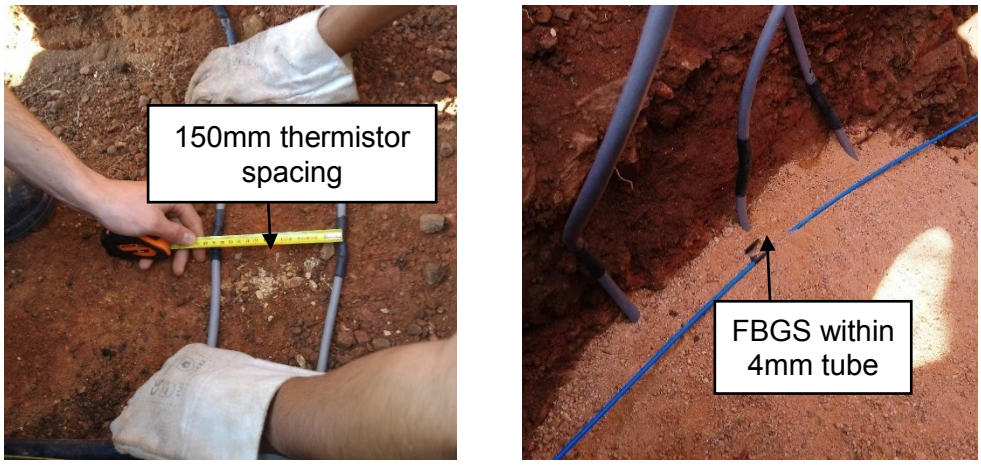

Figure 3-14: Installing sensors on the trench bottom

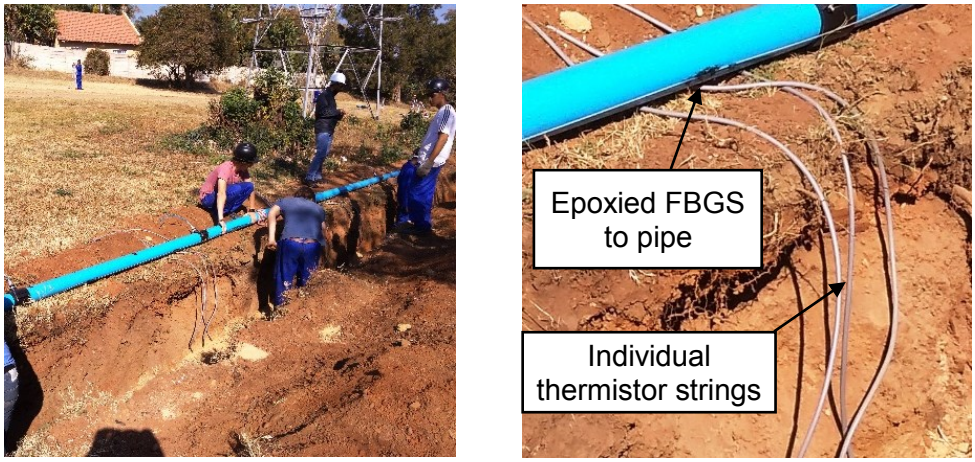

Figure 3-15: Epoxying FBGS to pipe base

After the epoxied FBGS bonded to the pipe base, the pipe was laid onto the sand cradle in the trench (see Figure 3-16). The sensor layout was realigned during pipe laying to ensure that the sensor locations were correct and that the strain and temperature sensors were aligned.

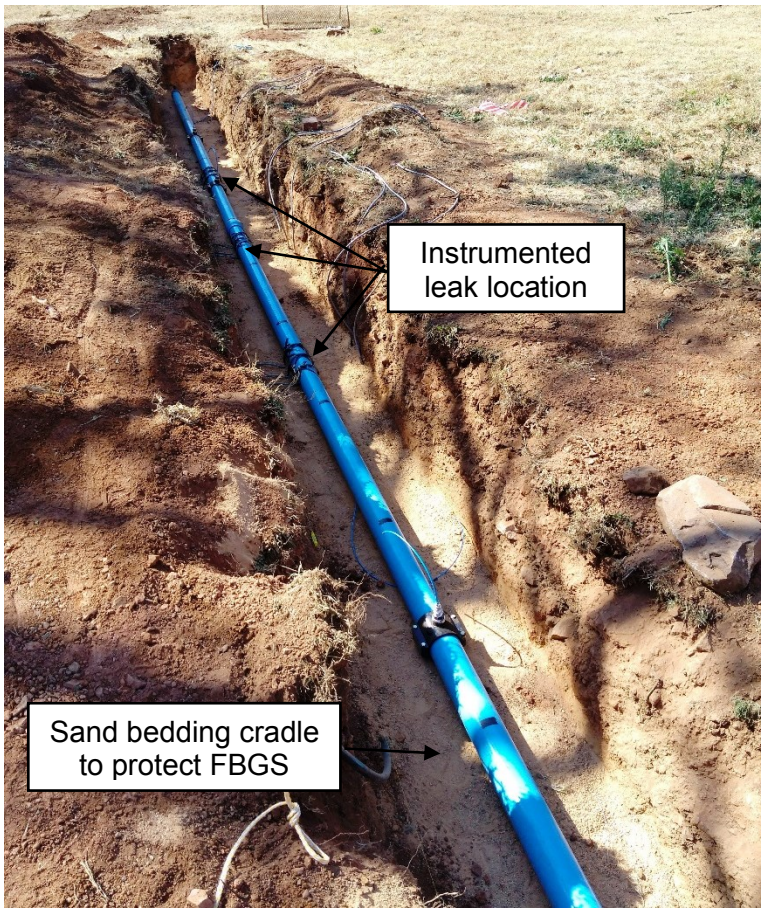

Figure 3-16: Instrumented pipe in trench

The pipe bedding consisted of a 100mm clean building sand (bedding) layer, covered by a 400mm sieved in-situ hillwash material fill blanket, compacted in 100mm layers with hand Tampers and finally un-sieved in-situ material for backfilling the remaining 200mm. A lightweight mechanical compactor ("wacker") was available on site, which was not used for the bedding blanket because it was suspected that it might damage the FBGS. The final layers of the backfill was compacted with the "wacker" and hand stampers. Each individual 100mm layer was wetted to achieve OMC prior to compaction (see Figure 3-17).

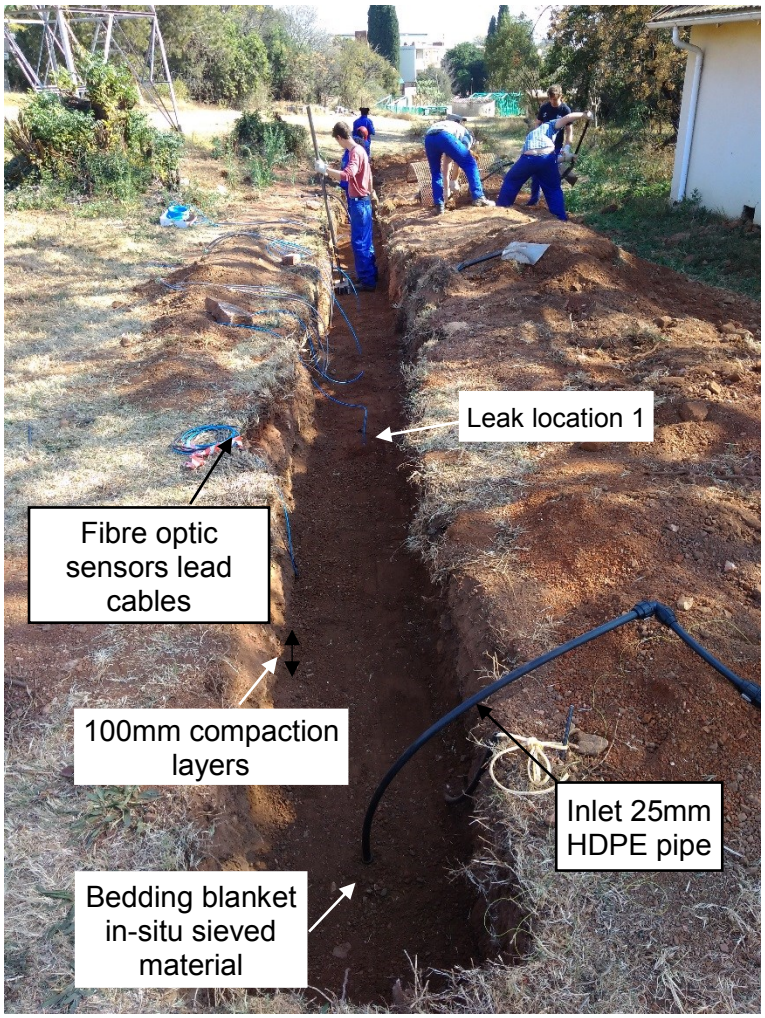

Figure 3-17: Backfilling pipe and sensors

The field installation was completed by ensuring that the trench is sufficiently compacted throughout and that there are no sharp edges or potential for erosion gullies on the surface that can form in close proximity to the trench during rain storms (see Figure 3-18). Care was taken to ensure that the pipe ends were sufficiently compacted, acting as thrust blocks. Arrangements were made so that the internal pipe pressure could be limited during testing at the upstream valve to prevent unnecessary and unintended leaks forming at connections,

joints and couplings. A downstream valve was provided that could be used to relieve the internal pipe pressure if necessary.

Figure 3-18: Finishing off installation

The pipe installation was allowed to settle and reach equilibrium for two weeks prior to testing commenced. Undergraduate civil engineering students assisted with the installation of the pipeline and sensors.

The installation was completed at the end of July 2017 and testing commenced in August. A number of different tests were carried out to determine the sensitivity of the fibre optic sensors within the PU tube and the epoxied fibre optic sensors.

3.4.3 Tests conducted

The tests conducted with the experimental setup were planned to primarily indicate the effectiveness of temperature changes around a pipe as leak indicator. Strain changes at the pipe base were investigated with secondary interest. A number of sub-questions had to be answered related to in-situ natural temperature cycles and soil-water interaction.
The following phenomena and questions were investigated:

- The daily temperature fluctuation at the installation site in both the soil and water.
- Can the daily temperature fluctuation be distinguished from that caused by a water leak?
- What is the effect of normal operational pressure changes in the water network on longitudinal strain development in a pipe?
- What are the effects of changes in support conditions to the pipe due to wetting for short and long term testing?

The tests conducted were categorised in short and long-term leaks. Short-term tests were conducted over a period of less than 2 hours compared to the latter being greater than 6 hours. The tests were limited in time duration as the storage capacity of the downstream water tanks was only 2 kilolitre and the leak initiation and propagation was of interest. This setup was envisaged as a starting point to investigate the effectiveness of both temperature and total strain changes as leakage detection parameters.

4. DATA ANALYSIS AND RESULTS

The data analysis chapter is grouped in five individual sections, discussing ground depth and water temperature in the first two sections. This is followed by a comparison of the water and ground temperature. The laboratory test phase is discussed next. The last section rounding off the analysis and results chapter contains the field phase.

4.1 Observed natural temperature changes in the ground

The monitoring of ground temperatures over the top 3m of the soil profile entered its twelfth month in December 2017. Figure 4-1 presents box & whisker plots of temperature variation with depth recorded every hour over a 12 month period for the year of 2017. Minimum, maximum and average temperatures are presented, as well as the 25th and 75th percentile values. The measurement array was commissioned towards the end of January which is the reason for the narrow temperature variation shown for that month.

It is evident that temperature variation rapidly reduces with depth. It is interesting to note that at a depth of 0.5m, the monthly temperature variation is of the order of 4°C, but that the maximum temperature variation appear to occur during the autumnal months of April and May, during which temperatures reduce from the higher summer values. The smallest temperature variation was measuring during August at the end of winter, with a noticeable increase in temperature variation occurring in September as the ground began to warm as spring arrived.

Below 0.75m, the depth below which water distribution pipelines would normally be buried, the hourly temperature variation compared over a month is generally less than 2°C. The fact that the temperature variation with depth is small is encouraging as it implies that temperature variations caused by water leaks should be readily discernible should such leak-induced temperature variation exceed 2°C.

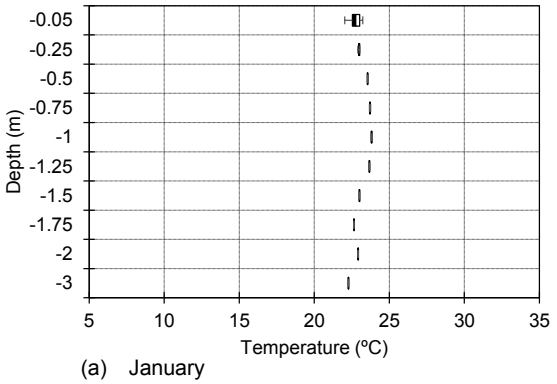

(a) January

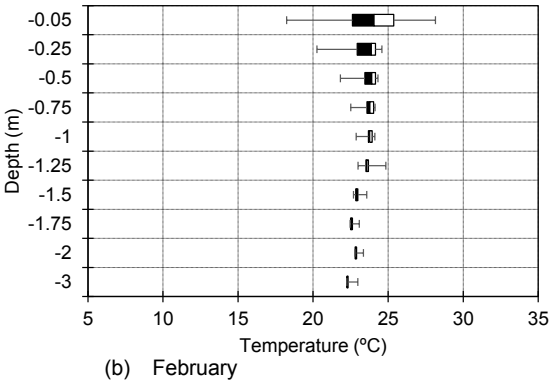

(b) February

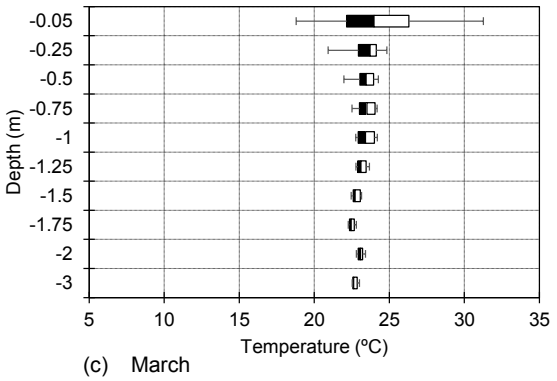

(c) March

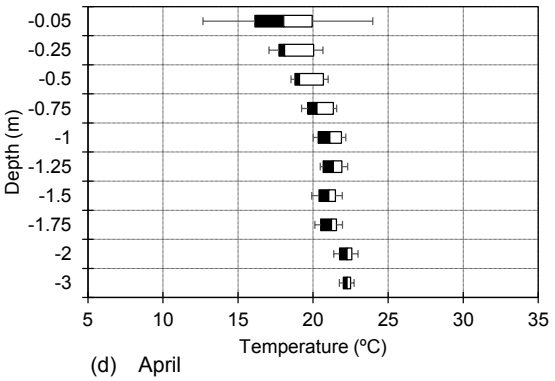

(d) April

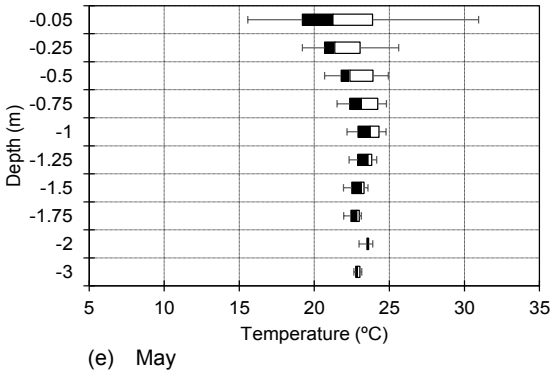

(e) May

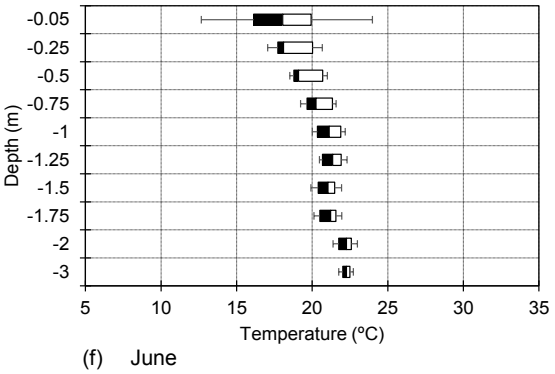

(f) June

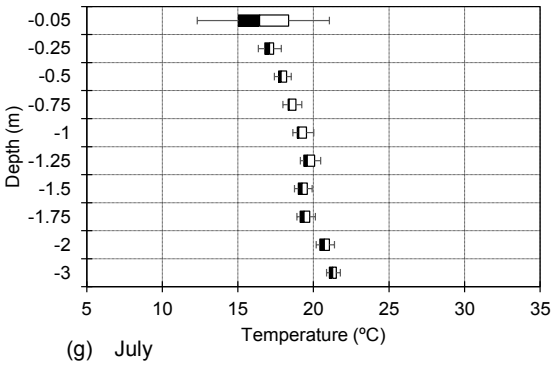

(g) July

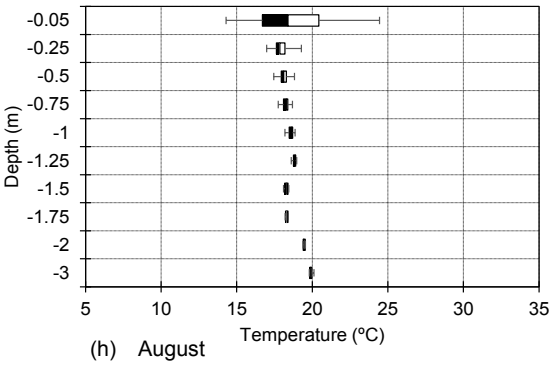

(h) August

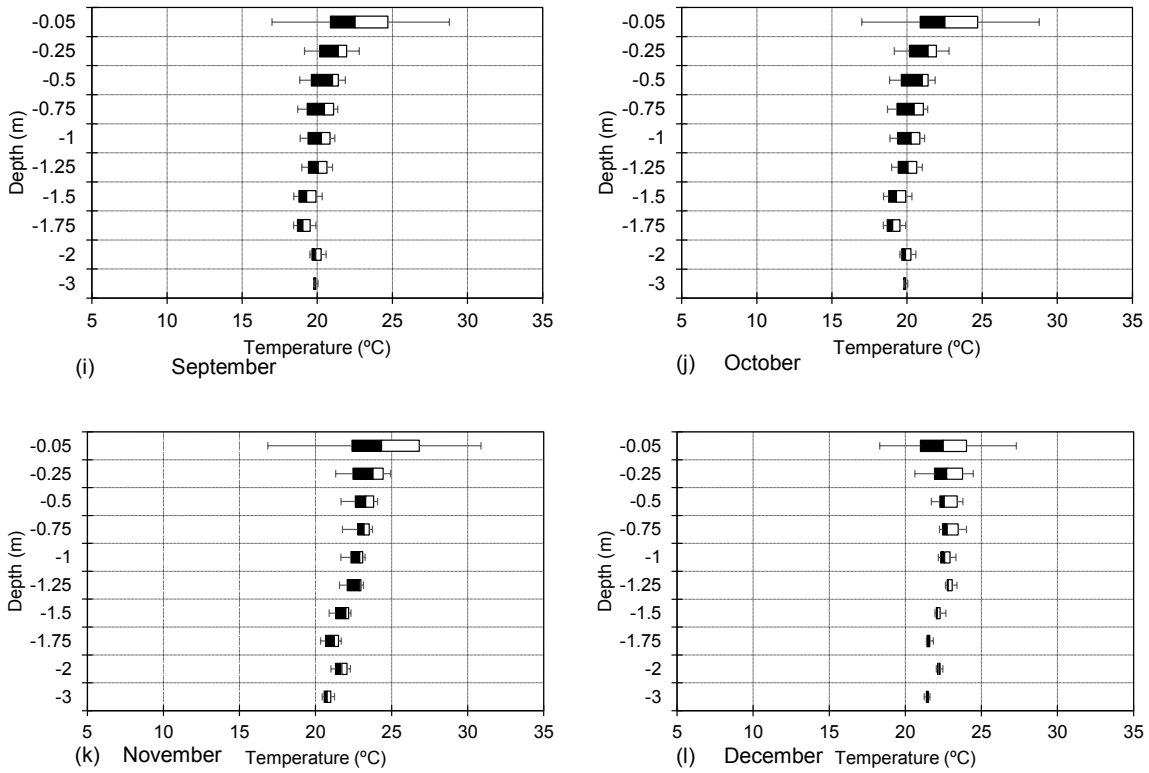

Figure 4-1: Box and Whisker ground temperature plots for 2017

Figure 4-2 below indicates ground temperature plotted on the primary vertical axis and daily rainfall data on the secondary vertical distance against time in months. A strong correlation between depth and seasonal temperature variation can be seen as well as major rainfall events influencing the top soil layers up to 1 meter depth. The lag in ground temperature response to seasonal temperature variation increases with depth with a minimum ground temperature at 0.25m occurring in July, while the minimum ground temperature at 3m depth was only reached in the beginning of September.

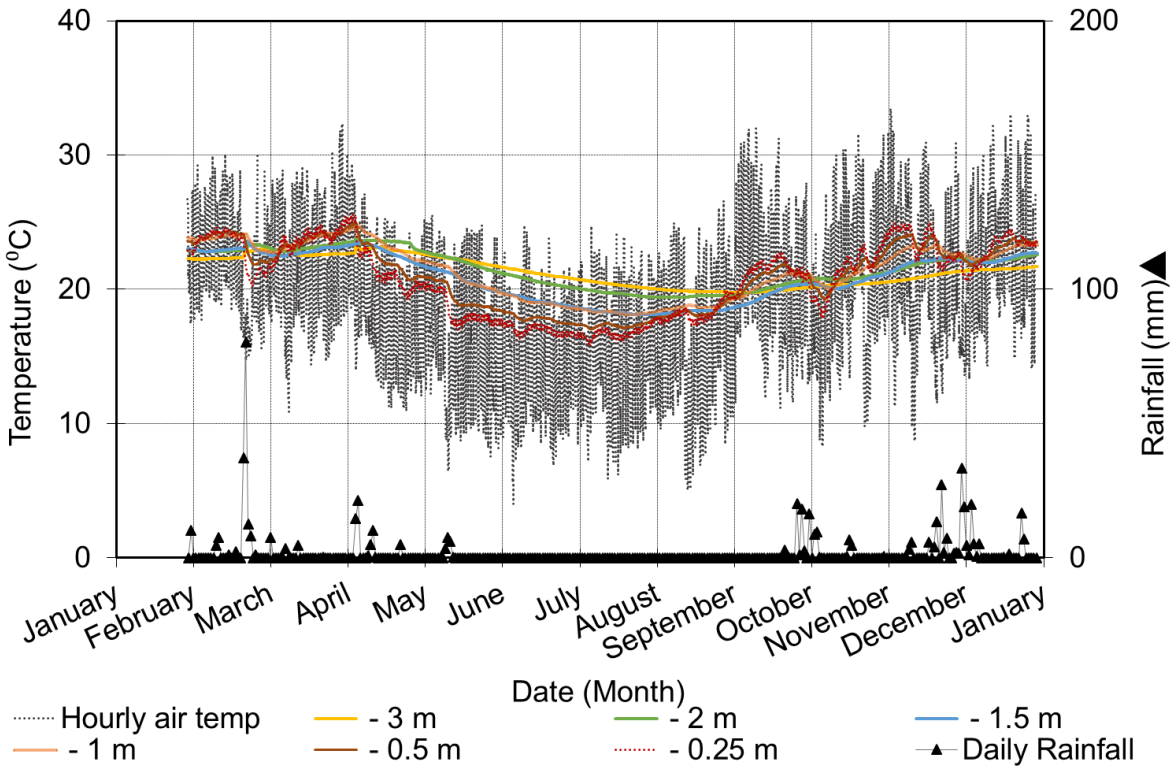

Figure 4-2: Soil temperature with depth and rainfall variation over the course of 2017.

The temperature variation with depth is shown in Figure 4-3 below for the months of February, May and July. These months represent a typical summer, transitional and winter seasonal period. It can be seen that during summer and winter months the temperature fluctuations taper off rapidly with depth as compared to the seasonal transition period, May.

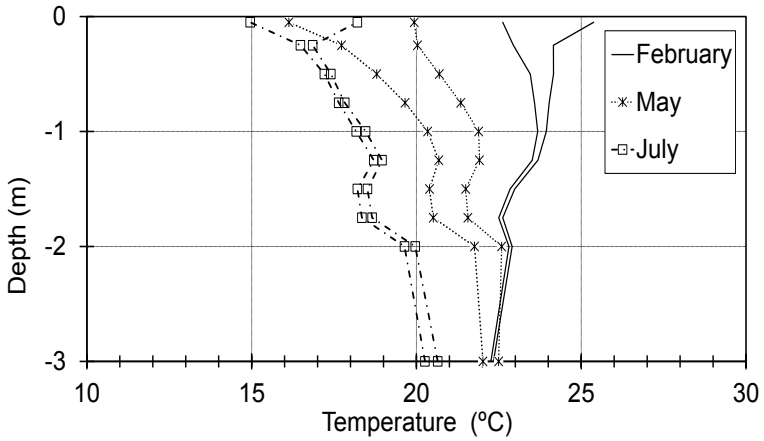

Figure 4-3: First and third quartile temperature variation with depth for summer and winter months

4.2 Temperature variation in water mains

A resistance temperature device (RTD) was installed upstream of a reservoir in Pretoria to determine water temperature within distribution mains. The data obtained from the experiment is summarised in this section. Figure 4-4 presents air and water temperatures recorded at the Pierre van Ryneveld reservoir in Tshwane during the course of May to October 2017. A clear daily fluctuation in water temperature is evident. However, it can be seen that the fluctuation in the water temperature is considerably smaller than the fluctuation in air temperature, being approximately only 2 to 3°C compared to air temperature variation of typically 15°C over the course of the monitoring period. It is interesting to note that the water temperature seemed to fluctuate around a relatively constant mean of approximately 15° with comparatively little variation. This represents a relatively large temperature differential of 3 to 5°C compared to the May and June soil temperature at depth presented in Figure 4-3 which is encouraging in terms of the potential performance of the monitoring system under investigation in this study.

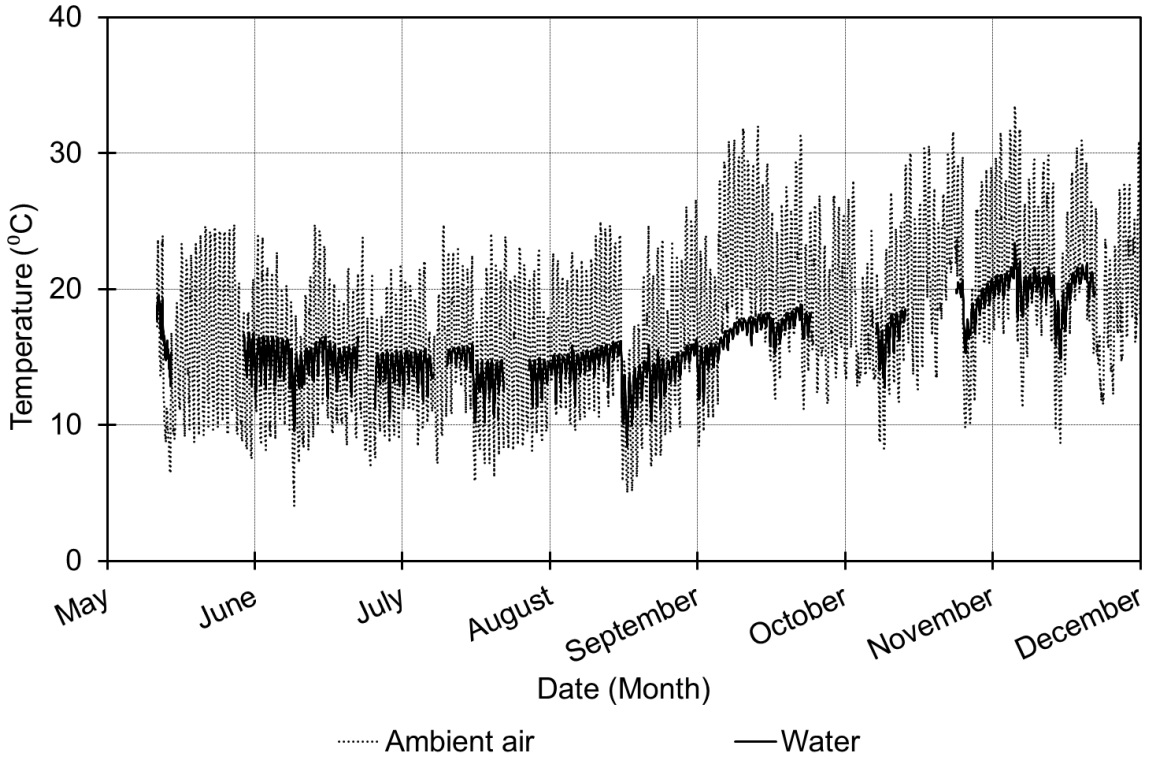

Figure 4-4: Air and water temperatures recorded at Pierre van Ryneveld reservoir (Tshwane) May to December 2017

4.3 Comparing water and soil temperature

The water mains and ground temperature variation is compared to indicate if the proposed detection system can function. Figure 4-5 below indicates the water mains temperature and the natural ground temperature variation with depth for the month of July. It is shown that the water temperature is different to the soil temperature at a typical depth at which water mains are normally installed. The water and ground temperature values are compared in Figure 4-6 over a period of seven months from May until December.

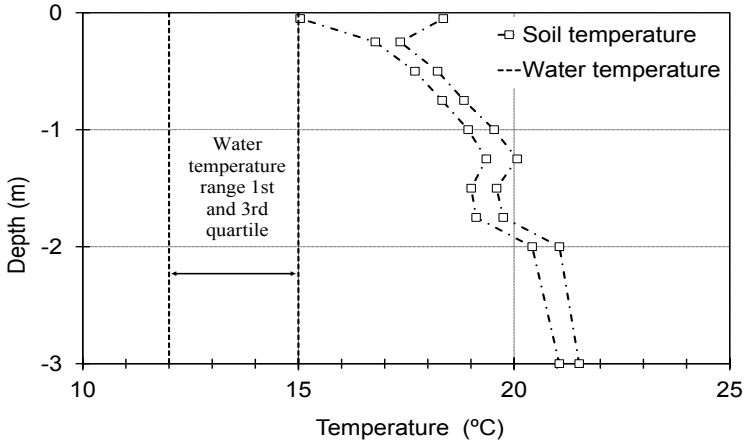

Figure 4-5: First and third quartile soil and water temperature variation July 2017

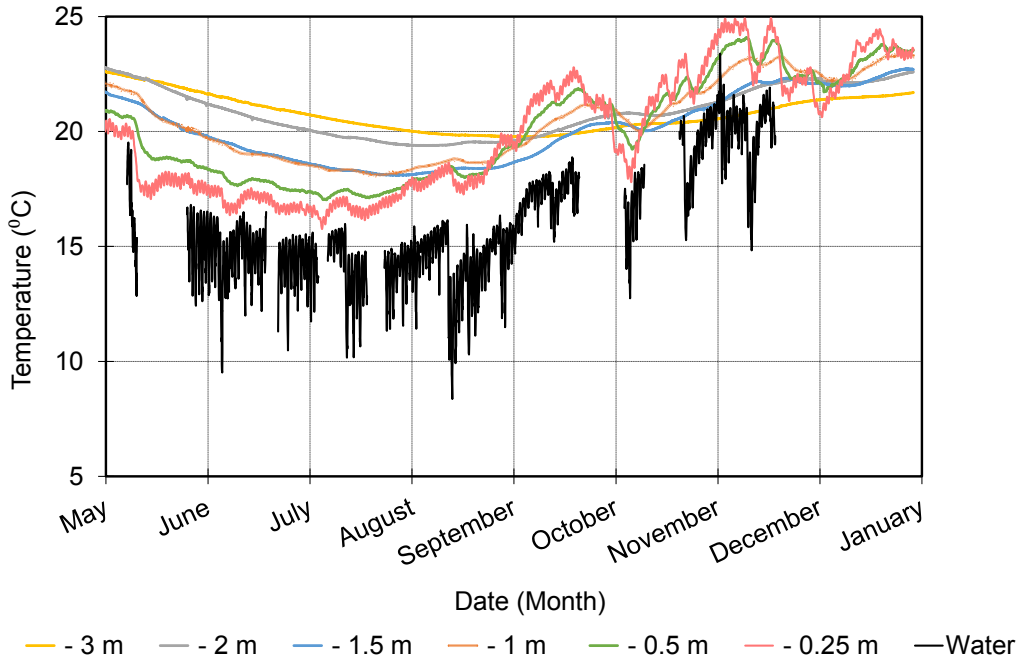

Figure 4-6: Ground and water temperature comparison

4.4 Temperature changes caused by water leaks (laboratory phase)

Laboratory experiments were conducted to determine the effect of a water leak on soil temperature and the suitability of using thermistors to detect a possible temperature change. A transparent container filled with quartz sand was used to conduct the test, with a nearby municipal connection used as water source. The advance of the wetting front observed during the experiment is illustrated in Figure 4-7, with the increase in wetting plume circled in a red dash dotted circle. Figure 4-8 presents temperature variation recorded during the first laboratory phase experiment. The leakage rate was 140ml/min and the water temperature measured at 24°C. The second laboratory leak test is shown in Figure 4-9, with a lower flow rate of 90ml/min and the water temperature measured at 21°C. It is evident from the temperature records that temperatures in the soil reduced markedly in response to the wetting front moving through the soil, which is promising in terms of the performance of the proposed leakage detection system. Thermistors were found to be efficient as measurement device in the field phase of the experiment.

Examining the temperature data more closely reveals an interesting phenomenon. As expected, the passing wetting front seems to result in a temperature reduction after passing a specific measurement location. However, it is evident from all temperature records that a small temperature increase (0.2°C – 0.5°C) was observed before the temperature reduction followed. This was an unexpected observation, but was consistently observed in all tests.

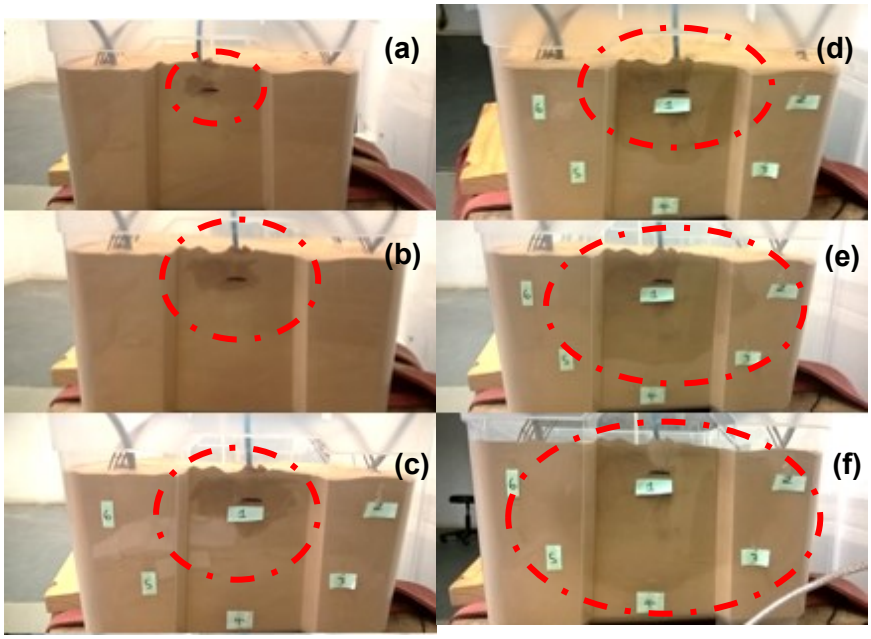

Figure 4-7: Advancing wetting front in laboratory test

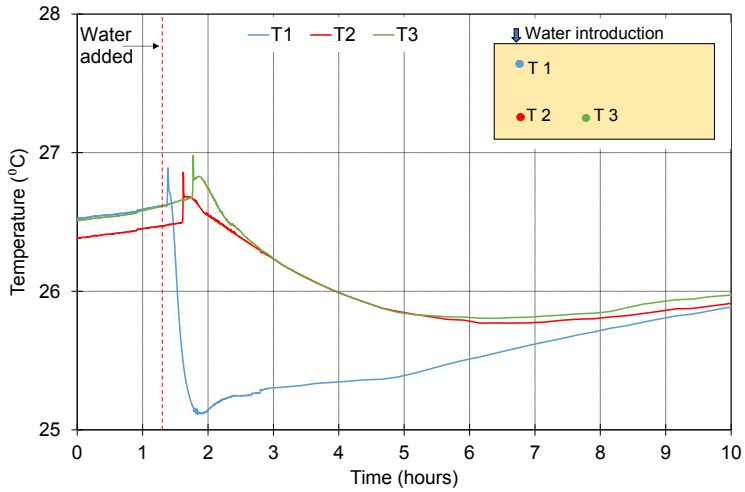

Figure 4-8: Temperature record from the first laboratory wetting test

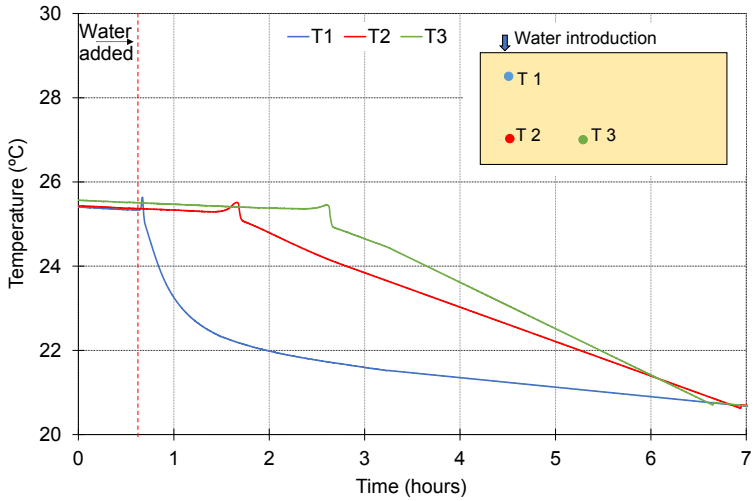

Figure 4-9: Temperature record from the second laboratory wetting test

The phenomenon was further investigated by carrying out wetting tests in another material, a red-brown silty slightly clayey silty sand collected from the University of Pretoria's experimental farm. Figure 4-10 presents an illustration of the simple experimental setup. The tests on the original material was repeated as control. The temperatures recorded during wetting of the soils are presented in Figure 4-11. It can be seen that the same phenomenon was observed, but that the temperature increase in the case of the red-brown sand was smaller.

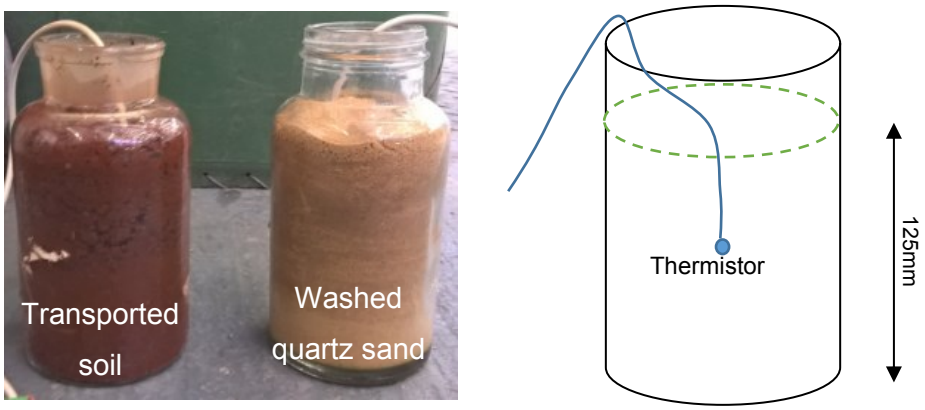

Figure 4-10: Wetting tests to investigate initial rise in temperature during passage of wetting front

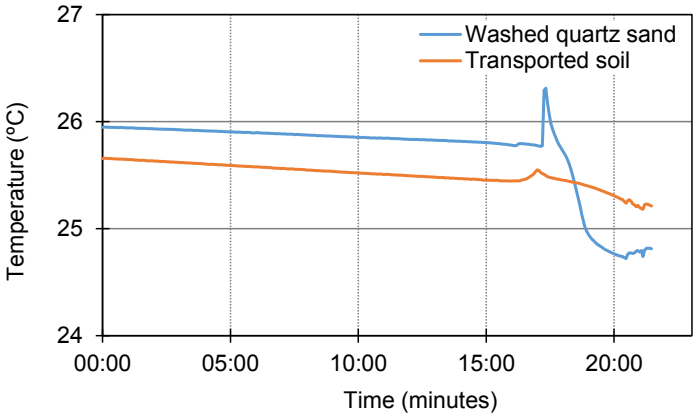

Figure 4-11: Temperature record from wetting test

A literature search revealed that the phenomenon can be attributed to the release of surface energy from the surfaces of the soil grains upon wetting with water (Sophocleous, 2010). The process of wetting of a solid surface with a liquid involves interaction between three interface types, i.e. solid-liquid, solid-air and liquid-air. Wetting results in an area of solid-air interface to be replaced by a solid-liquid interface. Each solid surface has its own specific surface energy which is associated with the way in which atoms are bonded into that solid (e.g. co-valent, ionic or hydrogen bonding) (Parks, 1984). A certain amount of energy, referred to as surface energy, needs to be added to a surface to allow atoms to be removed from the lattice structure. Wetting can result in a net increase or a net decrease in total surface energy. When energy is released upon wetting, wetting occurs spontaneously. Should energy be required to be added for wetting to occur, the surface will not wet naturally and will be hydrophobic (Wenzel, 1936). Wetting of quartz by water results in a reduction in the specific surface energy of quartz by about 72 mJ/m^2, thereby resulting in an energy conversion noted as temperature increase (Parks, 1984). Due to the fine grained particulate nature of soils, the surface area of a small volume of material quickly becomes large as grain size is reduced. Wetting a fine grained soil,

which is known to occur spontaneously, is therefore associated with a measurable release of surface energy. It is hypothesised that this release of some of the surface energy of the soil described above is responsible for the small rise in temperature associated with the passage of the wetting front. After passage of the wetting front the thermal mass of the colder liquid released by the leak results in a drop in temperature which, if measured, allows a leak to be detected which illustrates the potential for success of a leakage detection system based on temperature measurement installed in close proximity along a pipeline.

4.5 Temperature and strain variation caused by water leaks (field phase)

4.5.1 Introduction to field phase

A Class 9 110mm diameter 12m long uPVC pipe with 3 separate leak locations spaced 2m apart was used to test the effect of a water leak on in-situ soil temperature and possible strain development. Temperature changes and pipeline strains changes due to a possible softening of the support conditions are predicted to occur close to the leak location.

Each leak locations had 27 thermistors placed around it with a total of 8 FBGS attached longitudinally to the pipe and 8 FBGS loose within 4mm polyurethane pipe spaced 1m apart along most of the length of the 12m pipeline as illustrated in Figure 3-11. A Datataker DT85 logger was used to monitor 27 thermistors simultaneously, which represents all the thermistors at a given leak location. A Datataker DT615 logger was used to continuously monitor one thermistor string at a reference location over the entire study period to record soil temperatures with depth.

The pipeline was allowed a settling-in period of two weeks after installation before commencing initial daily FBGS readings. These readings were taken with a HBM FS22DI BraggMETER, logging all FBGS at 10Hz for a 15 minute period each day. This phase was proceeded by permanently installing the logger in a building in close proximity to the experiment to continuously monitor the FBGS at 1Hz.

Continuously monitoring the FBGS proved more effective than the short duration daily observations, as it indicated the daily temperature and strain variation over time which is necessary for a thorough interpretation of the data.

The internal pipe pressure was monitored at one minute intervals with an Onset Hoboware U12 logger and a 7 bar pressure transducer during the leak tests. See Appendix D for the calibration curve of the pressure transducer. The logging frequency of the thermistors during a leak test was 1 reading every 5 seconds or 0.2Hz. The logging frequency during dormant periods, where no leaks were induced, was set to 15 minutes to provide information on the magnitude of the daily temperature fluctuations. The temperature of the water exiting the pipe into a downstream storage tank was logged during the leak tests, as well as the temperature of the water in the pipeline during dormant periods. A thermistor was added during the final testing phase to measure the water temperature inside the pipe when the system is pressurised and the downstream valve closed. A thermistor recording ambient air temperature was also added as a nearby weather station stopped taking data.

During daily temperature fluctuation observations, the pipeline was isolated from the water distribution network before and after a leak was initiated, due to limited water storage capacity downstream of the experiment. The flow rate at the leak location was measured with a measuring beaker and stopwatch and the flow rate of the water entering the pipeline was determined with a gear type Class C flow meter.

Brief summary of the typical measuring regime during leak tests is presented below:

1.) The testing sequence was initiated by setting up the Onset Hoboware U12 logger with a pressure transducer with a 1 minute logging interval, initially the pressure transducer was left at atmospheric pressure to allow for base or “zero” reading to be determined for 10 minutes.
2.) The “dormant” data was then downloaded from the DT615 and DT85 loggers which measured resistance (temperature) of the thermistors at 1 hour intervals for the DT615 recording in situ soil temperature and 15 minutes for the DT85 recording thermistors at the leak locations.
3.) The logging frequency during the leak test was then set to a 5 second interval for the DT85 at the leak location (DT615 remained at a 1 hour logging frequency).
4.) DT85 logger was allowed to obtain base resistance readings for a few minutes before opening the main upstream, downstream valves to the experiment and initiating the leak.
5.) It was ensured that all the loggers and channels read ‘acceptable’ values, which were 4kΩ to 7kΩ for the thermistors, 4mA for the pressure transducer (at atmospheric pressure) and that the fibre Bragg readings were within a range from 1509nm to 1570nm.
6.) The leak was initiated by opening the main upstream valve, setting the flow rate at the leak location by disconnecting, leak tube at the surface and measuring the amount of

water with measuring beaker per time period with a stopwatch and using a gear type flow meter to determine flow volume into the pipeline at the test start.

7.) Depending on the required internal pipe pressure the downstream valve was closed to increase the internal pressure up to the network pressure.

8.) During the leak test a remote connection to the HBM BraggMETER was established to ensure that the logger is functioning “normally” and if an error did occur, the logger could be restarted remotely or other troubleshooting action taken.

9.) After the leak test was completed, the leak was stopped by closing the valve upstream of the pipeline and at the leak location.

10.) The water volume was read from gear-type flow meter to determine the amount of water that passed through the pipe during a test.

11.) Data was retrieved from all the loggers before resetting the logging intervals to their dormant rate of 15 minutes for the DT85 logger and 1 hour for the DT615.

12.) Temperature and Bragg data was continuously observed for a few days after the leak was terminated.

The above mentioned methodology was repeated at all three leak locations.

4.5.2 Leak tests conducted

The first test conducted was a short duration leak test for less than an hour to determine whether all the instruments were functioning as intended. After the initial fibre optic Bragg sensor problems were resolved and all the sensors gave reasonable outputs, longer duration tests were conducted at the various leak locations. For the tests the water within the pipeline was stagnant up to the initiation of the leak event. The leak was maintained for a few hours. Between the leak occurrences 3 days were given for the pipeline to return to its normal daily temperature fluctuation. During this period all the fibre optic sensors were logged.

The intention with the fibre optic sensors in the trench corner, isolated from mechanical strains within the 4mm tube was to only measure thermal strain changes, while effects of softening of the ground around the pipe would be measured by the FBGS attached to pipe. The latter was expected to be sensitive to both mechanical and thermal strains.

The thermistor string (TS) elevation layout for the various leak locations (LL) is shown in Figure 4-12 below. A cross section at one leak location is shown in Figure 4-13, which was the same for all the leak locations and thermistor stings 1 to 9.

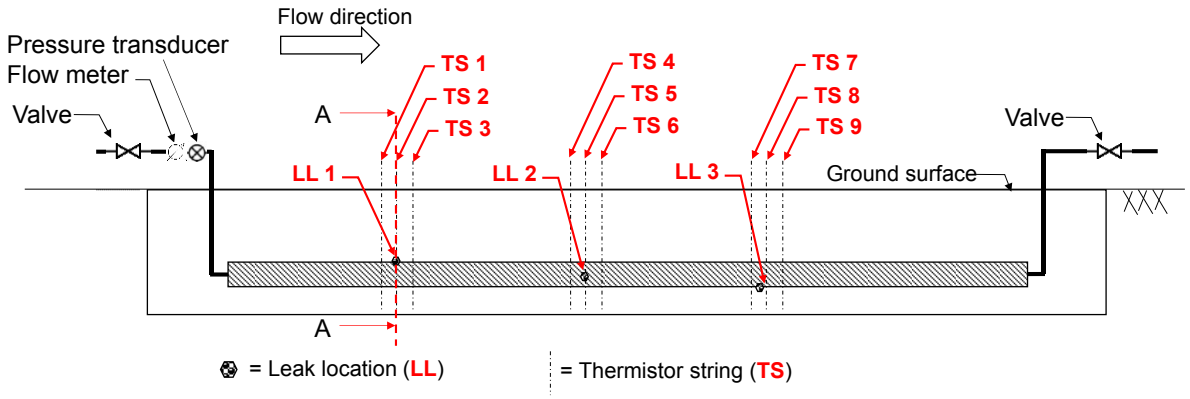

Figure 4-12: Thermistor string layout

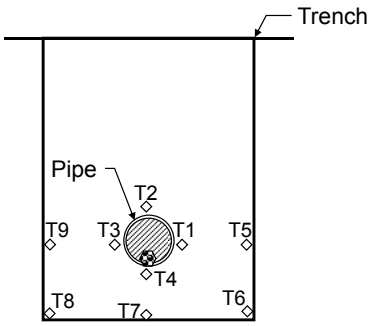

Figure 4-13: Thermistor layout per TS for section A-A

An elevation layout schematic of the FBGS layout is shown in Figure 4-14 and a cross section through the leak location is shown in Figure 4-15. The FBGS leak test data were obtained from the same tests producing the thermistor data.

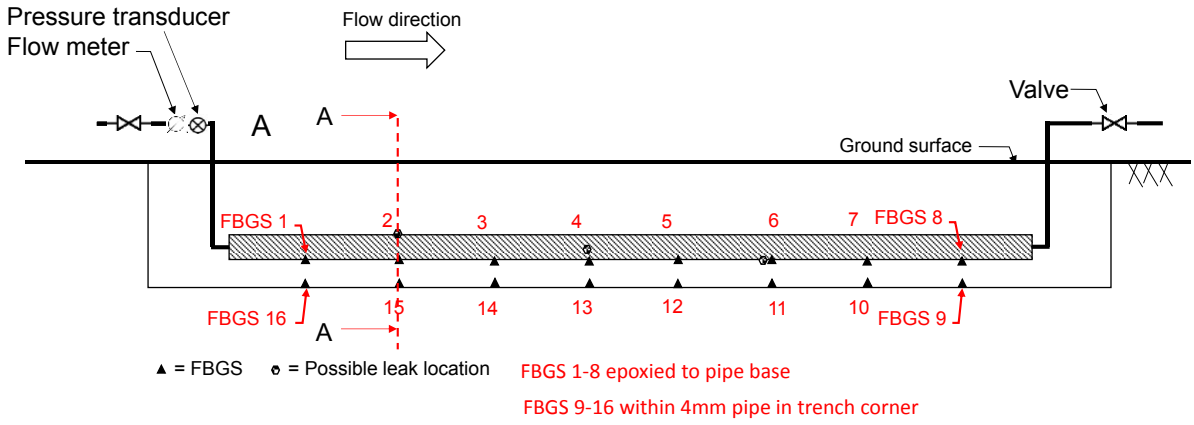

Figure 4-14: Elevation of experimental setup

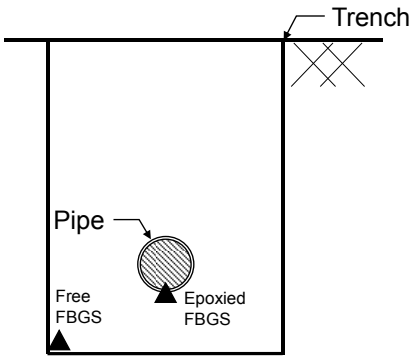

Figure 4-15: Cross section through the leak location showing the FBGS layout at section A-A

Each leak experiment is discussed separately with thermistor data or temperature data discussed first is followed by fibre Bragg grating data. Table 4-1 below indicates the tests conducted.

Table 4-1: Tests conducted

Test Nr.	Description
1	Medium duration (>5 hours and <1 days) at leak location 3
2	Medium duration at leak location 2
3	Medium duration at leak location 1
4	Long duration (>2 days) at leak location 2
5	Pressure vs. strain test with (data evaluation phase)

4.5.3 Temperature and strain calculation

4.5.3.1 Thermistor temperature calculations

Water and soil temperatures were obtained by logging the thermistor resistance values. The resistance values can be converted to temperature by a calibration formula and coefficients given by the manufacturer. The cable length were kept sufficiently short not to effect resistance-temperature relationship. The resistance of the cable was measured using a multimeter and it was determined that the value falls within the noise range of the logger and would therefore not have had to be accounted for during the calculation temperature values.

4.5.3.2 Fibre Bragg grating strain calculations

The strain calculation using fibre Bragg gratings (FBG) is more complex compared to, for example, thermistor data due to a certain baseline wavelength (lambda 0, l_0) corresponding to a specific total (ε_{total}) strain amount, being a combination of both thermal ($\varepsilon_{thermal}$) and mechanical strain ($\varepsilon_{mechanical}$). The thermal strain can be compensated by measuring the temperature changes in close proximity to the FBG, ideally with an uncoupled mechanical strain FBG, which can be used to subtract the thermal strain to obtain mechanical strain only. For this experiment, thermistors were used to measure temperature changes and to compensate the epoxied (bonded) FBG readings for thermal strain at the leak locations to only obtain mechanical strain. A thermistor varies in dimension and material composition to an FBGS thereby creating a difference in thermal behaviour.

Equation 4-1 below represents the relationship between the change in wavelength and the total change in strain and change in refractive index due to temperature changes. The first term (k x ε) of Equation 4-1 (Kreuzer, 2013) indicates gauge factor multiplied by the total strain present in the system. The second term of the equation relates to the change in refractive index caused by a change in temperature. The change in refractive index (α_δ) is small compared to the effect of the gauge factor.

$$\frac{\Delta l}{l_o} = k \times \varepsilon + \alpha_\delta \times \Delta T \qquad \text{Equation 4-1}$$

Δl = change in wavelength (nm)

l_o = base wavelength at test start (nm)

k = gauge factor (0.78)

ε = total strain

α_δ = change of the refractive index (5-8 10^{-6} / K)

ΔT = change in temperature (K)

The mechanical strains can only be obtained with Equation 4-2 where the thermal expansion coefficient of the specimen material (α_{sp}) to which the fibre Bragg grating is epoxied is governing. For the pipe made of uPVC being the specimen the thermal expansion coefficient was determined as 50.4e-6 per K and the change in refractive index was 5e-6 per K according to the manufacturer of the sensor (FBGS, 2017). The gauge factor is 0.78 as previously determined from literature and the manufacturer.

$$\varepsilon_m = \frac{1}{k} \times \frac{l_o}{\Delta l} - \left(\alpha_{sp} + \frac{\alpha_\delta}{k}\right) \times \Delta T \quad \text{Equation 4-2}$$

ε_m = mechanical strain

α_{sp} = thermal expansion coefficient of material

If no mechanical strain is present, the change in temperature can be determined by using Equation 4-3. In most cases it is unrealistic to assume that there are no mechanical strains present due to the sensitive nature of FBGS. Any bending, tension, compression or torsion will influence the change in wavelength of the FBGS.

$$\Delta T = \frac{\Delta l}{l_0} \times \frac{1}{k \times \alpha_{glass} + \alpha_\delta} \quad \text{Equation 4-3}$$

α_{glass} = change in refractive index of glass ($0.55 * 10^{-6}$ per Kelvin)

For the majority of FBGS where no temperature reading are present, the following formula was used to determine the total strain change which is representative of total thermal and mechanical strain, giving an indication of the total amount of strain to be expected. This approach was followed after it was seen that thermal temperature compensation techniques yielded similar results to that of non-compensated FBGS strain results. The current compensation technique has to be revised, by using mechanically uncoupled Bragg sensors to temperature compensate for total strain sensors. The focus of this study was to determine whether a leak event could be distinguished from natural temperature cycles and other phenomena, therefore observing a total strain compared to either only observing thermal or mechanical strain is not of concern.

$$\varepsilon = \left(\frac{\Delta l}{l_o}\right) / k \quad \text{Equation 4-4}$$

4.5.3.3 Pipeline strain changes due to internal pressure

The internal pressure in the pipe section, pipe dimensions and pipe material was used to determine the longitudinal strain to be expected in the pipe wall. The calculations are made to interpret the results obtained from fibre Bragg sensors. The relationship between pressure and strain is to be determined from the calculations. The pipe can be described as thin walled pressure vessel as the internal radius is 52.4mm and the wall thickness is 2.6mm giving a ratio of the internal radius over the wall thickness equal to 20.15, which is greater than the thin walled limit of 10 (Hibbeler, 2013).

The expected change in axial stress and strain due to a specific internal pipe water pressure with no confining pressure was determined with Equation 4-5 and Equation 4-6.

$$\sigma_1 = \frac{p \times r}{2 \times t} \quad \text{Equation 4-5}$$

σ_1 = longitudinal stress (5.4MPa)
p = pressure (536kPa)
r = internal radius (52.4mm)
t = wall thickness (2.6mm)

$$\varepsilon = \frac{\sigma_1}{E} \quad \text{Equation 4-6}$$

ε = longitudinal strain (1460με)
E = modulus of elasticity for uPVC (3.7GPa)

The principal circumferential stress due to an internal pressure of 536kPa was determine as 5.4MPa in the pipe wall. The modulus of elasticity obtained from literature is 3.7GPa for uPVC and the Poisson ratio is given as 0.4 (Zahoor & Kanninen, 1981). The longitudinal strain is therefore 1460με at 536kPa internal pressure. The overburden weight and soil restraints limit the amount of strain and inhibit the free movement of the pipe or thin walled pressure vessel. Other factors influencing the free expansion and contraction of the pipe are listed below:

- Friction between soil and pipe wall;
- End restraints;
- Pipe material;
- Pipe dimensions;
- Installation depth; and
- Joints and couplings along the pipe.

It is important to note that the fibre optic sensors were epoxied to the pipe base with great care to the best ability of the researcher. However, it cannot be guaranteed that all the sensors transferred the full strain experienced by the pipe. A spigot and socket (bell type or rubber ring) joins the two 6m pipe sections which does allow for some movement to occur between the two pipe lengths. The initial calculations indicated that at low pressures no thrust restraints would be needed. During testing it was found that a slight pull out between the pipe sections did occur, allowing for some free movement.

Description of the experimental results obtained for each test are presented below:

4.5.4 Leak test 1

The first leak test conducted was initiated on 13 September at 16h43 and closed on 14 September at 05h51. Therefore a total leak time of just over 13 hours was applied. The imposed average leakage rate was 0.61 l/min. The corresponding average flow rate through the pipe was 3.75l/min and the internal pipe pressure 36kPa. The outlet valve from the pipe was opened allowing water to discharge into a tank at atmospheric conditions to allow for water from the municipal network to flow through the pipe continuously.

4.5.4.1 Thermistor data leak test 1

The leak was initiated at leak location 3 (LL3) (see Figure 4-18 below). Thermistor string (TS) 8 was located at LL3 with TS9 0.15m downstream and TS7 0.15m upstream of LL3. A reference string TS1 which is located 4.15m upstream from LL3 was used to investigate a cross-section where no leak occurs.

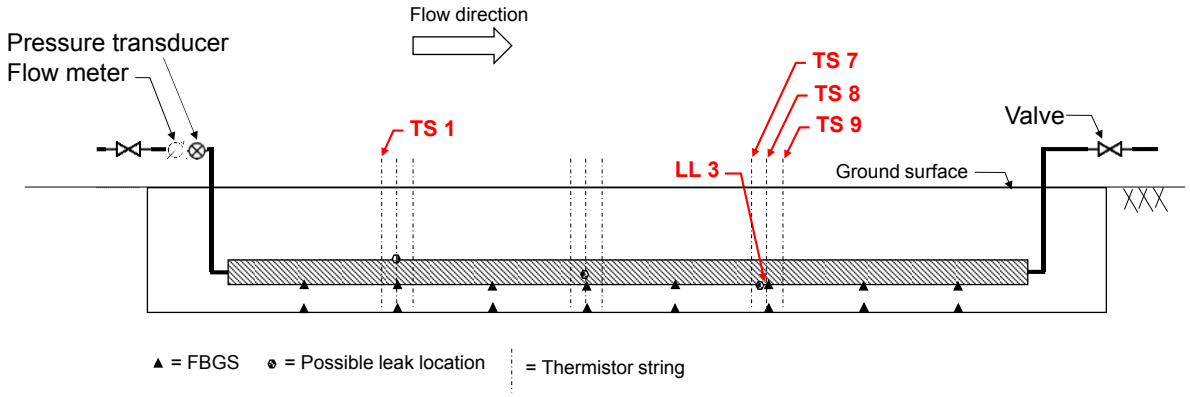

Figure 4-16: Elevation of experimental installation showing location of Leakage test 1

The thermistor data obtained is separated into data obtained in close proximity to the pipe (i.e. thermistors T1 – T4, see Figure 4-20) and in the trench perimeter (thermistors T5 – T9).

The water supply from the municipal connection was only opened when the leak was initiated. This was intentional and implies that the water in the pipe had been stagnant prior to commencement of the leak so that the temperature differential between the water in the pipe and the surrounding soil would have been minimal. The ability to detect a leak under such conditions (i.e. when the temperature of the water in the pipe was similar to the soil temperature) implies that a leak will be detected more easily under conditions when the water in the pipe had been circulating as there would have been a larger temperature differential between the water in the pipe and the surrounding soil.

The water temperature measured downstream of the pipeline in water exiting the pipeline during the test is summarised in Figure 4-17. An initial temperature spike can be observed due to warm stagnant water in the distribution network upstream of the test installation, which was flushed through the pipe after which a significant drop can be observed. The temperature spike was not intended to form part of the test sequence but provided an opportunity to examine the effect of such rapid water temperature changes on the temperatures around the pipe.

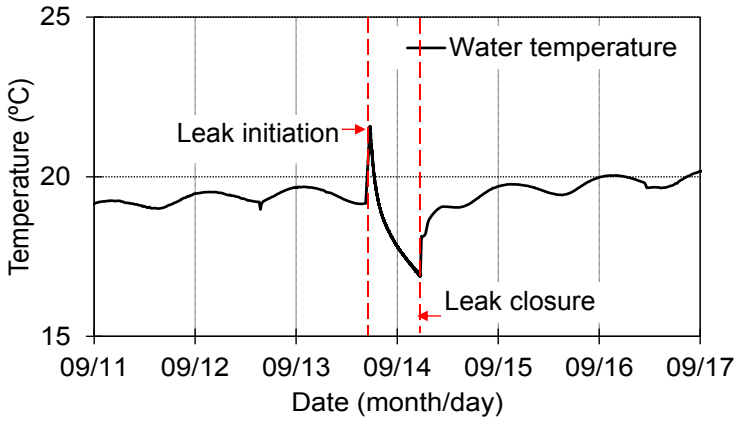

Figure 4-17: Water temperature during the first leak test measured downstream

The thermistor data for the leak test at LL3 is summarised in Figure 4-18 to Figure 4-21. The left graph in Figure 4-18, indicates temperature readings from the thermistors around the pipe (thermistors T1 to T4) and the right graph indicates readings from the thermistors in the trench perimeter (corners) (thermistors T5 to T8). Figure 4-18 applies to thermistor string TS8, installed in-line with the leak location LL3. Figure 4-19 and Figure 4-20 present similar data for thermistor strings TS7 and TS9, respectively located 0.15 upstream and downstream of the leak location. Figure 4-21 present temperatures recorded at thermistor string TS1, located away from the leak location and is included for reference purposes. The left dotted red line on each graph indicates the leak initiation and the right line indicates the leak closure. The leak location was at the crown of the pipe.

It is evident that the magnitude of the temperature change was greatest at the leak location and smaller upstream and downstream of the LL3 at TS7 (Figure 4-19) and TS9 (Figure 4-20). The reference cross-section TS1 in Figure 4-21 indicates that the thermistors around the pipe noted a change in a temperature but the thermistors in the trench corners did not. This is caused by T1-T4 being laid around the pipe in close contact to the pipe, whereas T5 –T9 are laid in the trench corner therefore they are only minutely affected by water flowing through the pipe. Voids within the soil matrix act as thermal barriers in unsaturated soil, however if leak occurs the pockets are filled with water increasing thermal conductivity.

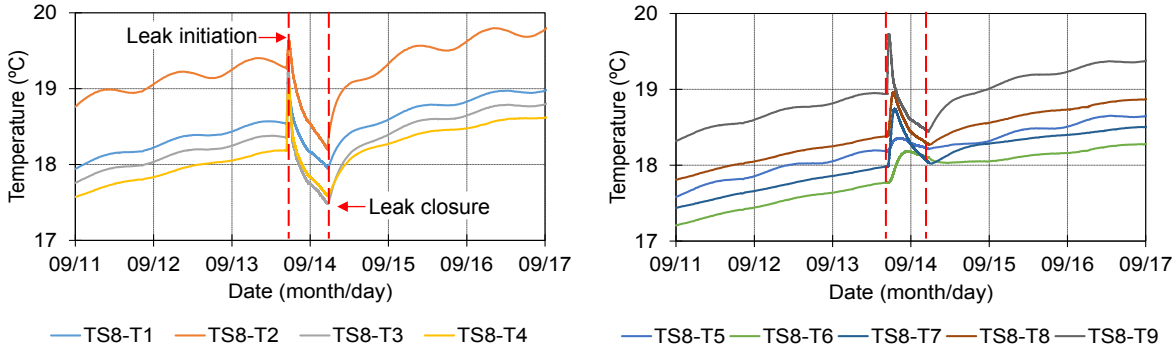

Figure 4-18: Temperature changes at leak location LL3 (TS8)

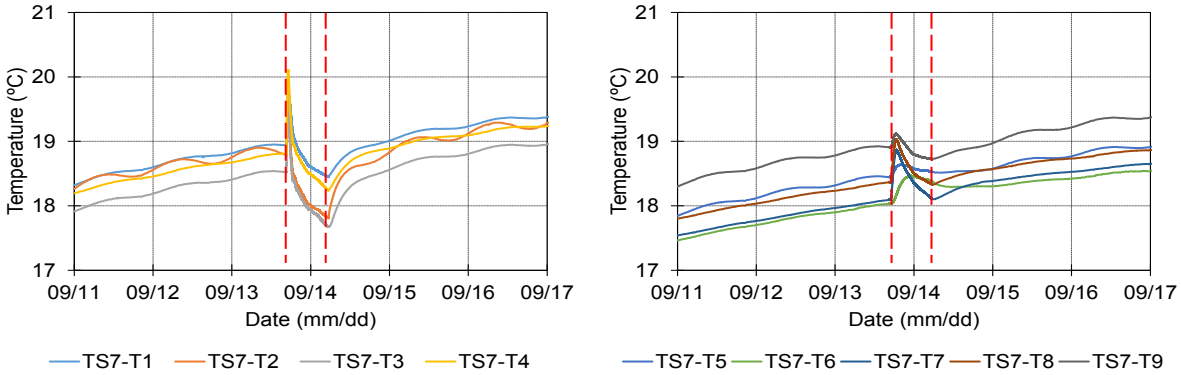

Figure 4-19: Temperature changes 0.15m upstream of leak location LL3 (TS7)

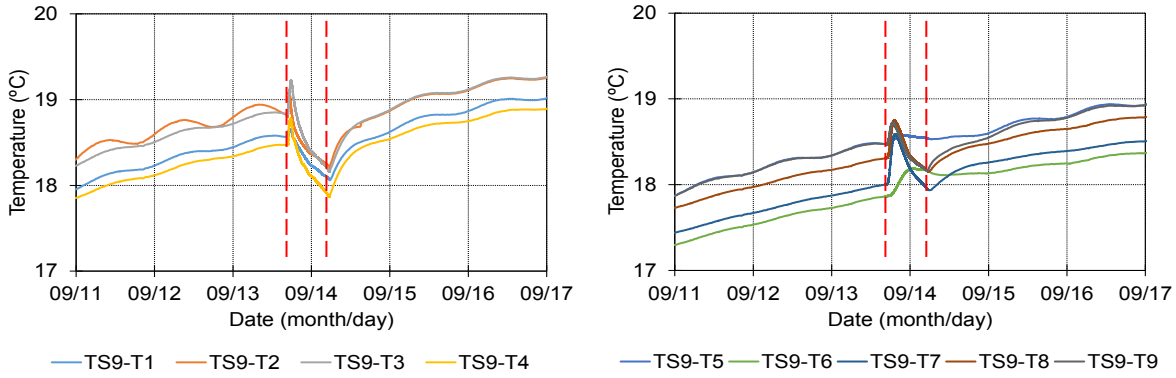

Figure 4-20: Temperature changes 0.15m downstream of leak location LL3 (TS9)

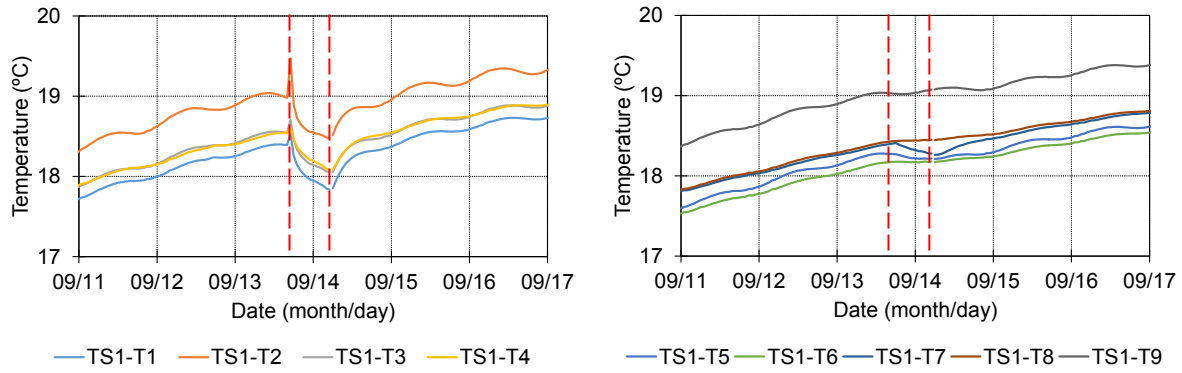

Figure 4-21: Temperature changes at reference string TS1 away from the leak location

Temperature distribution around leak location

The data was used to create a two dimensional temperature profile contour plot to visualise leak-induced temperature changes around the leak location. Figure 4-22 indicates a two dimensional (2D) contour plot for thermistor string TS7 (0.15m upstream), TS8 (at the leak location) and TS9 (0.15m downstream). It is evident from the visualisation that the temperature behaviour immediately upstream and downstream of the leak were similar and differed somewhat from the situation at the leak location. Before the leak occurred a clear horizontal temperature stratification can be seen (left column, Figure 4-25) compared to a cooling bulb forming around the leak location during the leakage test (right column). In addition to the absolute temperature plot, a differential temperature plot was created indicating the change in temperature before and during the leak event in Figure 4-23. A clear temperature stratification can be observed on the 2D contour plots before the leak was initiated.

Discussion

The success of the proposed leakage detection system depends on the ability to detect leakage-induced temperature changes around a pipeline and to distinguish such temperature changes from those resulting from changes in the water temperature circulating through the pipe. The abovementioned test provided an opportunity to compare temperature changes observed due to warmer water circulating through the pipe to compare to temperature changes when warmer water is allowed to leak from the pipe for a short period (13 hours). Comparing the temperature responses measured in direct contact with the pipe (left hand side in Figure 4-18 to Figure 4-20), responses at and away from the leak location appear similar. The

temperature changes at the leak was however somewhat larger than away from the leak. However, when comparing temperature changes along the perimeter of the pipe trench it appears that insignificant changes occurred where a leak was not present, while at the leak location, significant temperature changes were observed. This suggests that observing temperatures some distance removed from the pipe perimeter may allow leaks to be identified. It is also pointed out that leaks of any significance will not be of short term nature so that they are likely to cause long term changes in the ground temperature. Comparing temperature records over time with baseline values should therefore allow leaks to be identified with relative ease.

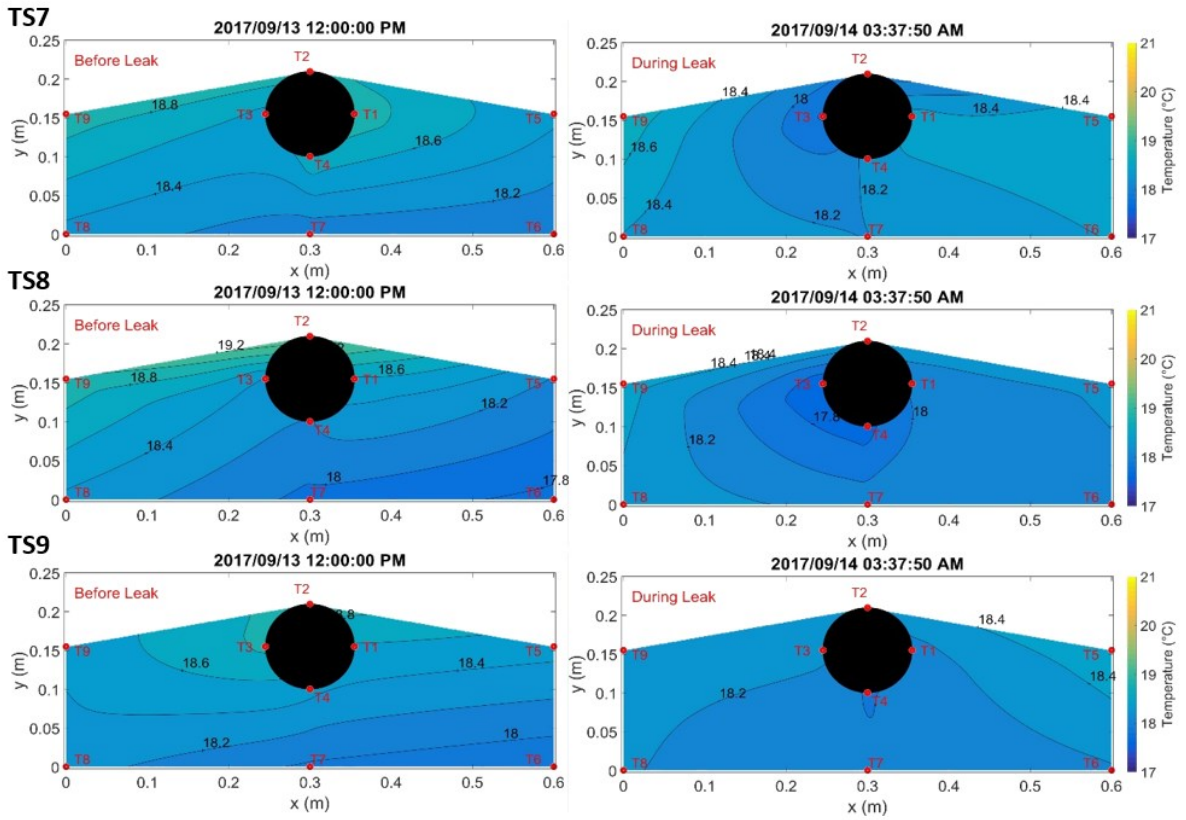

Figure 4-22: Temperature profile around LL3 before (left) and during (right) the leak for leak test 1

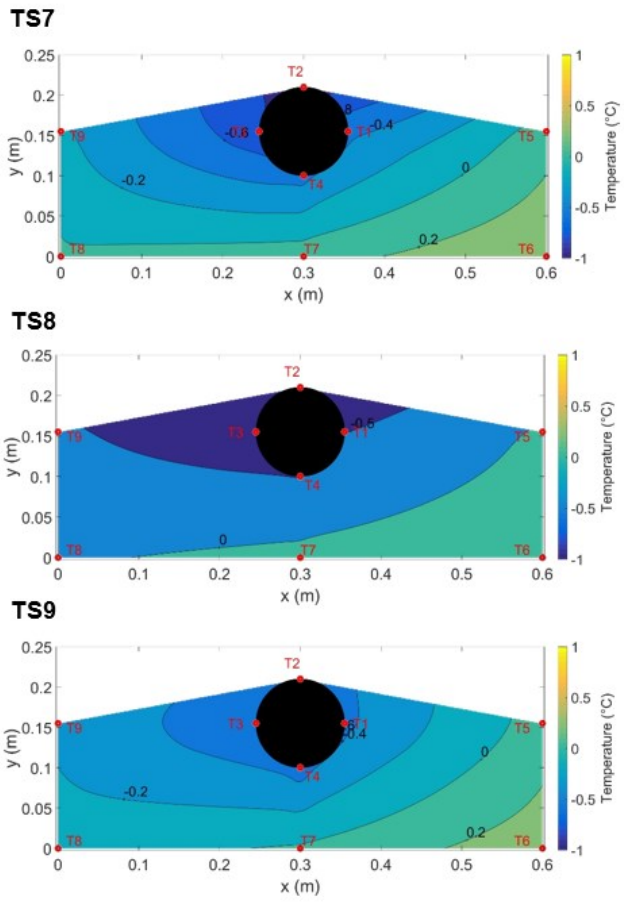

Figure 4-23: Temperature change profile around LL3 for leak test 1

4.5.4.2 Fibre Bragg data leak test 1

An elevation layout schematic of the first leak test FBGS layout is shown in Figure 4-24.

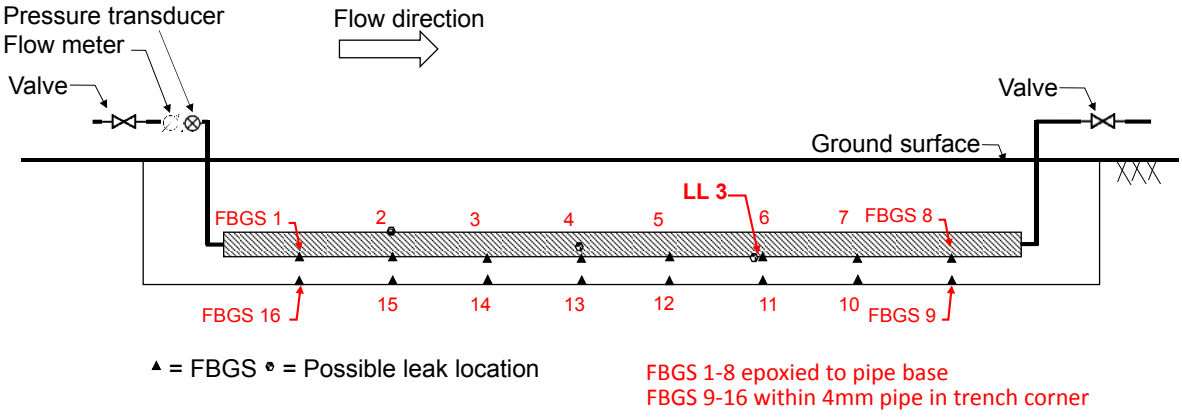

Figure 4-24: Elevation of experimental setup for LL3

Figure 4-25 and Figure 4-26 present the strain changes observed at the base of the pipe (FBGS 1 to 8) and in the trench corner (FBGS 9 to 16) respectively. The graph was obtained by using a central moving average of the raw data over a three minute interval. To decrease the size of the graph every tenth point was plotted, ensuring that important events are not lost. The base strain readings were taken one day before the test started. The vertical axis therefore represents the change in strain observed during the leak test and not the absolute strain. The first vertical red dotted line indicates the leak initiation and the second dotted line indicates leak closure. Larger strains were observed closer to the leak location compared to further away as shown by the results from FBGS 6 (at leak location LL3), 7 and 8 (downstream of the leak location). Free FBGS 11, at the leak location, registered the greatest strain of all the free FBGSs. Strains from the epoxied FBGS are about one order of magnitude larger than those from the free FBGS. The two figures below indicate uncompensated strains, meaning thermal and mechanical strain are shown.

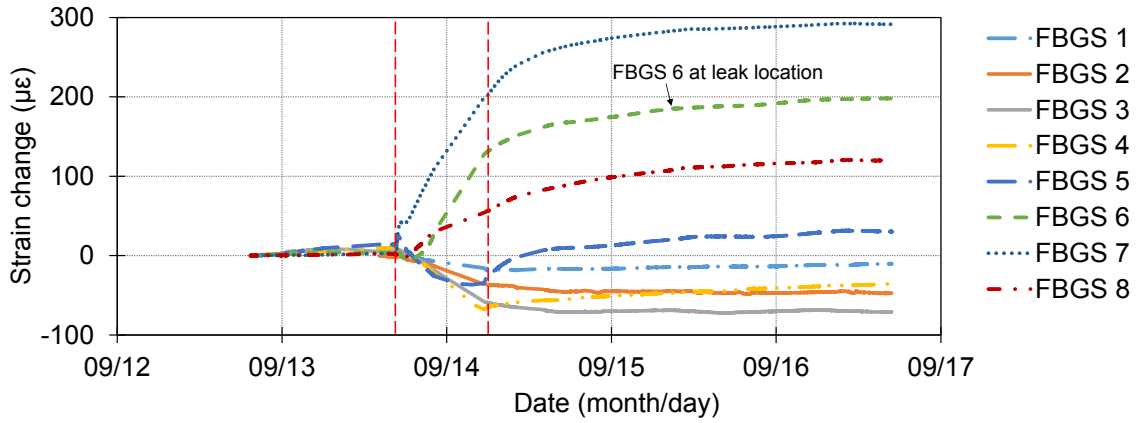

Figure 4-25: Strain changes over time for Leak test 1 from epoxied FBGS

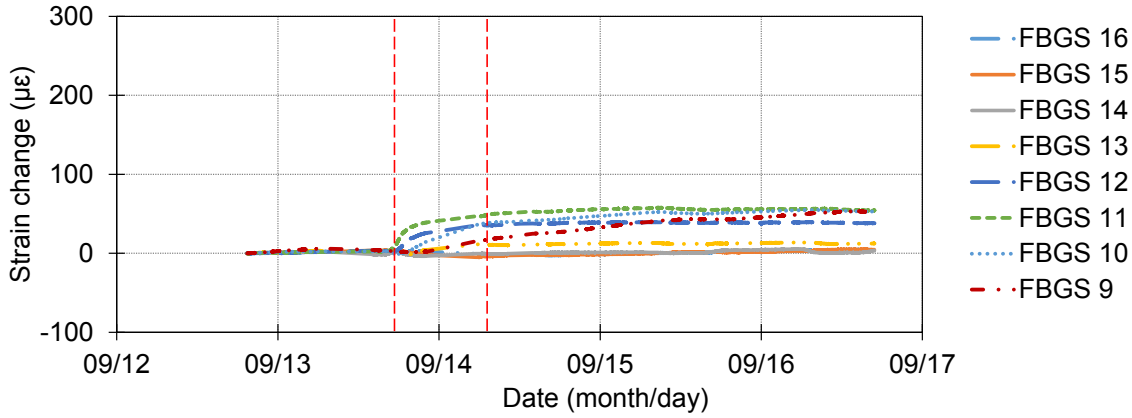

Figure 4-26: Strain changes over time for Leak test 1 from free FBGS

It was of interest to determine the proportions of strains measured on the pipe resulting from thermal and mechanical effect respectively. The total strains observed were therefore adjusted by applying temperature correction. Temperature compensation was only available at the leak locations where thermistor data was available, i.e. at FBGS 6 and 11 in leak test 1. Figure 4-27 and Figure 4-28 show the compensated and original curves for FBGS 6 and 11. The temperature compensated strain graph is indicated in dark green and the non-temperature compensated graph is indicated in a square dotted light green line. It is evident that temperature compensation is not critical for this investigation as it did not significantly impact the research results for FBGS 6 and 11 due to the small temperature changes induced by the leak.

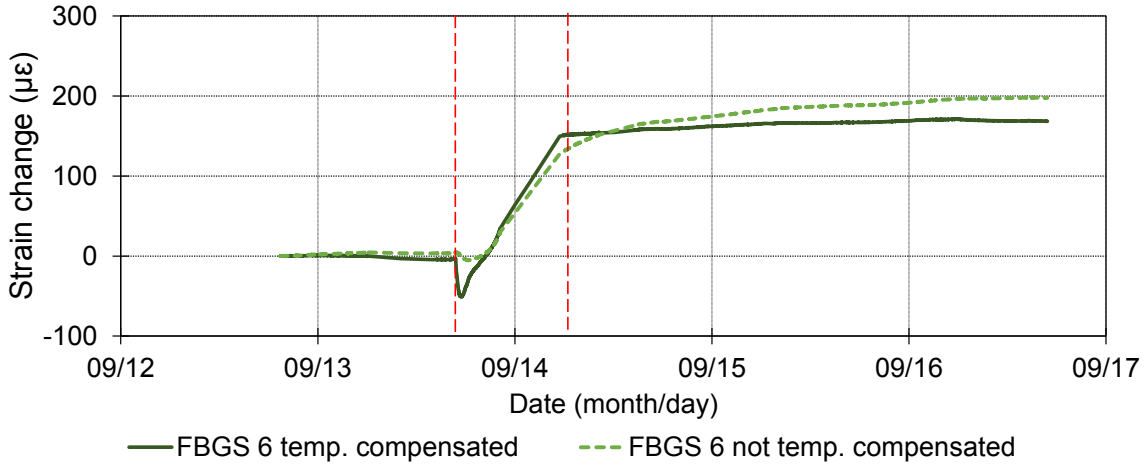

Figure 4-27: Comparison of temperature compensated vs non-compensated strains for epoxied FBGS 6

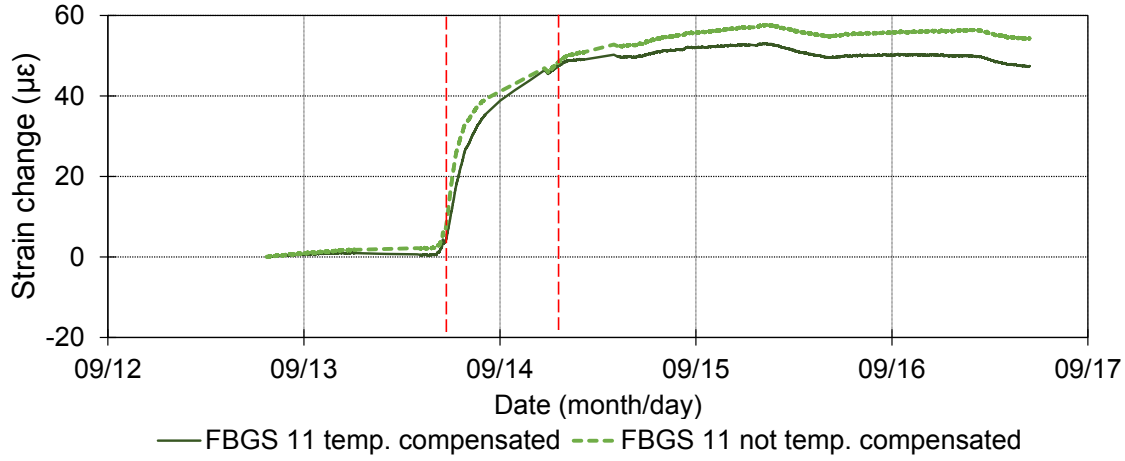

Figure 4-28: Comparison of temperature compensated vs non-compensated strains for free FBGS 11

Leak-induced strain development along pipeline

If the epoxied Bragg data (FBGS 1 to FBGS 8) is shown in terms of sensor location (distance) over time as shown in Figure 4-29, it is clear that strain values increase over time in close proximity to the leak where a support softening is occurring due to wetting. The time intervals per strain sections have been chosen to illustrate significant strain changes per time interval. The time intervals are given relative to the leak initiation time.

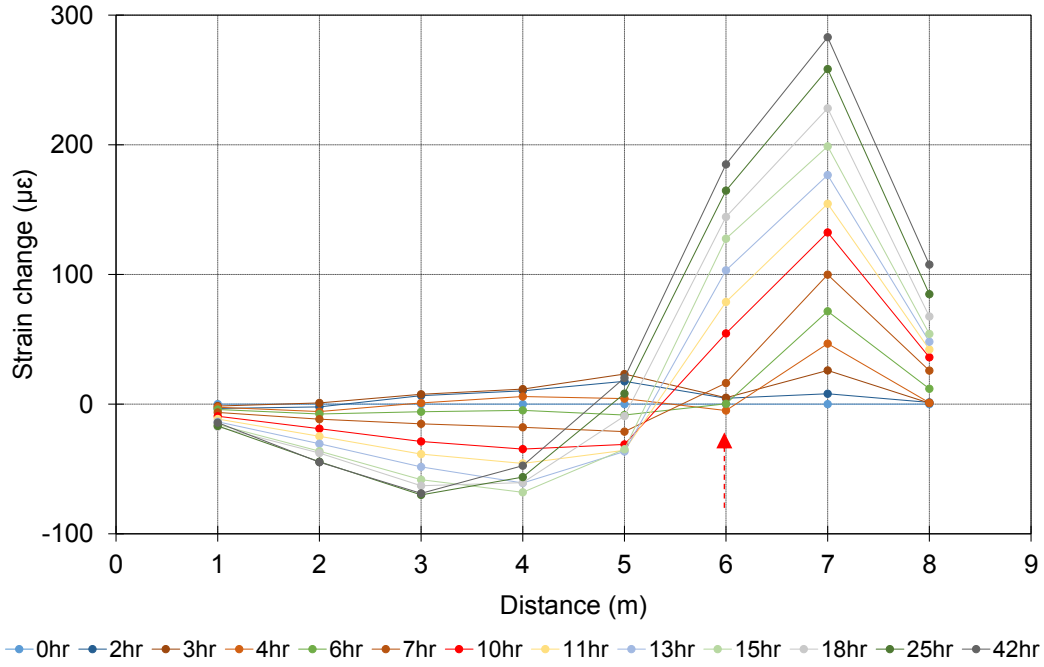

Figure 4-29: Epoxied FBGS strain development over distance during leak test 1

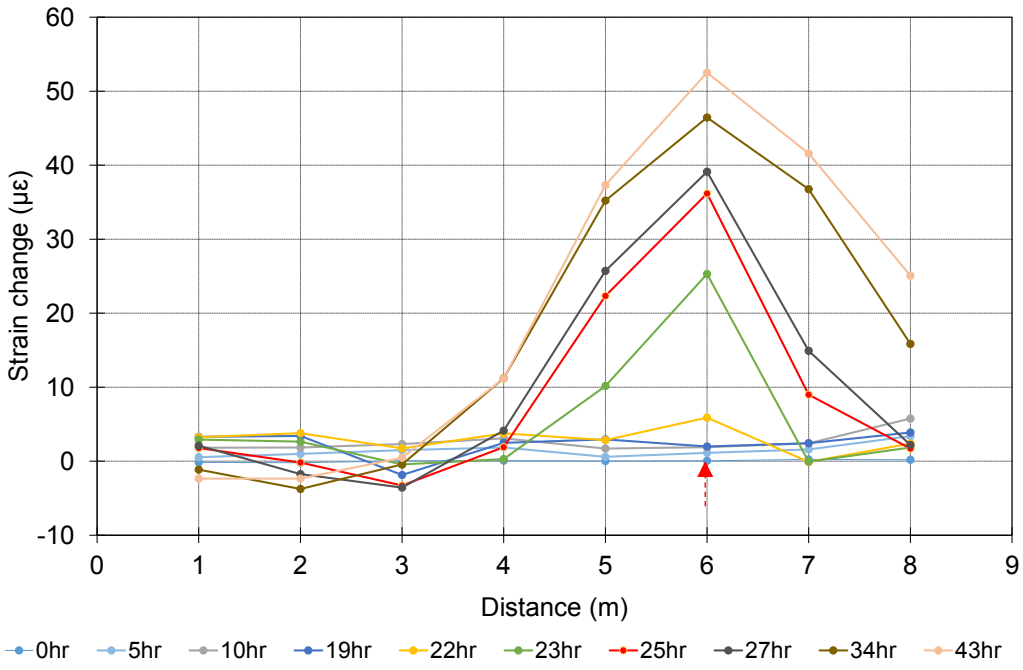

Figure 4-30: Free FBGS strain development distance during leak test 1

Discussion

Comparing strain readings from the free and fixed FBGSs reveal an order of magnitude difference in the strain magnitudes measured in the case of the epoxied sensors relative to free sensors. It appears that wetting of the ground results in softening, causing a change in the support conditions around the pipe manifesting as strain changes which are an order of magnitude larger than those induced by thermal effects only. It therefore appears highly beneficial to attach the fibre optic cable to the pipe as this increases the sensitivity of the leakage detection system considerably. However, it is necessary to investigate strain changes resulting from normal pressure fluctuations which occur in a pipe system during operation to make sure that these changes can be distinguished from those resulting from a leak.

4.5.5 Leak test 2

The second leak test was conducted from 17 September at 08h09 to 16h13 at leak location 2 (LL2). The flow rate entering the pipeline was 4.35l/min and the leakage flow rate was 0.83l/min with an average pressure of 24kPa during the leak test.

4.5.5.1 Thermistor data leak test 2

The thermistor layout of the second test is shown in Figure 4-31. Thermistor string TS5 is located at the leak locations (LL2), TS4 is 0.15m upstream of LL2 with TS6 0.15m downstream. TS1 was again used as a control to indicate the change of temperature around the pipe where no leak occurred.

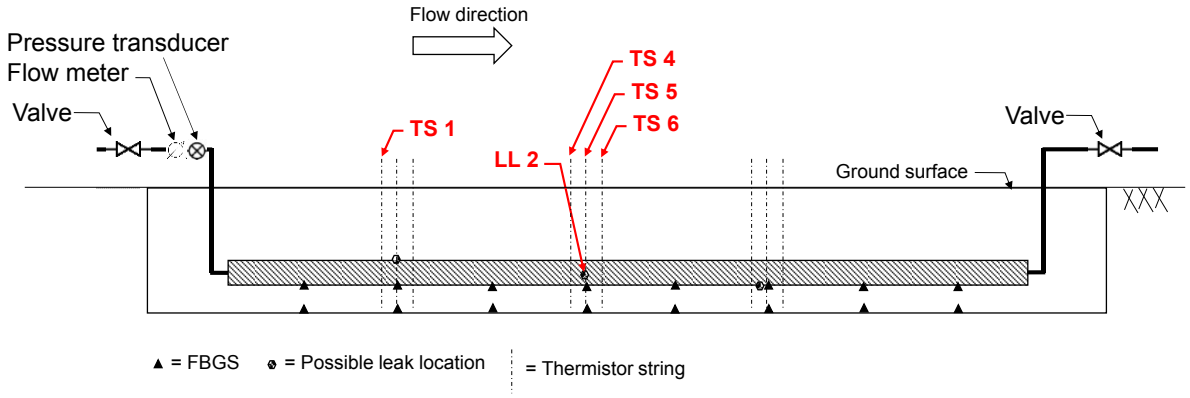

Figure 4-31: Elevation of experimental setup showing location of Leakage test 2

The same methodology used for the presentation of data from Leakage test 1 at LL3 is also used for the second leak test at LL2. The data from the leak location itself (thermistor string TS5) is shown first (Figure 4-33). Thereafter data from 0.15m upstream at TS4 is shown in Figure 4-34 and finally data from 0.15m downstream at TS6 is shown in Figure 4-35. Data from the reference string TS1 is shown in Figure 4-36. The water temperature during the leak test is presented in Figure 4-32.

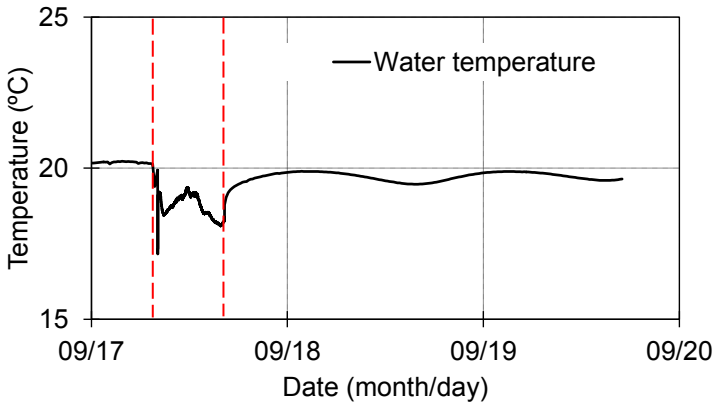

Figure 4-32: Water temperature during the second leak test at LL2

The temperature around the pipe changed immediately at TS 5 upon commencement of the leak while a lag time can be observed at TS4 and TS6. The magnitude of temperature change was small due to the relatively small differential temperature of less than one degree Celsius

between the water in the pipe and the soil temperature. The same temperature trend present in the water temperature graph can be observed at all the thermistors, where an initial negative temperature spike was caused by stagnant water upstream of the test section. The water temperature trend observed was directly transferred to the adjacent thermistor strings. The reference string TS1 did not register a major change in temperature because the thermistors were not in direct contact with the water and the uPVC pipe acted as a weak thermal insulator.

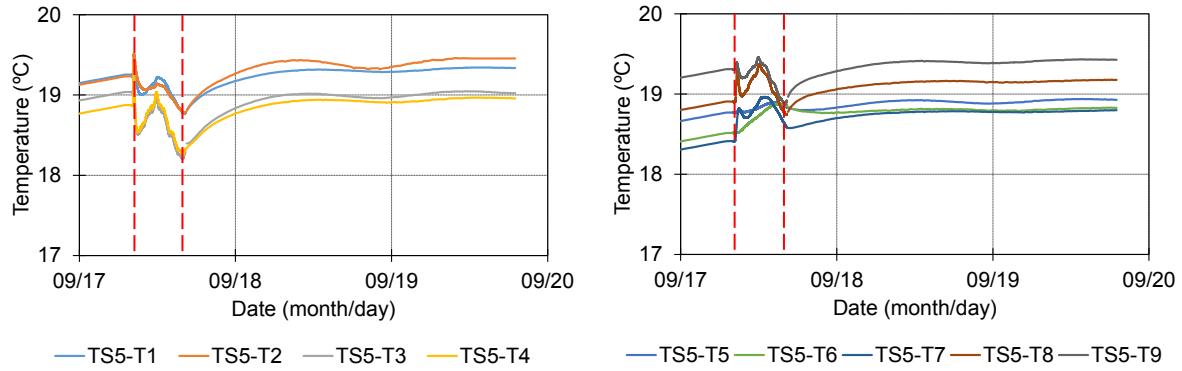

Figure 4-33: Temperature change at leak location LL2 (TS5)

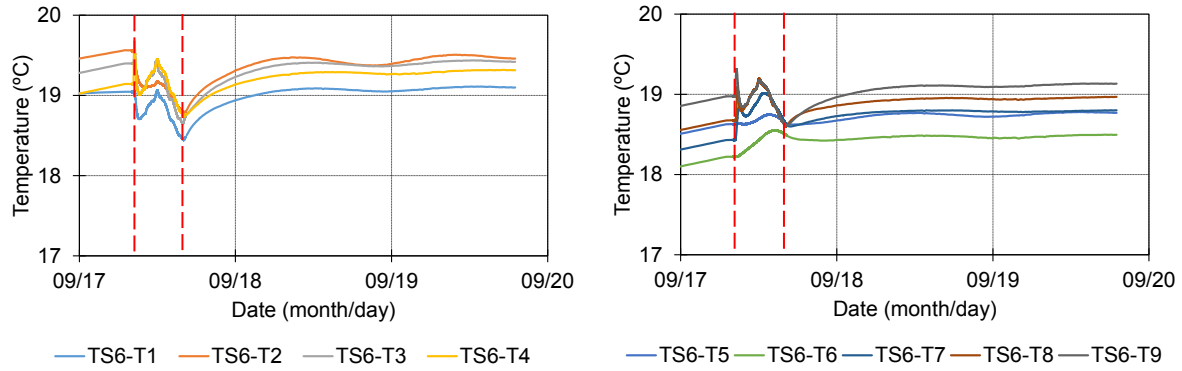

Figure 4-34: Temperature change 0.15m upstream of leak location LL2 (TS4)

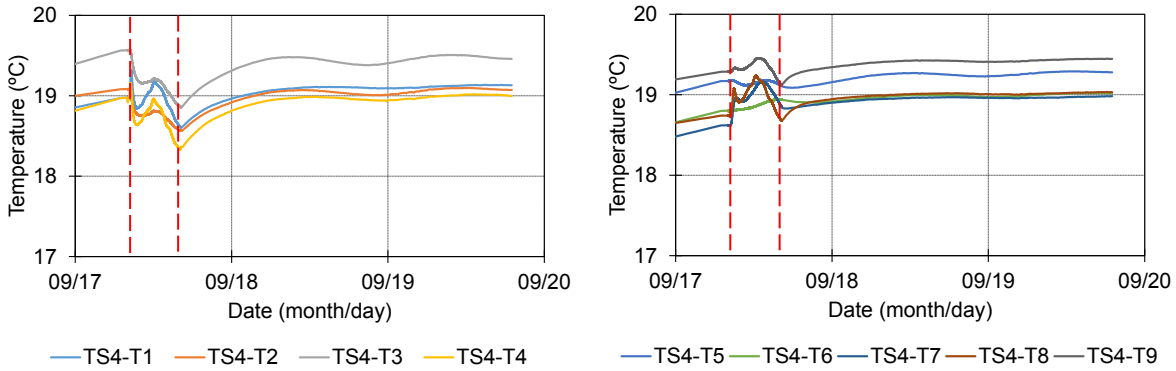

Figure 4-35: Temperature change 0.15m downstream of leak location LL2 (TS6)

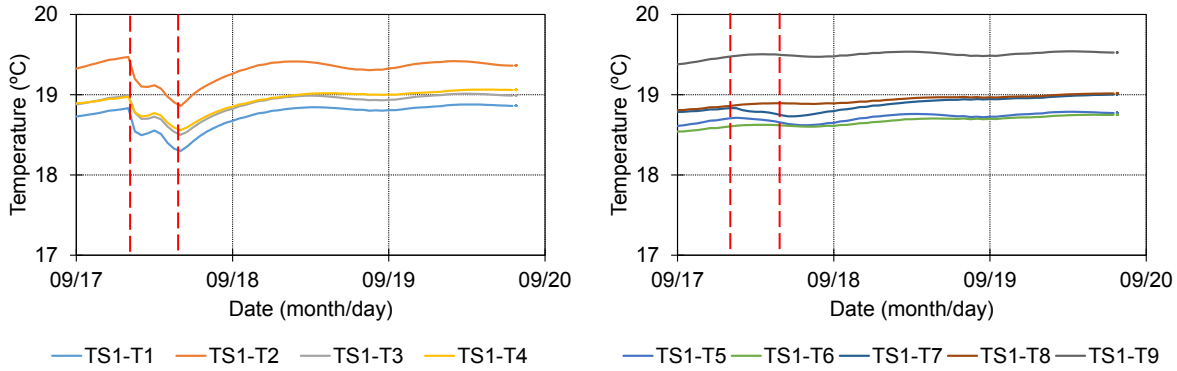

Figure 4-36: Temperature change at reference string LL2 (TS1)

Temperature distribution around leak location

Figure 4-37 presents a 2D contour plot of temperature observed before the leak was induced in the left column and during the leak in the right column. The differential temperature before and during the leak is shown in Figure 4-38. Before the leak was initiated a clear temperature stratification or bands could be seen in the left column and a small discontinuity at the pipe due to changes in thermal properties. A clear temperature stratification can be observed with depth before the leak test was initiated. It is evident that a leak caused a cooling or heating bulb, depending on the temperature differential, to form around the leak location, which spread over time as can be seen in the right column. The images are shown from top to bottom in the direction of flow, i.e. TS4 is in the first row, TS5 is in the middle (at the leak) and TS6 is downstream of the leak in the last row.

Discussion

During leakage test 2 the influx of warm water into the pipe did not occur so that the temperature differential between the water in the pipe and the surrounding soil was smaller. Despite the smaller temperature differential clear temperature changes were observed caused by the leak. As in the case of Leakage test 1 it appears that leakage will be most reliably detected by measuring temperatures some distance from the pipe, i.e. in the corners or invert of the pipe trench. While all thermistor in the string registered leak-induced temperature changes, thermistors located along the invert of the pipe registered somewhat larger temperature changes than those located adjacent to the pipe. This suggests the pipe invert to be the more optimal position for the temperature sensors.

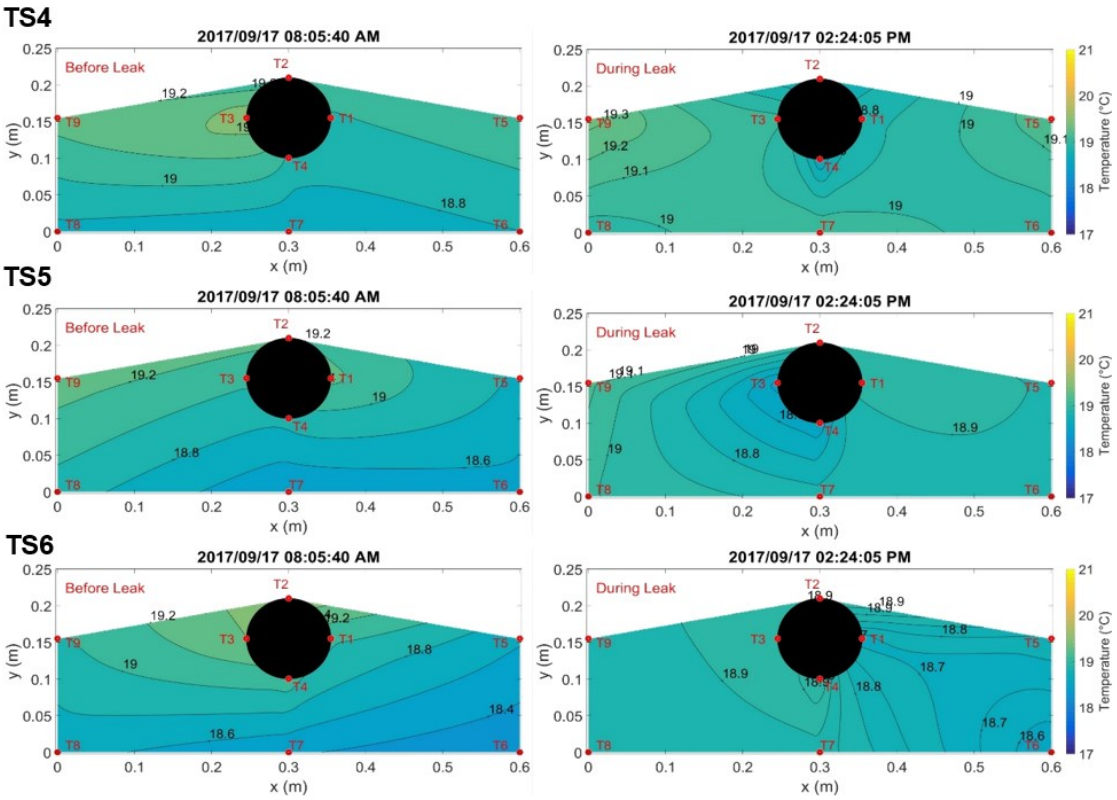

Figure 4-37: Temperature profile around LL2 before (left) and during (right) the leak for leak test 2

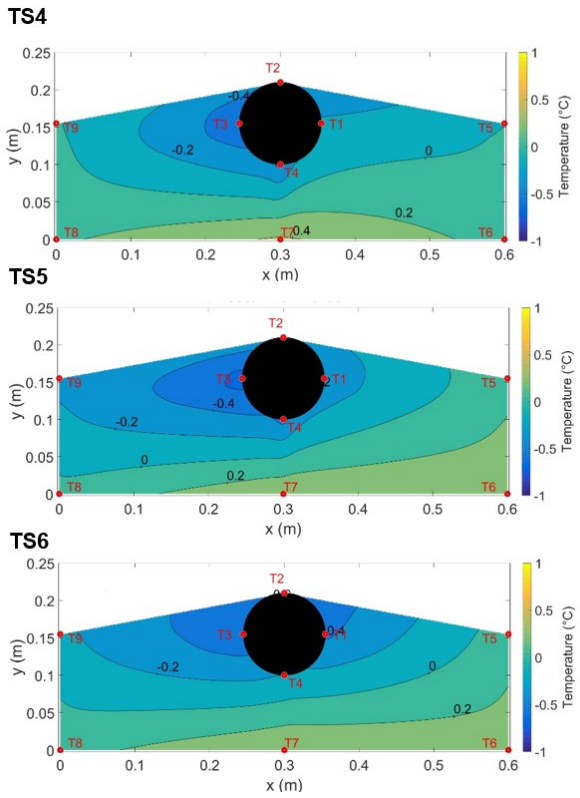

Figure 4-38: Temperature change profile around LL2 for leak test 2

4.3.2.2 Fibre Bragg data leak test 2

The second leak test was conducted at LL2, with epoxied FBGS 4 and free FBGS 13 being the closest to the induced leak location. Figure 4-39 below indicates the experimental FBGS layout for the second induced leak test.

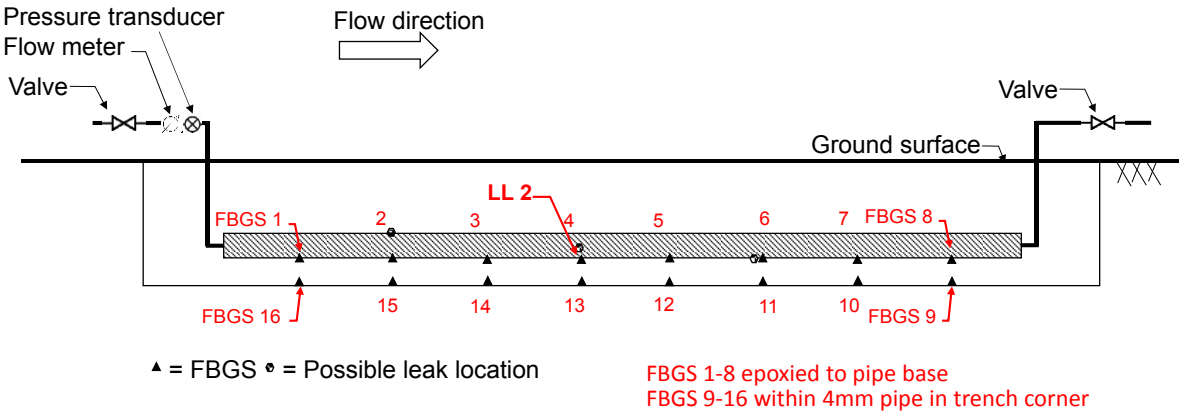

Figure 4-39: Elevation of experimental setup for Leak test 2 LL2

Figure 4-40 (epoxied FBGS) and Figure 4-41 (free FBGS) indicate changes in strain obtained during the test. Interestingly FBGS 5 located 1m downstream of the leak location registered the largest strain change of all epoxied FBGS despite it not being the closest to the leak location. FBGS 6, located 2m downstream also shows a significant strain change. Figure 4-41 dictates that the largest strain change for the free fibre sensors occurred at FBGS 13, which is the immediately adjacent sensor to the leak, located in the trench corner.

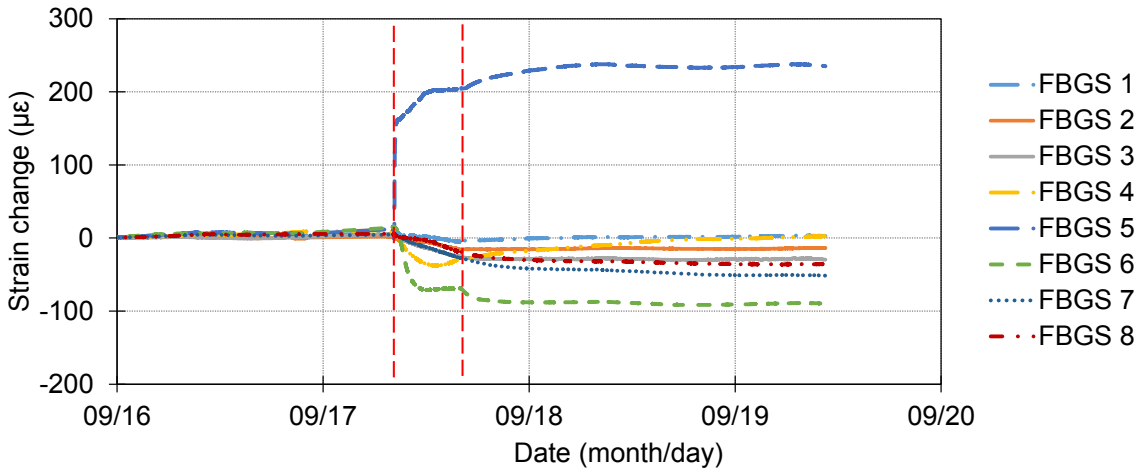

Figure 4-40: Strain changes over time for leak 2 from epoxied FBGS

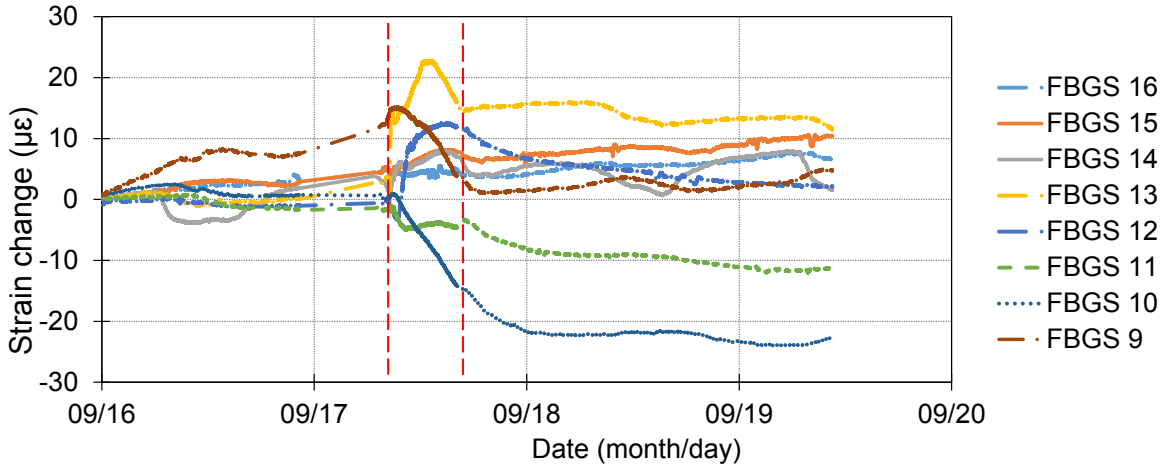

Figure 4-41: Strain changes over time for Leak test 2 from free FBGS

As for Leakage test 2 temperature compensation was done for FBGS 4 and FBGS 13 using data from thermistors TS5-T4 and TS5-T8 respectively. It is evident from Figure 4-42 that there is a substantial difference in strain between compensated and uncompensated strain values, this can be attributed to the lag in reaction of the uPVC compared to the theoretical behaviour. Figure 4-43 that no significant changes can be observed between compensated and uncompensated strain values. This means that the thermal strain component is insignificant for this study compared to mechanical strain component due to the small changes in temperature. Alternatively it can be argued that the temperature compensation technique applied, i.e. using a thermistor to measure temperature which is used to compensate for thermal strain change, is not the most effective method.

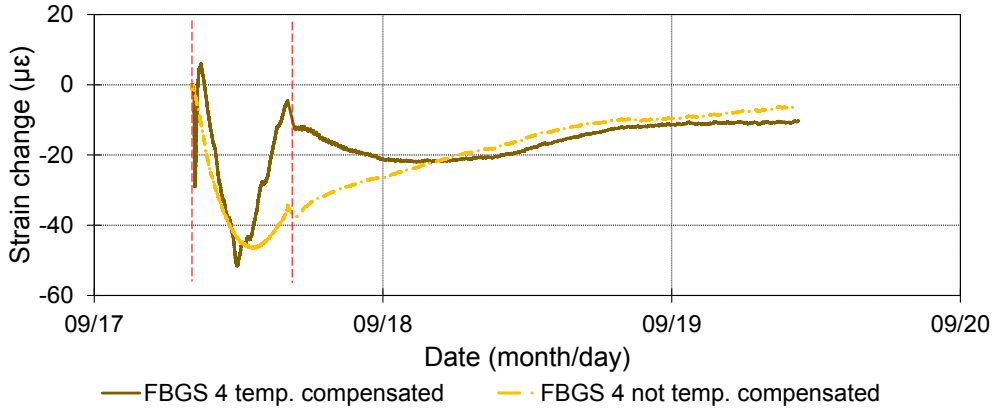

Figure 4-42: Comparison of temperature compensated vs uncompensated strains FBGS 4

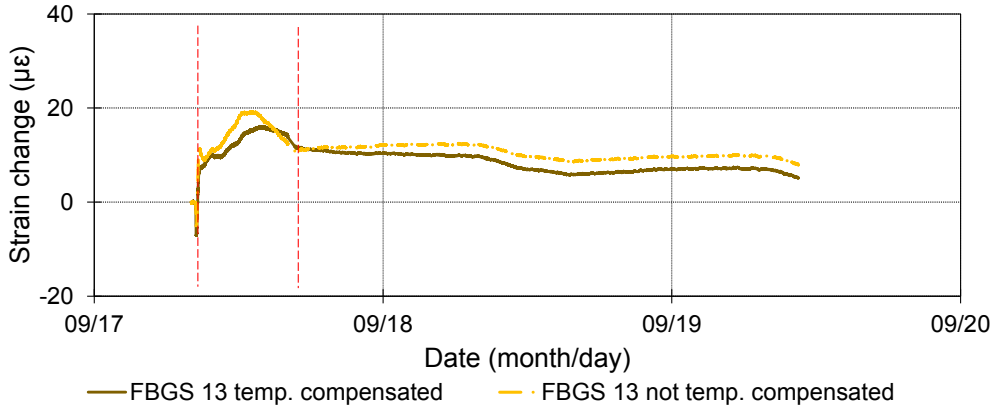

Figure 4-43: Comparison of temperature compensated vs uncompensated strains FBGS 13

Figure 4-44 is obtained if the changes in strains are plotted over distance according to time intervals after the leak event has been initiated for epoxied FBGS. As the leak event progresses a clearly discernible change in strain in close proximity to the leak location can be observed. Red arrows have been added to indicate an increase in strain at the leak location. The greatest strains can be observed at the joint at 5m distance at FBGS 5. The figure depicts a continuously supported beam, which bends in close proximity to the leak location (4m distance). The beam goes into tension just downstream of the leak location and in compression at either side of the leak event. Tension in this case would be of the strain changes are positive as the cable is epoxied to the pipe base and compression is a negative strain change. Figure 4-45 indicates the changes in strain over distance for the free FBGS, the greatest change in strain can be observed at the leak location itself at the 4m distance marker at FBGS 4.

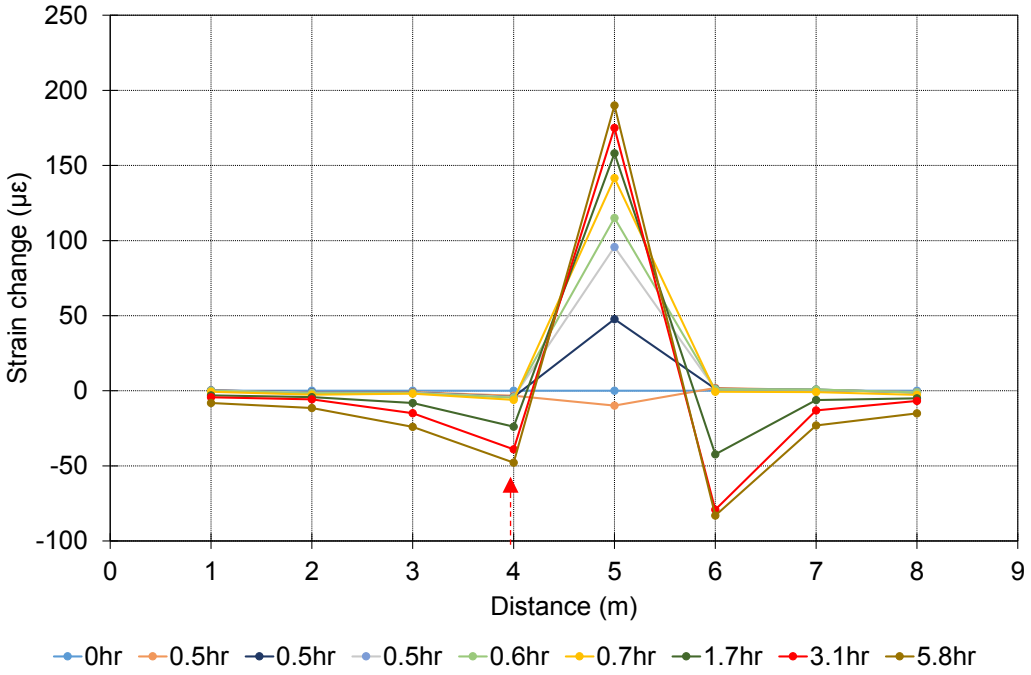

Figure 4-44: Epoxied FBGS strain development over distance during leak test 2

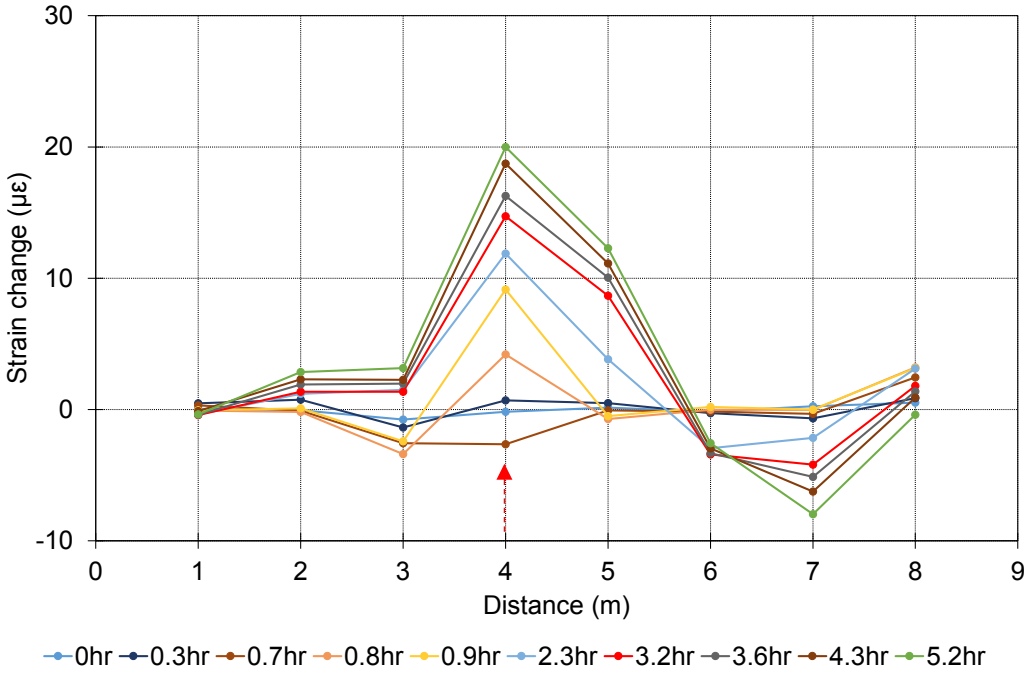

Figure 4-45: Free FBGS strain development over distance during leak test 2

Discussion

Again, it is shown that clearly measurable strain changes occurred in the pipe and that these could be measured to an exceptional resolution. Strain changes due to mechanical effects

caused by softening of the pipe support (bedding) were again an order of magnitude larger than temperature-induced strain changes resulting from the leak. An important observation from this test is that the maximum mechanical strain change did not occur immediately opposite the leak location. This can be explained by considering the way in which the pipe deflects in response to a softening of its support (bedding) upon wetting. It is proposed that non-uniformities in the pipe bedding and an asymmetric spread of leakage water around the leak location due to the slope can explain the asymmetric strain changes observed. The exact magnitude of strain changes themselves are not of so much interest, but rather the fact that a strain change occurred.

4.5.6 Leak test 3

The leak was initiated on 19 September at 19h39 and was closed the following day at 12h46. The average flow rate entering the pipe was 6.7l/min and the initial leakage rate was 0.54l/min the average pressure during the test was 34kPa.

4.5.6.1 Thermistor data leak test 3

The third leak test was conducted at leak location (LL) 1 as shown with the thermistor layout in Figure 4-46 below. The reference thermistor string (TS) used for this test was TS4 (1.85m downstream of leak location LL1). Thermistor string TS2 is at the leak location, TS1 0.15m upstream of the leak and TS3 0.15m downstream. The thermistor layout for each string was the same for this test setup as for the previous tests.

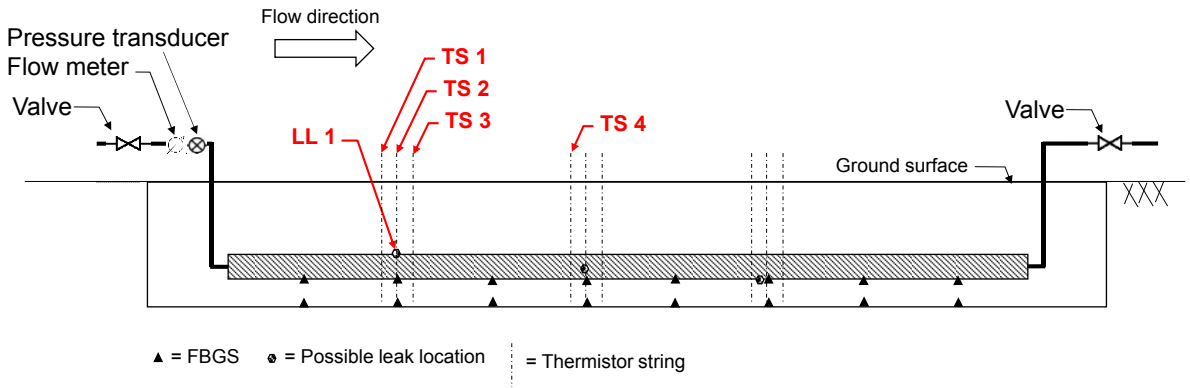

Figure 4-46: Experimental elevation schematic of test 3 at LL1

Stagnant water upstream of the installation had cooled down significantly prior to the test and explains the initial cooling spike in Figure 4-47. The initial spike was followed by a gradual increase in water temperature as water was flushed through the pipeline.

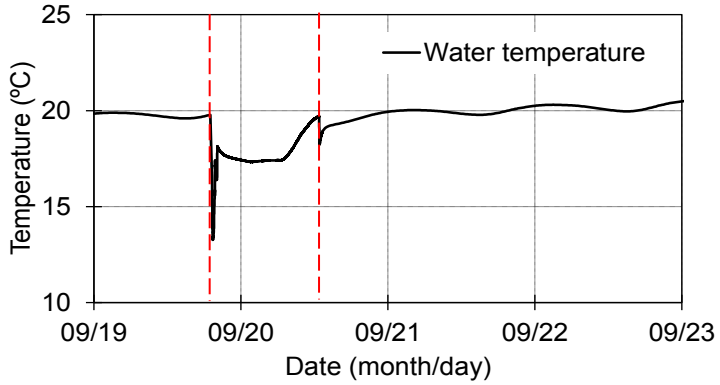

Figure 4-47: Water temperature during the second leak test at LL1

The temperature data obtained with the thermistors is summarised in Figure 4-48 to Figure 4-51 indicates temperature changes at the leak location LL1 based on TS2. It is evident that similar temperatures were measured around the pipe (thermistors T1 to T4 of thermistor string TS2, left figure) and that it reacted rapidly to the change in water temperature caused by the leak. The temperature in the trench corner did not change significantly at all the 'perimeter' thermistors (T5 to T9). Only TS2-T9 reacted significantly to the change in water temperature at the leak location (see Figure 4-48). The same trend can be observed at TS1 (Figure 4-49) and TS3 (Figure 4-50). The reference string TS4 (Figure 4-51) behaved similar to the thermistor strings at the leak location. The difference in behaviour in this test is related to the flow of water around the pipe. The leak location was at the top of the pipe, which does not affect the temperature profile around the pipe over a long time duration, however just after the leak occurrence the leak location on the pipe does affect the temperature profile. The pipe trench slopes from LL1 towards LL3 which explains why temperature changes were registered at some of the thermistors at LL2.

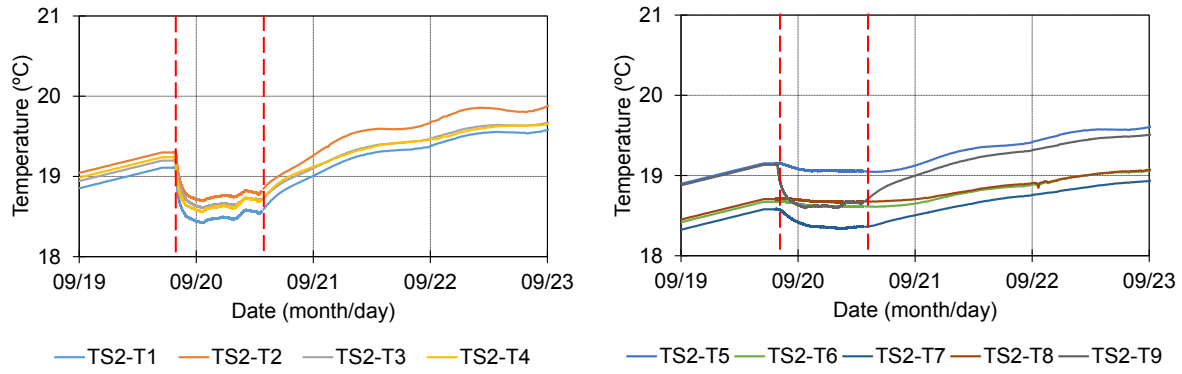

Figure 4-48: Temperature change at leak location LL1 (TS2)

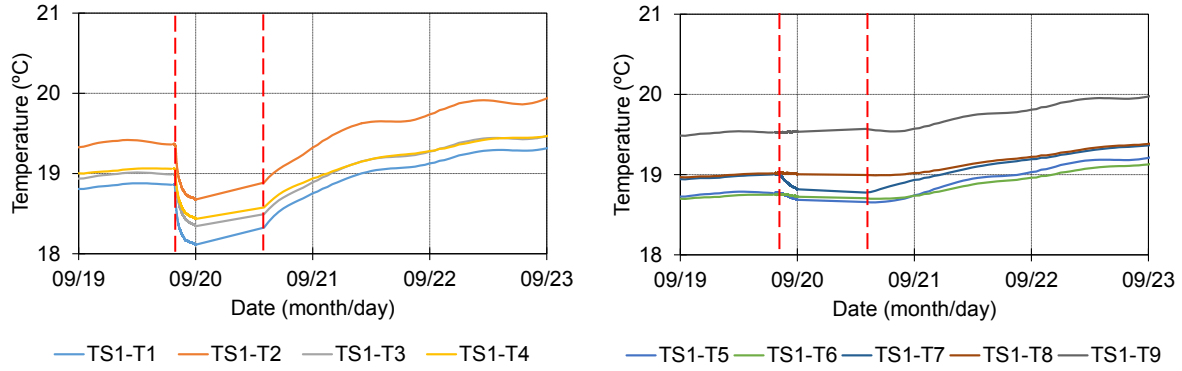

Figure 4-49: Temperature change 0.15m upstream of leak location LL1 (TS1)

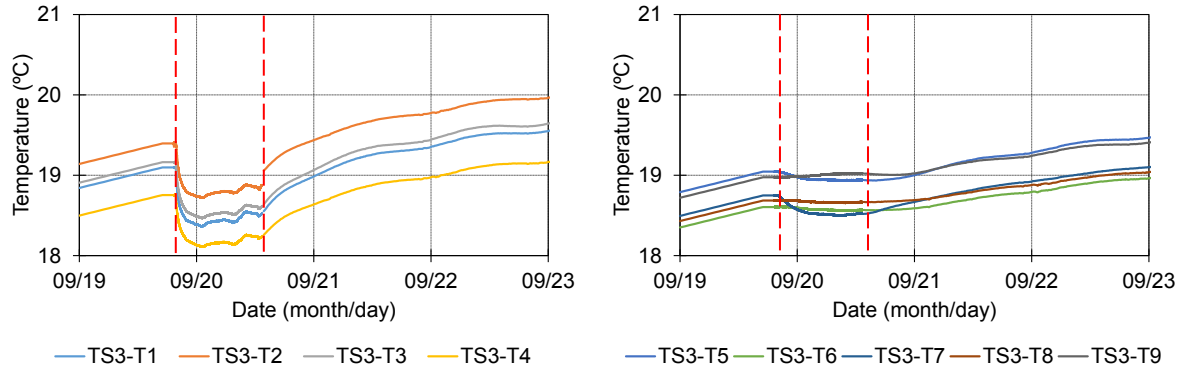

Figure 4-50: Temperature change 0.15m downstream of leak location LL1 (TS3)

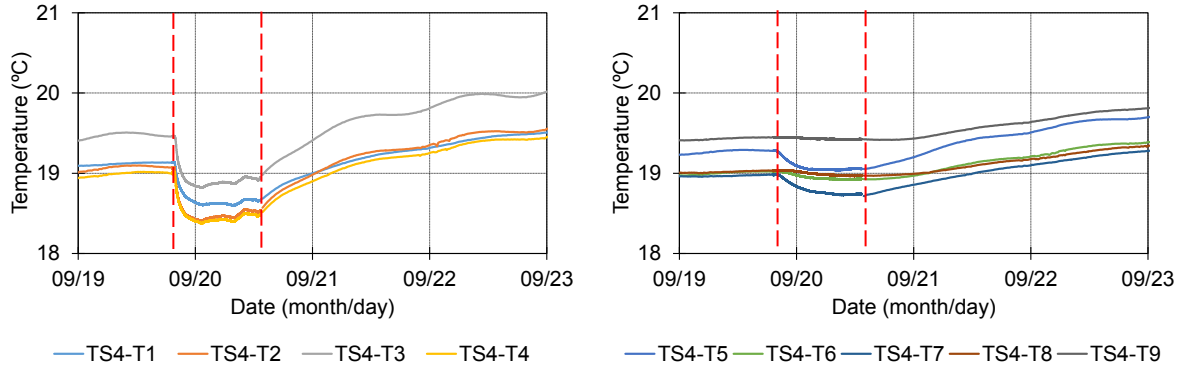

Figure 4-51 Temperature change at reference string LL1 (TS4)

Temperature distribution around leak location

Figure 4-52 presents a 2D contour plot of the temperature data obtained at and around LL1 with TS1 (0.15m upstream), TS2 (at the leak location) and TS3 (0.15m downstream). Again a clear temperature stratification with depth can be observed in Figure 4-52 before the leak was initiated (left column) with a temperature discontinuity at the pipe. During the leak test a clear cooling bulb (right column) formed around the LL1 which reached thermistor T8 and T6 which were most distant from the pipe in the trench corner. A temperature differential plot is shown in Figure 4-53, showing the change in temperature before and during the leak event.

Discussion

Results similar to the previous tests were obtained, i.e. indicating that leaks can be detected by measuring temperature changes around the pipe. The effect of the gently sloping pipe trench may result in water flowing in the direction of the slope so that temperature changes can occur a short distance away from the leak location.

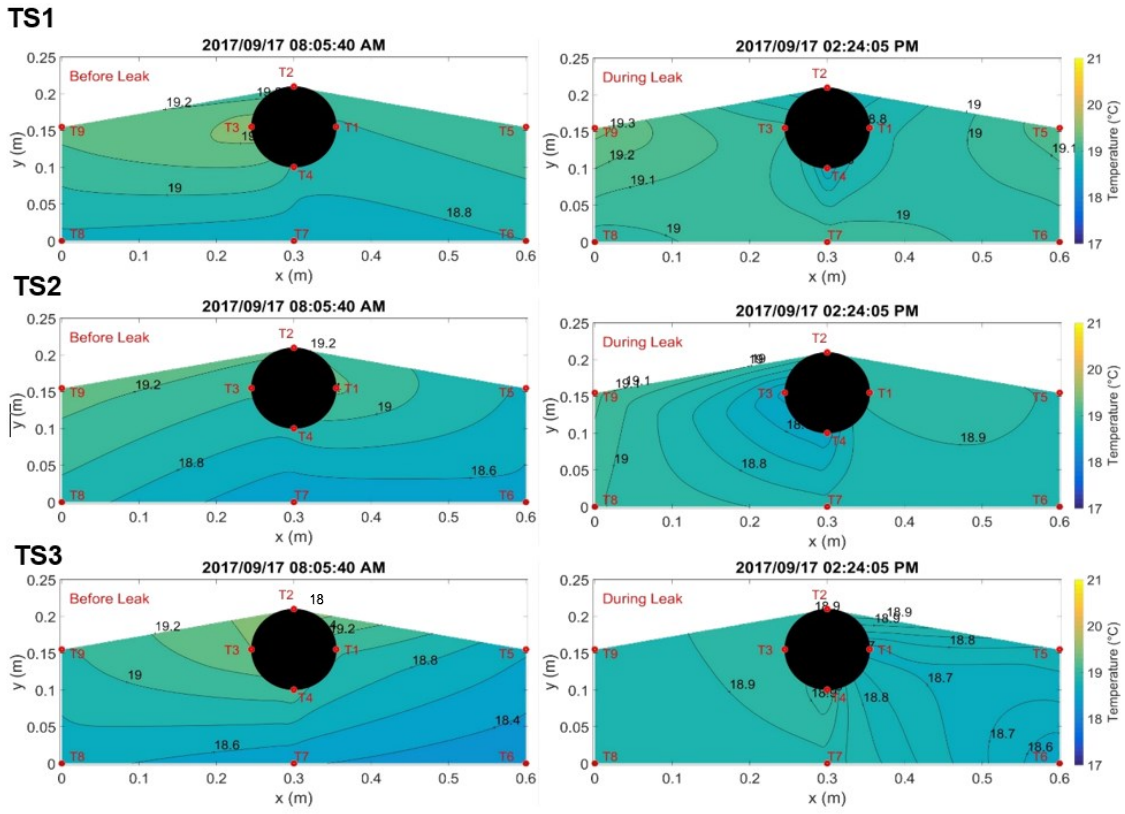

Figure 4-52: Temperature profile around LL1 before (left) and during (right) the leak for leak test 3

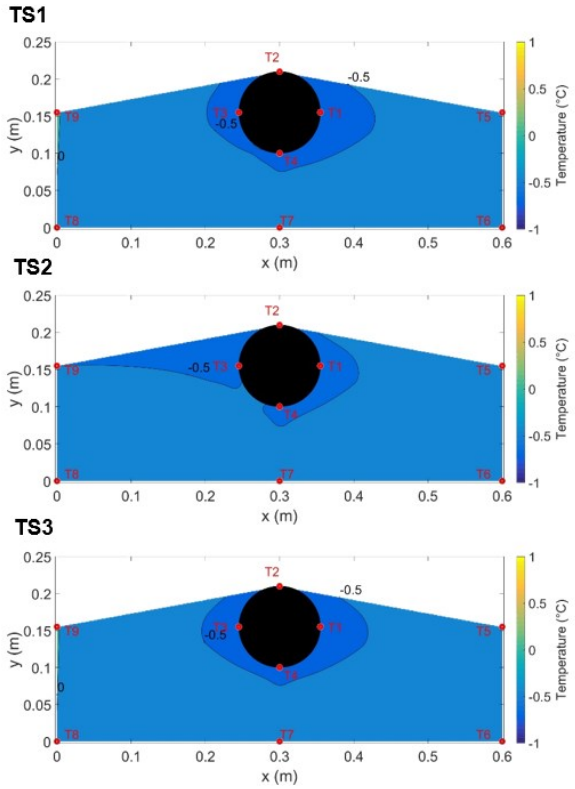

Figure 4-53: Temperature change profile around LL1 for leak test 3

4.5.6.2 Fibre Bragg data leak test 3

The third leak test was initiated at LL1 as shown in the thermistor layout in Figure 4-54. FBGS 2 and FBGS 15 are the closest fibre optic sensors to the leak location.

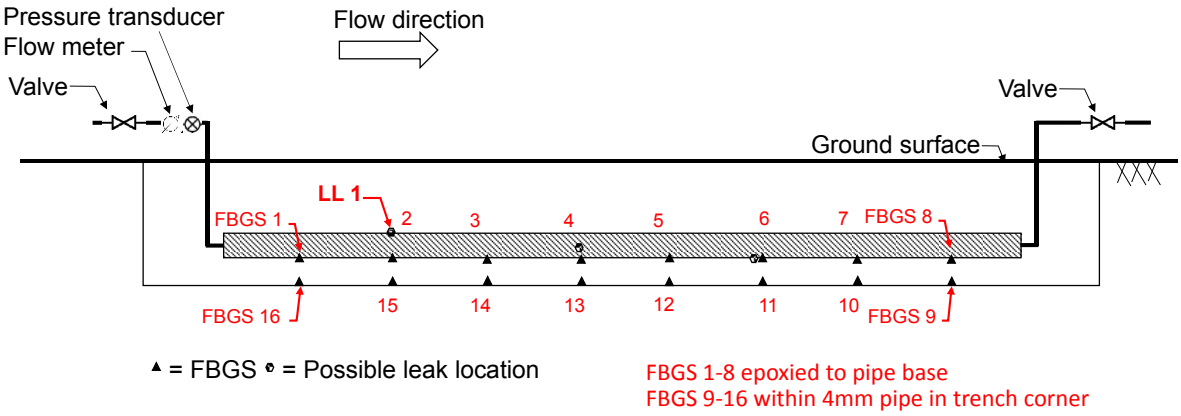

Figure 4-54: Elevation of experimental setup for Leak test 3 LL1

The strain change for the epoxied and free FBGS are shown in Figure 4-55 and Figure 4-56 respectively. It is evident that the previous leakage events had an impact on the subsequent leakage tests: The first test softened the support (bedding) around the pipe, leading to strains

over a greater length of pipe during the subsequent compared to the first. The epoxied FBGS further from the leakage source seem to recover rapidly after the leak was closed. However, at the leak location FBGS 2 and 3 seem to have undergone a more permanent deformation. Results from the free FBGS presented in clearly registered compressive thermal strain changes resulting from the leak. A clear daily temperature variation is also evident on the free temperature sensitive sensors as temperatures recovered in the soil during the days after the leak.

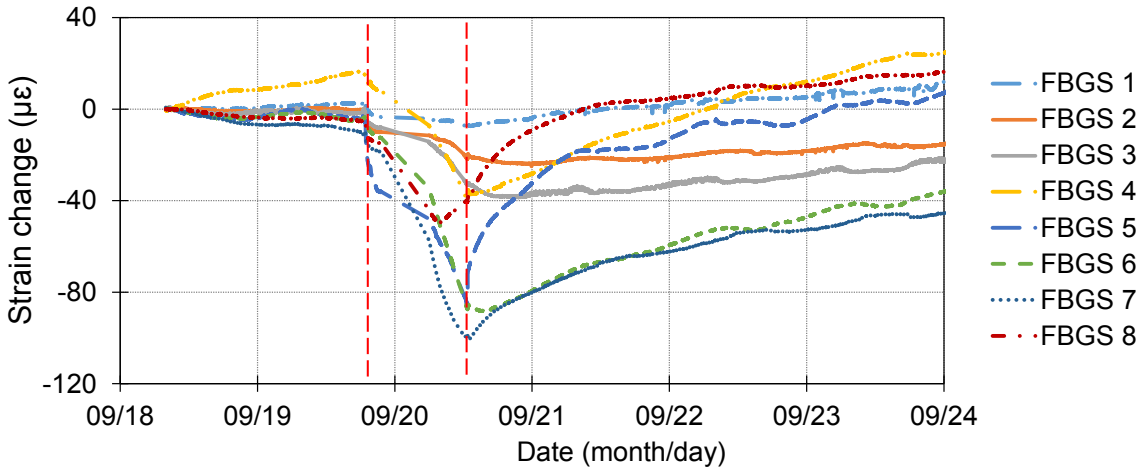

Figure 4-55: Strain changes over time for leak test 3 from bonded FBGS

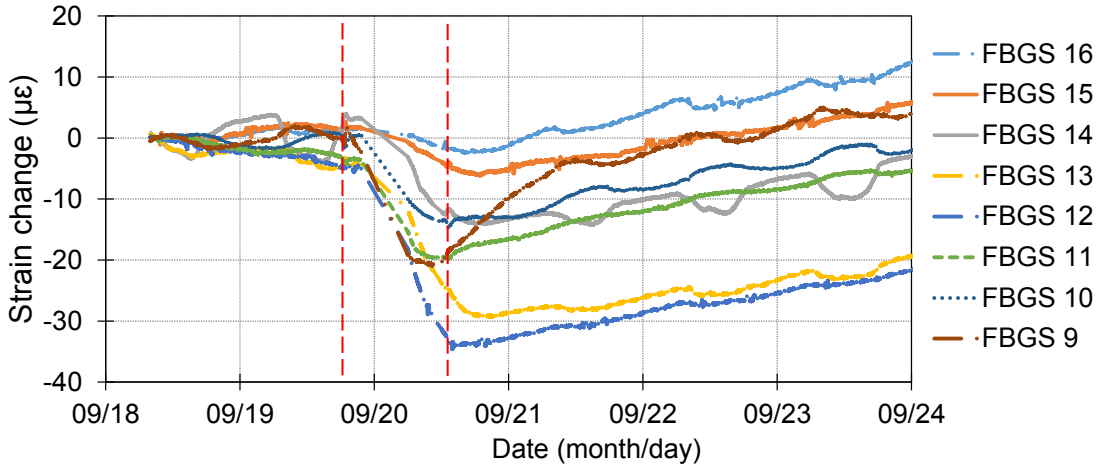

Figure 4-56: Strain changes over time for leak test 3 from free FBGS

Temperature compensation had a minor effect on the strain changes for the free FBGS 15 as shown in Figure 4-58. A considerable strain change of 30 με could be noted for the compensated epoxied FBGS 2 compared to uncompensated results. The difference in compensated vs. uncompensated strain results, even though substantial, is unimportant for

this study, as a change in strain due to a leak event was registered. The total (uncompensated) strain change was caused by a combined thermal and mechanical action.

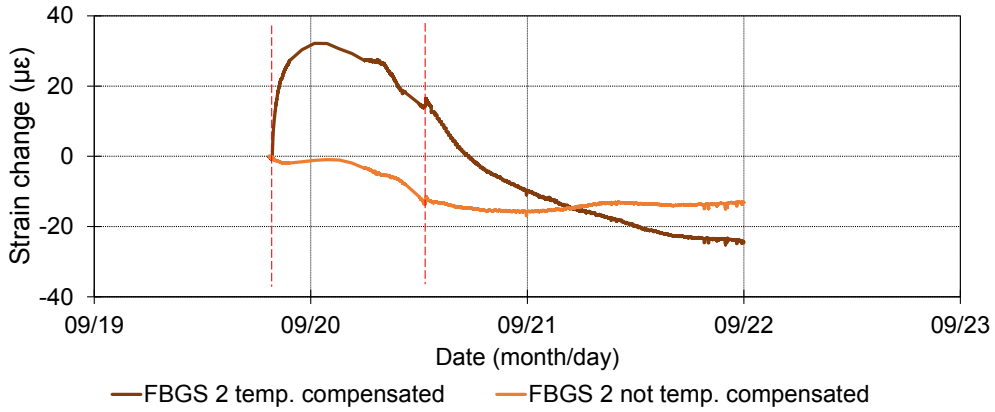

Figure 4-57: Comparison of temperature compensated vs uncompensated strains FBGS 2

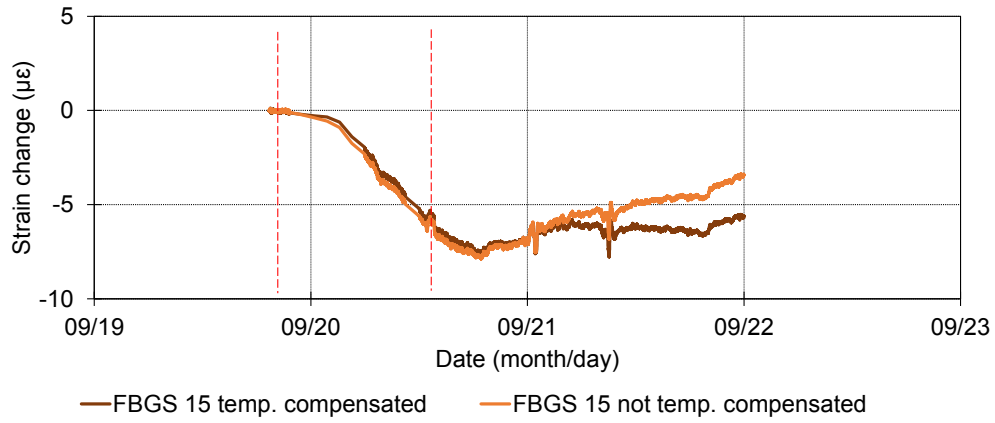

Figure 4-58: Comparison of temperature compensated vs uncompensated strains FBGS 15

If the epoxied Bragg data (FBGS 1 to FBGS 8) is shown in terms of sensor location (distance) over time for leak test 3 as shown in Figure 4-59, it is clear that strain develops over time in close proximity to the leak locations where a support (bedding) softening is occurring due to wetting. The previous leak events at LL3 and LL2 did have a significant effect on strain development along the pipeline as can be observed in the figure below where the most downstream leak location indicates the biggest strains. In Figure 4-60 the free FBGS strain development is shown over distance. The greatest strains are noted close to the joint where the previous leak was initiated at distance marker 4m and 5m (FBGS 4 and FBGS 5) being close to the joint.

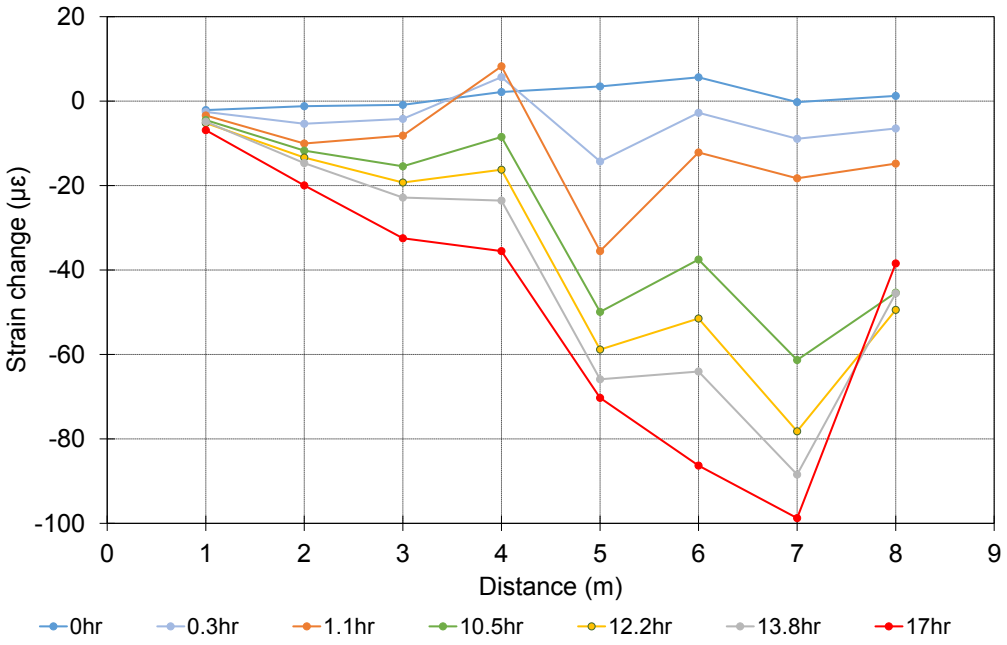

Figure 4-59: Epoxied FBGS strain development over distance during leak test 3

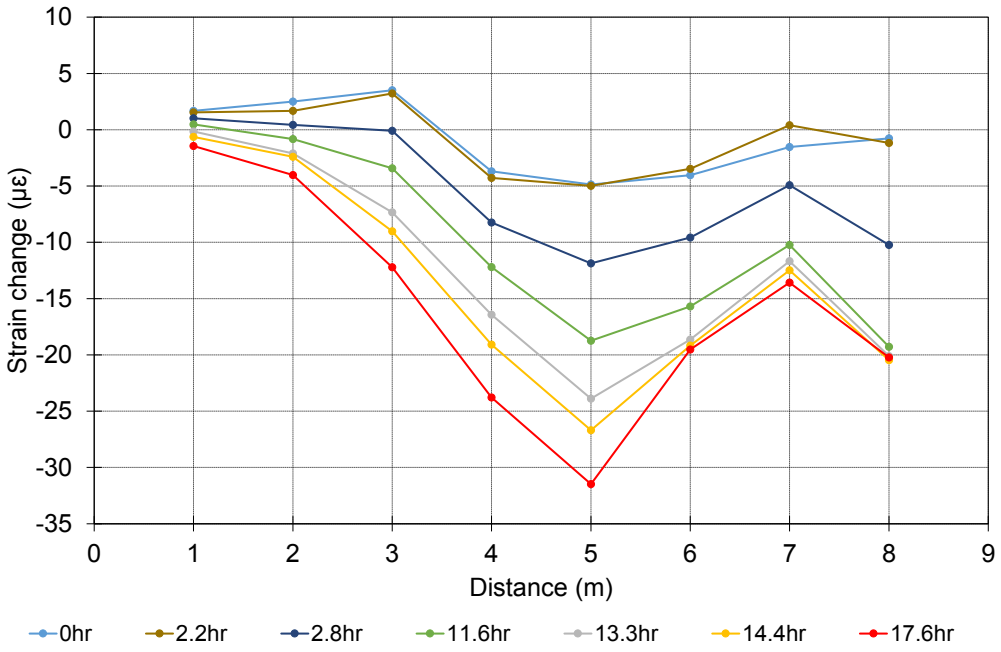

Figure 4-60: Free FBGS strain development over distance during leak test 3

Discussion

It is evident from the FBGS data that strain values as recorded in the experimental setup are sensitive to changes in support (bedding) properties around a pipe. Initially the FBGS isolated from external mechanical strains within the 4mm tube in the trench corner were envisaged to measure only temperature effects, but the wetting patch did appear to have a significant impact on the support condition around the small conduit, causing some bending to occur as illustrated by the fact that strain readings did not return to their initial values prior to the leak as the temperature of the ground recovered. This illustrates the benefit of also measuring mechanical strain resulting from a leak as it increases the sensitivity of the measurement system. Results to date suggest that a leakage detection system comprising of FBGS capable of recording both mechanical and thermal strains would provide a highly sensitive means of leak detection for pipelines or other infrastructure suitable for instrumentation by means of such sensors.

4.5.7 Leak test 4

The fourth leak test was conducted under the full network pressure, which was throttled upstream of the leak location in the previous tests. The final leak test was conducted at LL2 with the same sensor layout as used for leak test 2. LL2 is in close proximity to the pipe joint where a rubber ring joint connection joined the two 6m pipe sections. The upstream valve, connecting the municipal water supply to the field installation, was fully opened and the downstream valve, connecting the field installation to the storage tanks, was fully closed. This setup was used to determine the effect of network pressures on the strain behaviour of the pipe which had to be assessed to determine if strain changes from a leak event could be distinguished from that caused by natural network pressure variation.

Water was flushed through the pipe for 1.5 hours before pressurising it. The pipe was pressurised at 18h23 on 6 November and left at full network pressure throughout the night. The leak was initiated in the early morning at 6h33 on 7 November to eliminate stagnant water with an elevated temperature from being flushed through the field installation. This can occur as there is a black HDPE pipe connecting the field installation to the water mains above ground. The leak was left open for 31 hours until 13h12 on 8 November. The average pressure head during the test was 54 meters. The leak flow rate was 1.6l/min, amounting to a total leakage volume of 3620l or 3.620m^3 of water being introduced into the ground around the pipe leak.

The water flow rate during the leak event from the water mains to the field installation was low due to the downstream valve being fully closed and the upstream valve fully open, with only the leak location allowing water to exit the pipeline. The water upstream of the pipe, which is exposed to sunlight and the ambient air temperature fluctuation acted as a heating element by increasing the temperature of the water injected into soil surrounding the leak during the day and drastically decreasing the temperature around the leak during night time.

A thermistor was placed inside the feeder line on the same level as the horizontal centreline of the main 110mm uPVC pipe (Figure 4-61). An air temperature sensor was added next to a building in the shade to correlate ambient air and water temperature, explaining the heating effect observed in the soil surrounding the leak. The ambient air temperature sensor was added as the nearby weather station data was not available anymore.

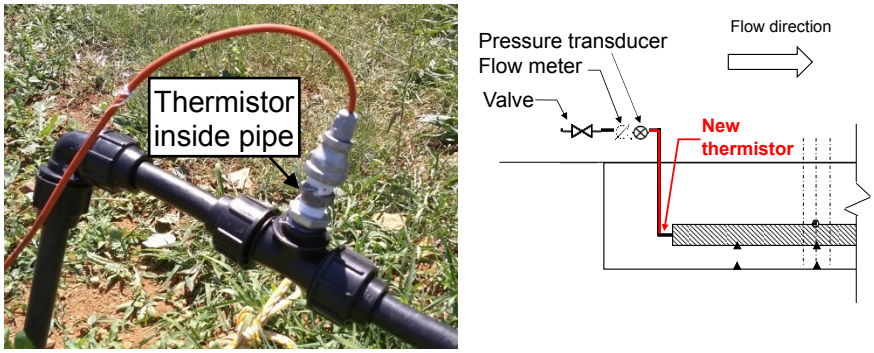

Figure 4-61: Thermistor inside of pipe to measure water temperature during test

4.5.7.1 Thermistors data leak test 4

The thermistor data was obtained from TS5 at the leak location, TS4 0.15m upstream of the leak location and TS6 0.15m downstream of the location. TS1 the reference string was located 2.15m upstream of LL2. The water pressure variation during the test is shown in Figure 4-63 and the water temperature changes inside the pipe are shown in Figure 4-62. The dashed red vertical lines indicate the leak initiation and closure. The red circle in Figure 4-62 indicates the change in water temperature during the flushing event and the subsequent recovery shortly after the flushing was conducted. The pressure behaviour was as expected. Throughout the evening an increase in pressure can be observed due to filling of the municipal reservoir feeding this part of the water network which then decreased gradually throughout the day as

water was being used from the reservoir. The spikes observed throughout the pressure dataset is attributed to short duration water use in close proximity to the installation.

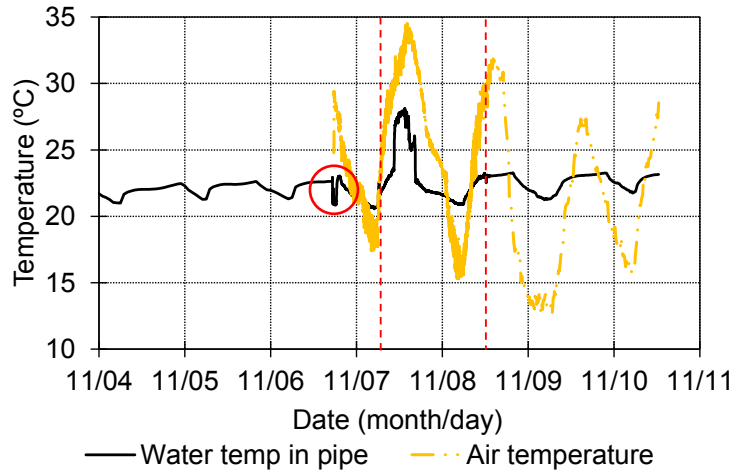

Figure 4-62: Water and air temperature

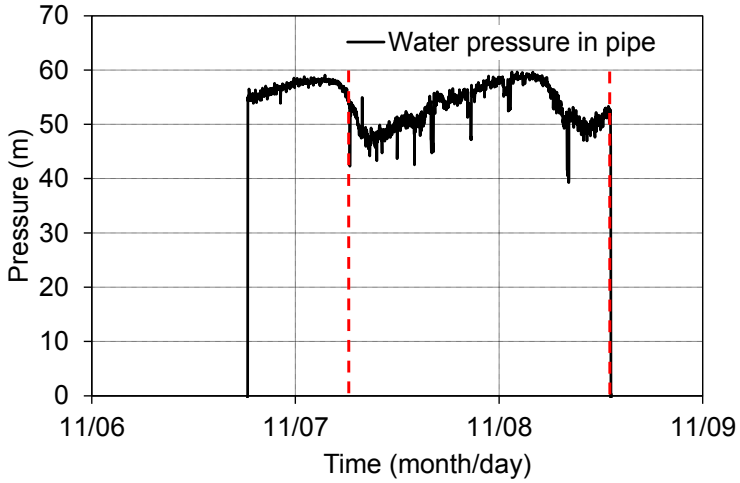

Figure 4-63: Water pressure in pipeline

Thermistor data from soil around pipe

Figure 4-64 below indicates thermistor data for TS5 at the leak location followed by Figure 4-65 and Figure 4-66 indicating data for TS4 and TS6 being 0.15m upstream and 0.15m downstream of the leak location. Figure 4-67 acts as reference string TS1. The left graph column are for the thermistors located in close proximity to the pipe (TSx-T1 to TSx-T4) and the right graph column presents the thermistors in the trench corner (TSx-T5 to TSx-T9). The figures indicate that during the initial flushing of the pipeline a rapid decrease in temperature

was observed which is not only noticed by thermistors in close proximity to the pipe (left column graphs below) but also in the trench corner (right column graphs below). When the leak was initiated after the pipeline was pressurised again a rapid decrease in temperature was observed, followed by an increase in temperature due to an increase in ambient air temperature and sunlight exposure of the pipe upstream of the test installation. The ambient air temperature and water temperature experienced the same sharp increase in temperature as seen in the saturated soil around the leak. The thermal changes at LL2 at TS 5 (Figure 4-64) were greater compared to TS4 (Figure 4-65) and TS6 (Figure 4-66). The reference string TS1 (Figure 4-67), located 2.15m upstream of LL2, indicates a similar trend to the thermistor strings in close proximity to the pipe. During the leak test TS1-T6 placed underneath the pipe in the pipe base indicated the greatest change in temperature due to its close proximity to the pipe and because the pipe formed a thermal discontinuity between the upper soil layers and the sensor.

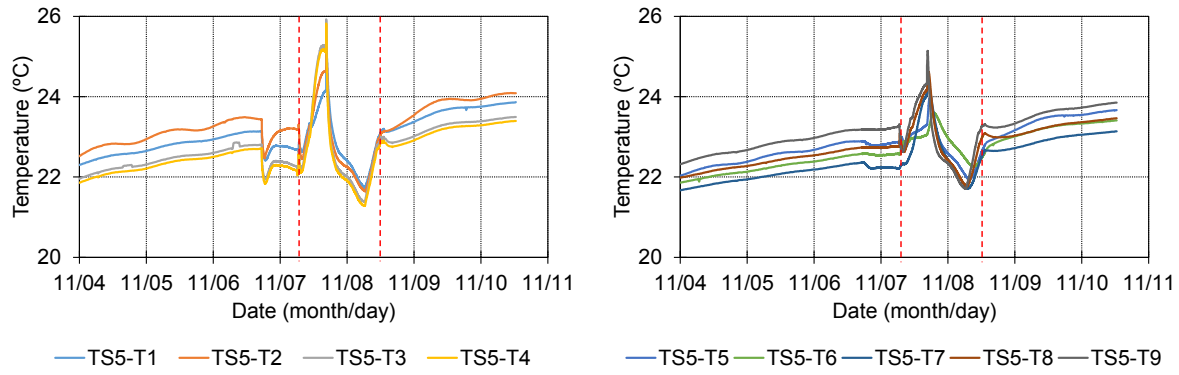

Figure 4-64: Temperature changes at leak location LL2 (TS5)

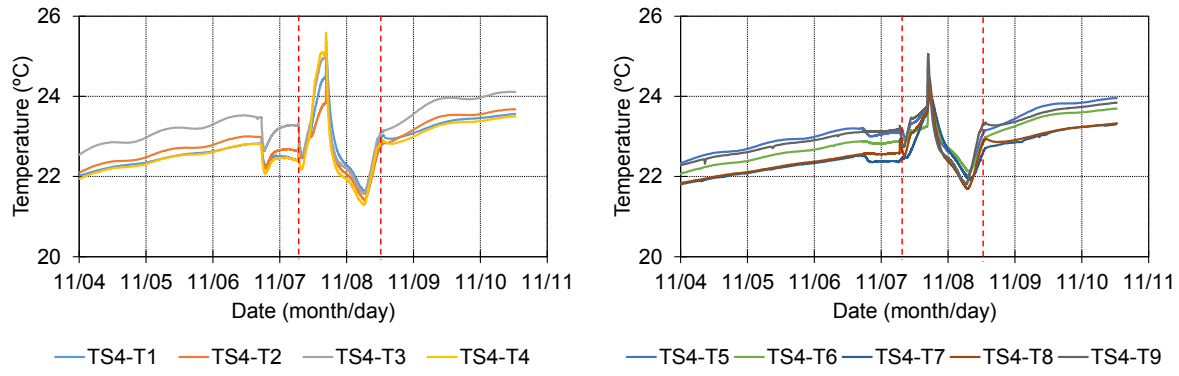

Figure 4-65: Temperature changes 0.15m upstream of leak location (TS4)

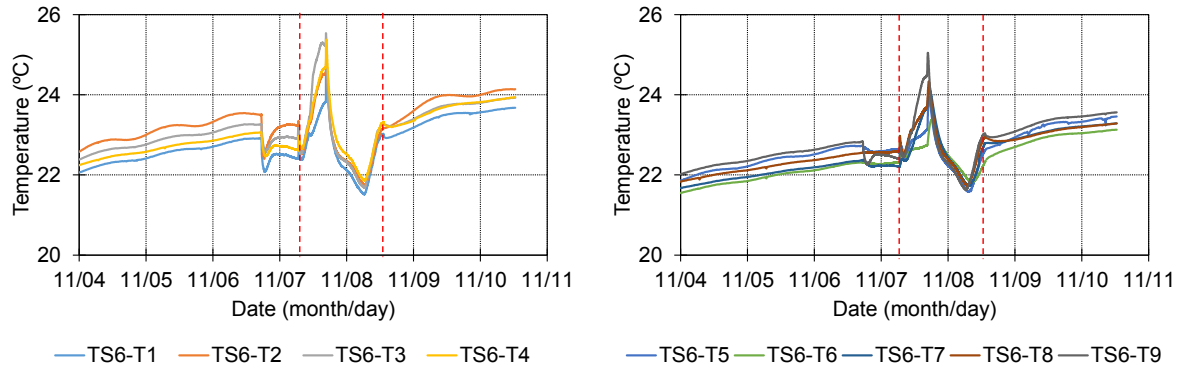

Figure 4-66: Temperature changes 0.15m downstream of leak location (TS6)

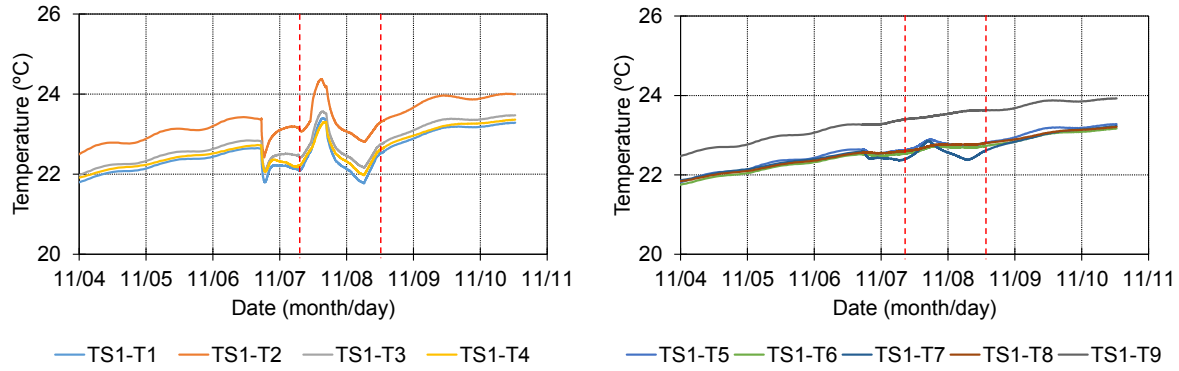

Figure 4-67: Temperature changes at reference location (TS1)

Temperature distribution around leak locations

A leak test under elevated internal pipe pressure increased the risk of having background leaks on the experimental pipeline. It is evident that temperature changes caused by the water in the pipe can be observed throughout the pipe trench even in the trench corner relatively far from the leak event at the reference string TS1 (TS1-T5 to TS1-T9). A temperature spike caused by the exposed upstream pipe section acting as heating element is clearly discernible.

A 2D temperature contour plot around the leak is shown in Figure 4-68 before (left column) and during the leak event (right column). The temperature difference before and during the leak test is shown in Figure 4-69. A temperature plume can be seen around the leak point which dissipates upstream and downstream of the leak location.

Discussion

It is evident that a noticeable change in temperature was observed during the leak event, indicating that temperature change is likely to be a successful as a leak indicator.

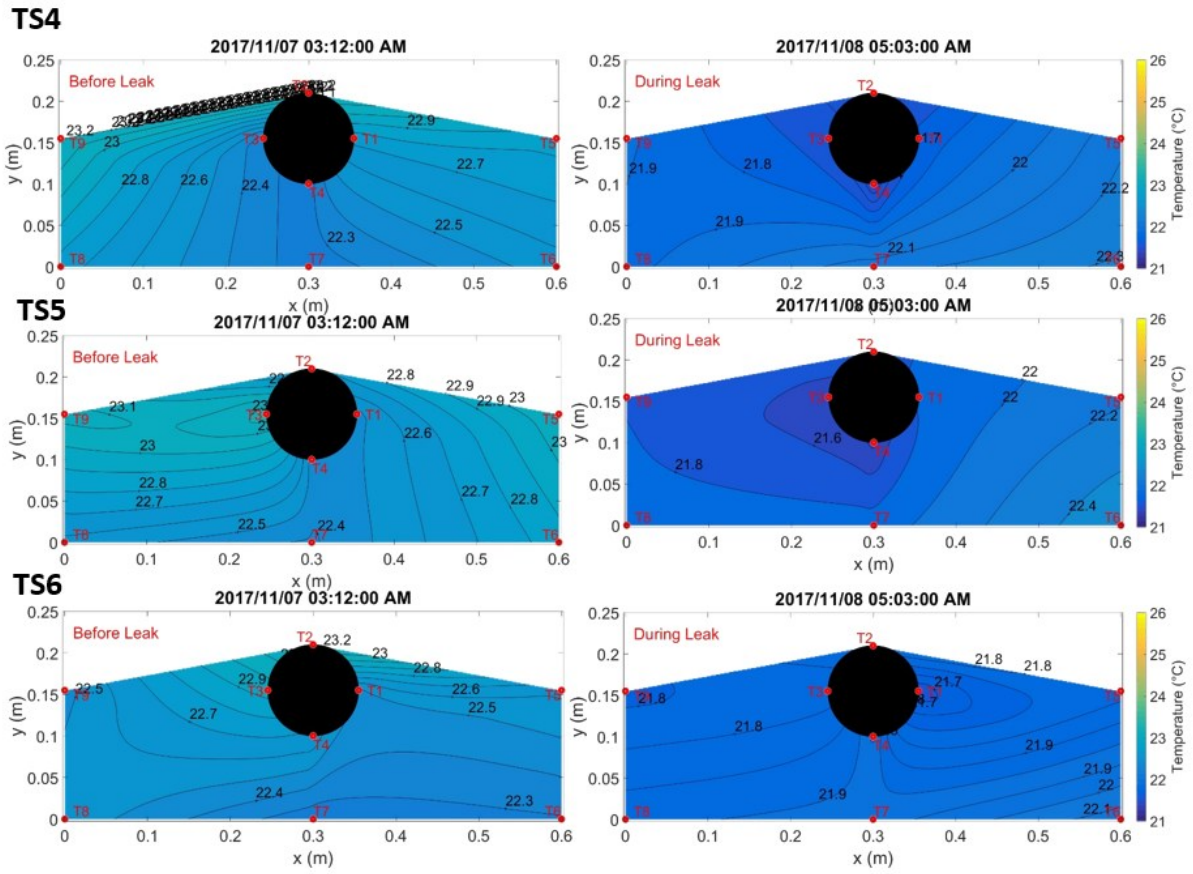

Figure 4-68: Temperature profile around LL2 before (left) and during (right) the leak for leak test 4

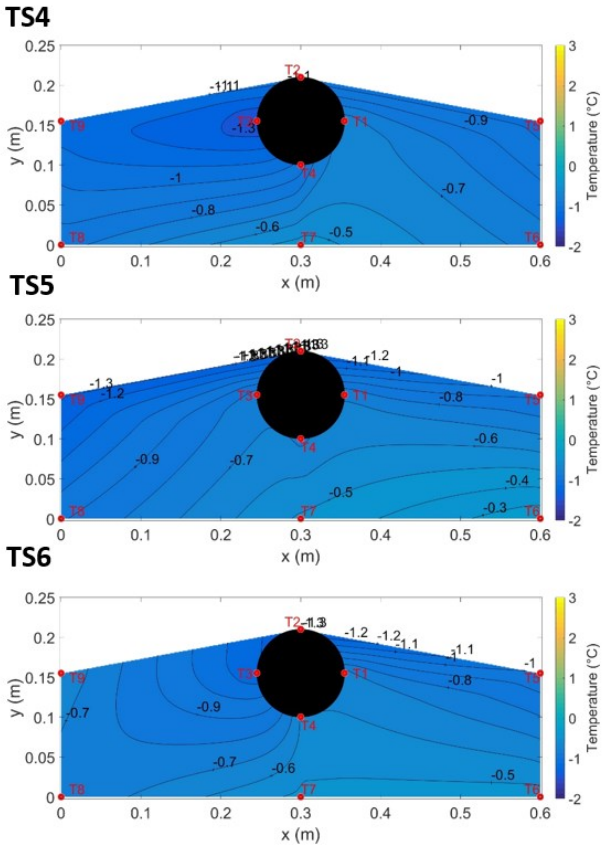

Figure 4-69: Temperature change profile around LL2 for leak test 4

4.5.7.2 Fibre Bragg data leak test 4

The fibre Bragg grating data at LL2 for leak test 4 was obtained from the same sensor layout used for leak test 2. The epoxied FBGS in Figure 4-70 reacted to the pressure changes in the network as can be seen by the instantaneous strain development during pressure fluctuations in the network, or sharp peaks and crests. The free FBGS in Figure 4-71 in the saturation zone, i.e. FBGS 12 to FBGS 16, remained under constant strain up to the initiation of the leakage event and the progression of the wetting front. The FBGS in close proximity to the leak started reacting by indicating an increase in strain.

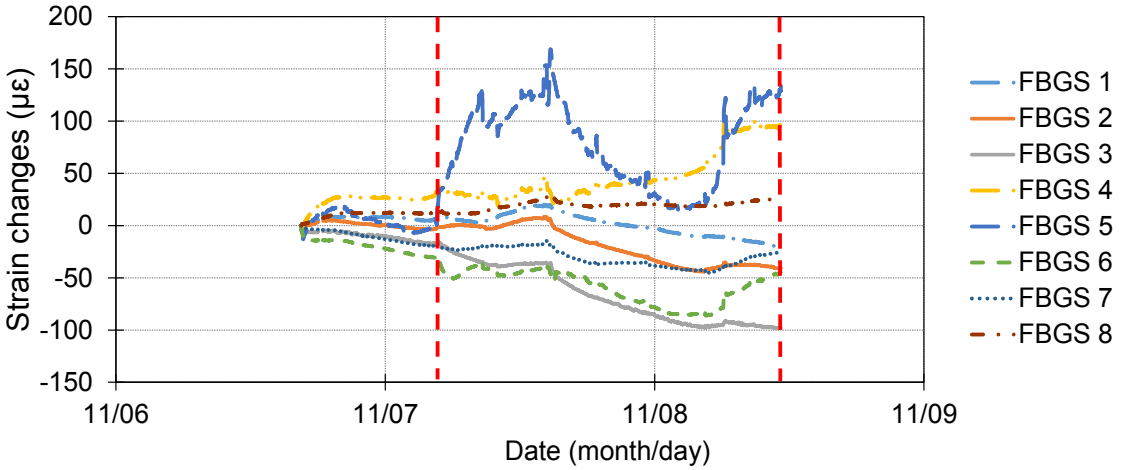

Figure 4-70: Epoxied FBGS during leak test 4

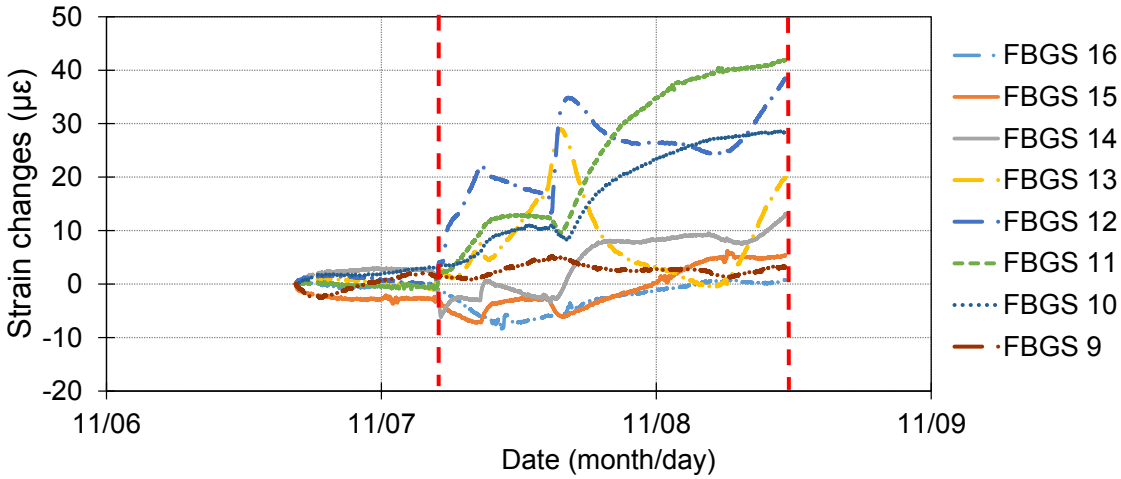

Figure 4-71: Free FBGS during leak test 4

Instead of comparing the individual sensors with each other over time as shown in Figure 4-70 for epoxied FBGS and Figure 4-71 for free FBGS, the sensor array is shown over its distance as strains develop. For the epoxied FBGS the greatest strain can be observed close to the joint at the 5m distance marker or FBGS 5, as the joint allows for movement. Initially however the leak location reacts first as can be seen at 36 hours with the blue coloured line. The free FBGS indicate major strain developments close to distance marker 5m

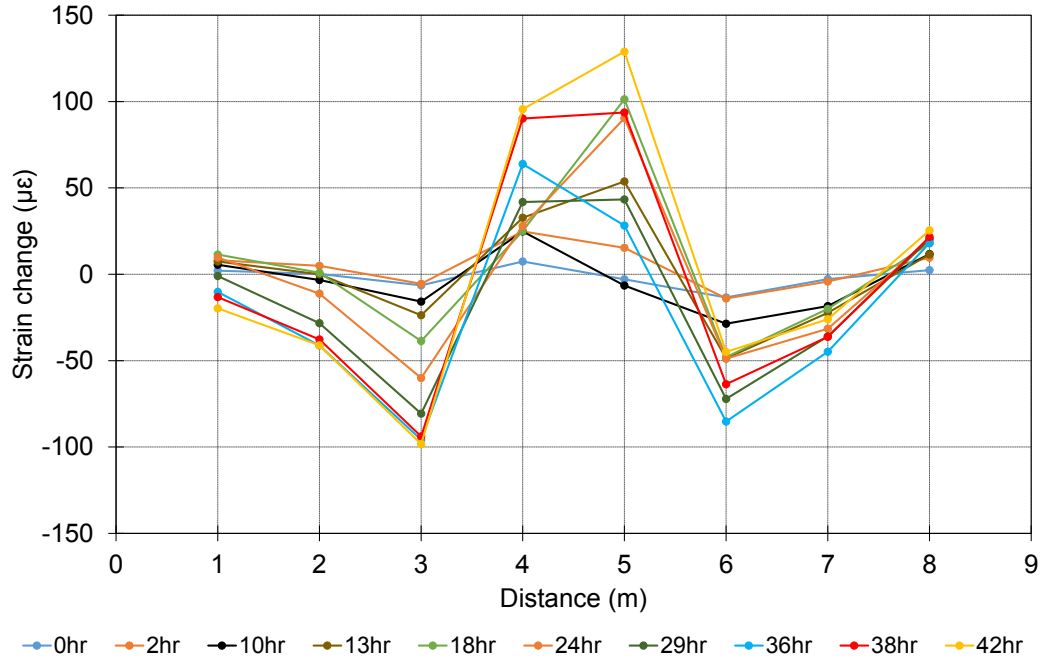

Figure 4-72: Epoxied FBGS strain development over distance during leak test 4

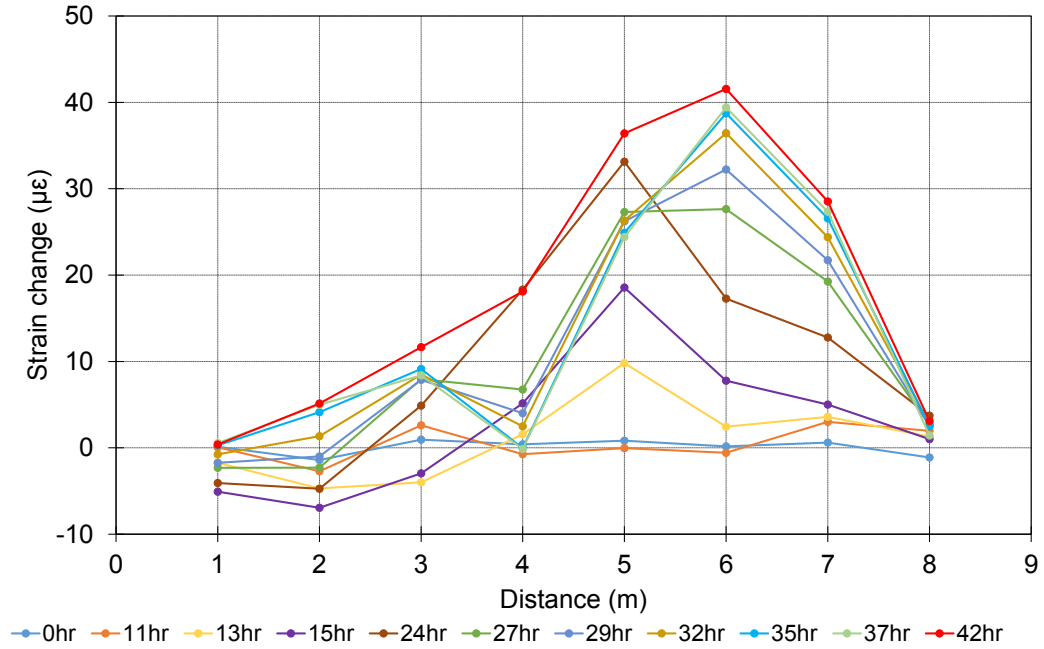

Figure 4-73: Free FBGS strain development over distance during leak test 4

Comparing strain to pressure

The measured strain changes are shown on the primary vertical axis against time for the epoxied FBGS and the registered network pressure is plotted on the secondary vertical axis

in Figure 4-74. The major jump at the start of the test sequence is caused by the initial pressurisation, which is not incorporated in Figure 4-72 and Figure 4-73. The data was re-zeroed to only show fully pressurised conditions and not the initial pressurisation, which skews the data set. It is important to note that the epoxied FBGS in close proximity to the pipe joint (FBGS 4, FBGS 5 and FBGS 6) react the most to pressure changes. Especially FBGS 5, which is at the joint, reacted to every slight change in pressure due to the joint being mobile relative to the adjacent points.

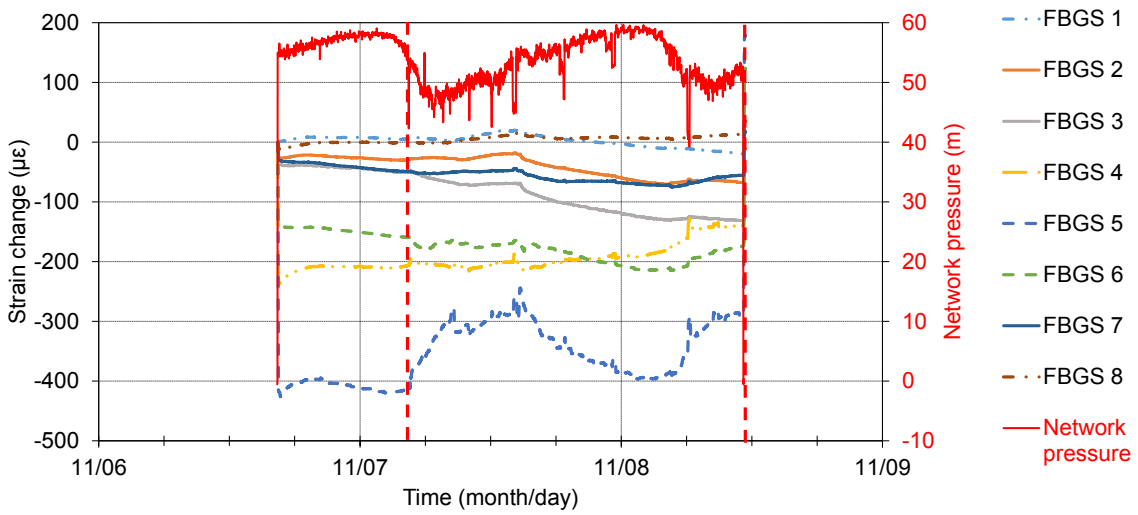

Figure 4-74: Pressure and strain vs. time for epoxied FBGS for leak test 4

Discussion

It is important to emphasise the sensitivity of FBGS as any changes in external loading or internal pipe pressure can be observed and measured. The pipe joint is freely movable and can contract and expand by a small margin, thereby indicating major strain developments in close proximity to joint with FBGS 5 at joint FBGS 4 upstream of joint and FBGS 6 downstream of joint. A measuring cable attached to the pipeline can detect noise originating from operational changes which would overshadow softening events, however operational changes would be indicated as rapid event (spike) compared to softening, which would be a gradual change in strain. A measuring cable mechanically uncoupled from the pipeline, which is freely movable within a thin tube filled with low viscosity oil in the trench corner, exhibited a brief lag time for total strain development compared to the epoxied FBGS and are more immune to operational pressure and flow changes, therefore making a more ideal measurement location.

4.5.8 Pressure and strain behaviour

The relationship between internal pipe water pressure and longitudinal pipe strain was investigated. This was done to understand to the extent of the soil and backfill confining pressure around a pipe and how the pipe joint allows movement under increasing internal pipe pressure. For this test the water pressure inside the pipeline was altered by opening and closing the upstream and downstream valve. The internal water network pressure was used as pressurisation medium. The pressurisation was induced in steps with the outlet valve initially being open to atmospheric conditions (therefore imposing 0 m of pressure head) to finally being completely pressurised with the downstream valve closed, while the upstream valve remained open to the network pressure. It was determined that over weekends, when little water was consumed, water pressure increased to a maximum of 65 meters. In general, the water pressure however remained below 60 meters. The pressure and longitudinal strain behaviour within the pipeline was investigated (should be first sentence of this section with a reason why). The pressurisation cycle was repeated three times to investigate possible hysteresis effects in the system and permanent deformation.

Figure 4-75 below indicates changes in strain on the primary vertical axis with internal pipe pressure on the secondary vertical axis over time. The initial pressurisation cycle caused a major strain effect in the region of the pipe joint at FBGS 5 the dark blue dotted line. As the distance to the centre of the pipeline or pipe joint was increased, the strain effect during pressurisation reduced (see Figure 4-75). The FBGS closest to the joint (FBGS 4, FBGS 5 and FBGS 6) strained the most. A negative strain translates to a compressive force as the internal pipe pressure was increased (right vertical axis).

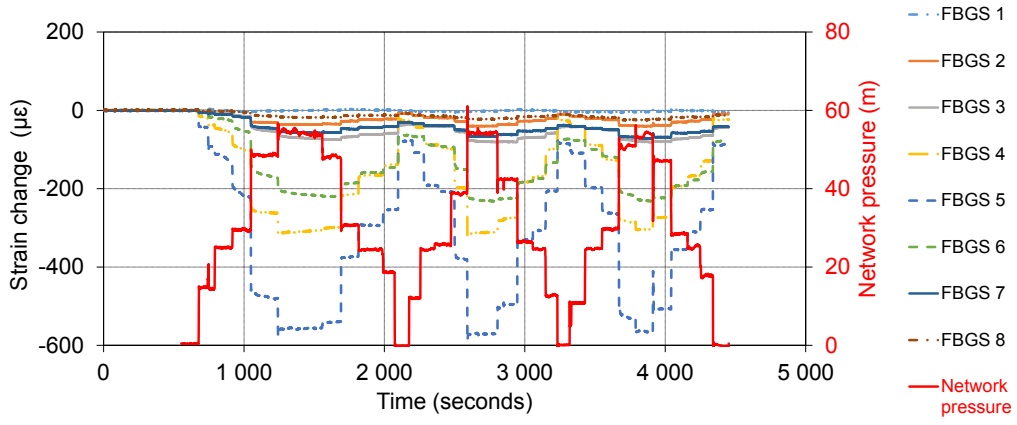

Figure 4-75: Epoxied FBGS pressurisation cycles

A similar phenomenon observed for the epoxied FBGS can be seen for the free FBGS in the trench corner but with strain changes of a much lower magnitude. This leak test was carried out where a previous leakage event had occurred, therefore the soil was saturated. Data from the free FBGS are separated in two diagrams, i.e. close to a saturated zone (leakage test being conducted shortly before this test) and an unsaturated zone. Compared to unsaturated soil, the saturated zone, represented by data from FBGS 16 to FBGS 13 in Figure 4-76, is likely to be relatively incompressible. It can be seen that some pressure was transferred to the FBGSs in the trench corner through the fairly incompressible soil. The unsaturated zone (represented by data from FBGS 13 to FBGS 16 in Figure 4-77) can be described as being more compressible, transferring seemingly insignificant pressure to the FBGSs in the trench corner during the pressurisation test.

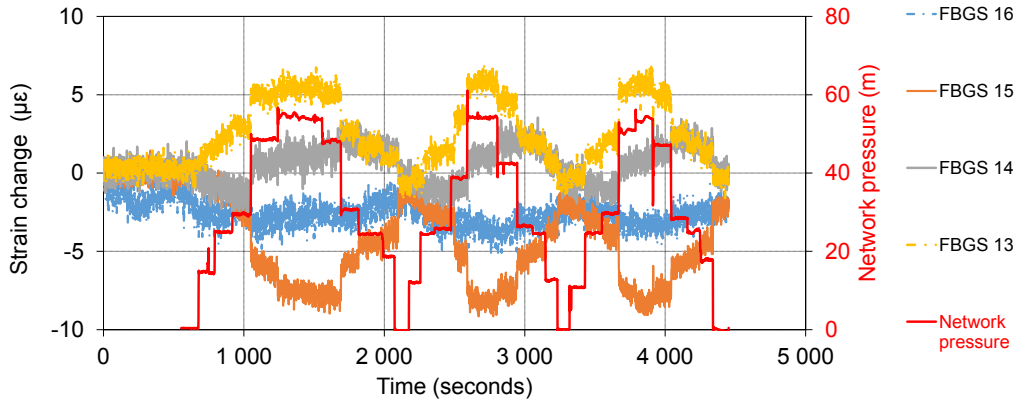

Figure 4-76: Free FBGS pressurisation cycles (saturated)

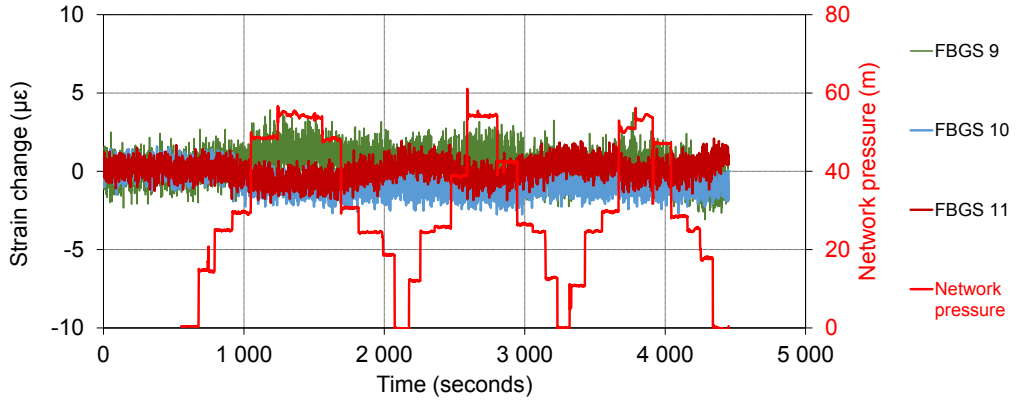

Figure 4-77: Free FBGS pressurisation cycles (unsaturated)

A different approach to the above Figure 4-75 to Figure 4-77 has been chosen to represent the strain change data over distance instead of time. Various pressure increments in meters have been chosen to represent strain changes for the different FBGS. The epoxied FBGS are

shown in Figure 4-78 and the free FBGS are shown in Figure 4-79. It is evident that the joint located in close proximity to the 5m distance mark (FBGS 5) indicates the greatest movement for the epoxied FBGS in Figure 4-78. The free FBGS in Figure 4-79 indicate the greatest strain development at the most recent leak location at the 4m distance mark at FBGS 4. The zone between 1m to 5m mark can be described as saturated, due leakage tests conducted shortly before commencing the pressurisation test. Distance mark 6m to 9m in the same figure has had time to dry out and is therefore termed partially unsaturated. The partially unsaturated zone does not transfer the pipe pressure to the free FBGS and therefore only small strains were observed.

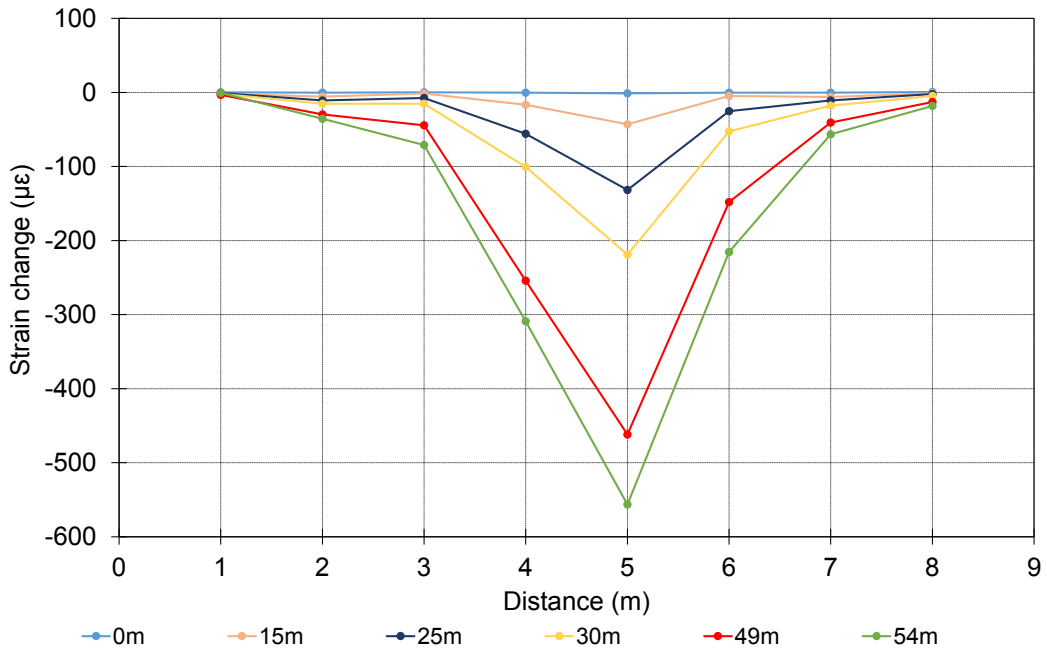

Figure 4-78: Epoxied FBGS pressurisation cycles over distance for various pressures

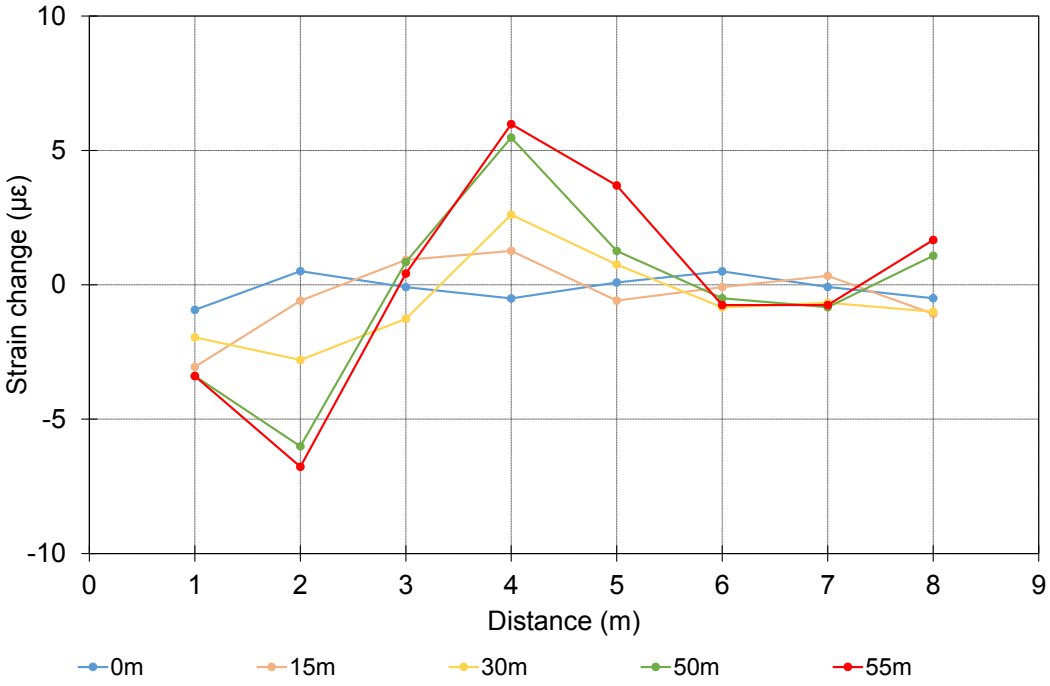

Figure 4-79: Free FBGS pressurisation cycles over distance for various pressures

Hysteresis in terms of the axial strain and internal pressure response of the system was investigated by plotting the strain for the FBGS against pressure for all the cycles. Figure 4-80 presents the results for the epoxied FBGSs and Figure 4-81 the results of the free FBGSs. The epoxied FBGS do exhibit slight hysteresis due to the joint allowing the pipe to contract freely during the first cycle. The second and third pressurisation cycle did not indicate further slippage or permanent deformation. The free FBGSs recovered to their initial state after pressurisation except for FBGS 12, located between the saturated and unsaturated zones, showing a significant change in strain during the first cycle which did not recover.

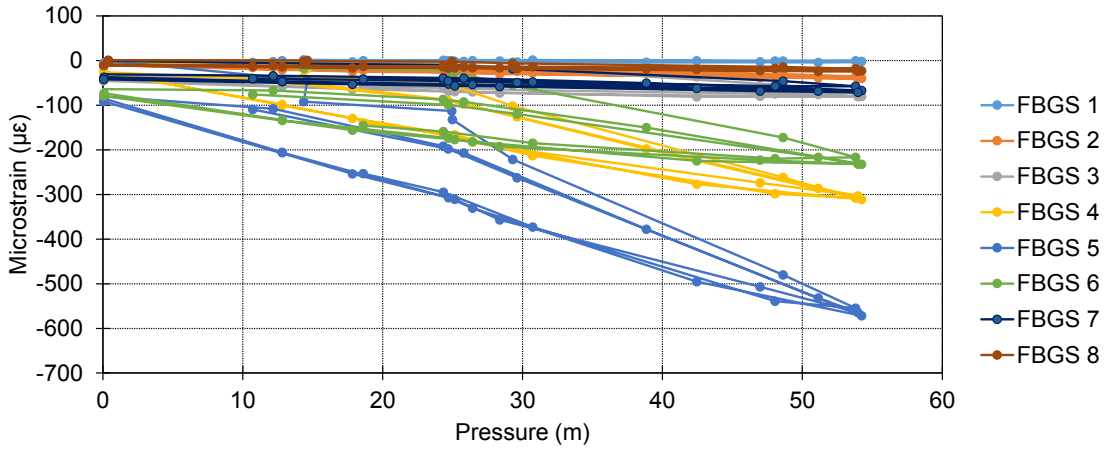

Figure 4-80: Epoxied FBGS pressure vs. strain

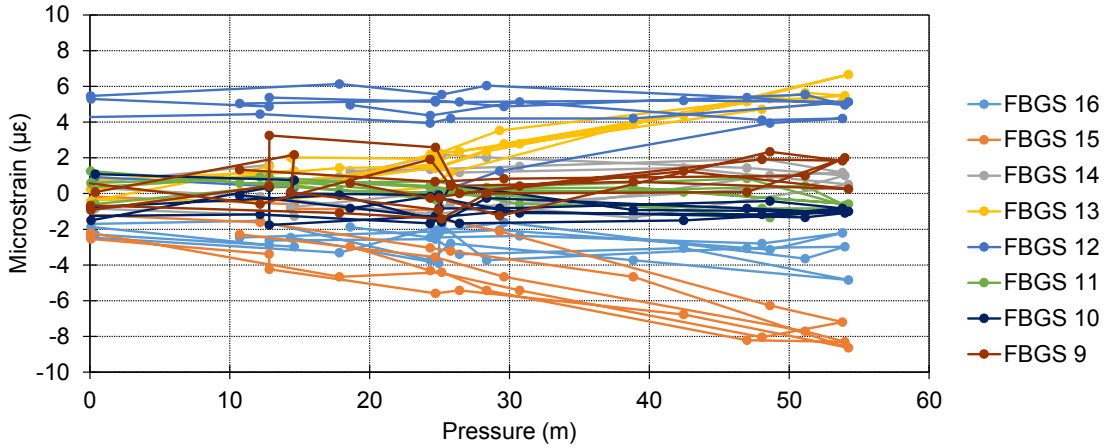

Figure 4-81: Free FBGS pressure vs. strain

Pressure changes in the pipeline affected attached pipeline sensors. However, the sensors which were free from the pipeline in the trench corner only reacted to internal pipe pressure fluctuation after the soil had been saturated, becoming less compressible. A higher saturation level can be associated with a leak and can therefore act as a further leakage indicator if operational pressure changes can are transferred to the trench corner.

5. CONCLUSIONS AND RECOMMENDATIONS

5.1 Conclusions

Under the test conditions with typically unsaturated soils in Pretoria on the experimental farm, natural temperature variation over time in the ground rapidly reduce with depth so that, at the depth where pipelines are likely to be installed, i.e. below 0.6m, the variation in temperature is less than 2° over the course of a month. This small temperature variation is encouraging in terms of the potential effectiveness of the proposed leakage detection system, as it implies that leakage induced temperature changes will be readily distinguishable from background temperature fluctuation. Rainfall events have a significant effect on soil temperature as it increases the thermal conductivity of the soil and causes a significant heat flux, affecting ground temperatures. Sudden changes in ground temperature observed by a leak detection system should therefore be interpreted in the context of the rainfall record.

Temperature measured in water mains at the Pierre van Ryneveld reservoir are substantially (at least 2 to 3°C) lower than the ground temperatures measured to date, implying that leakage induced temperature changes should be easily detectable. This was highlighted by combining the water mains and ground temperature in Figure 4-6.

The laboratory experiments suggests that the passage of a wetting front in the ground is associated with a significant reduction in temperature behind the front which should be detectable to warn of leaks. An interesting phenomenon associated with the release of surface energy upon wetting results in a slight temperature increase during passage of a wetting front. This is however soon followed by a net reduction in temperature associated with the passage of the colder water emanating from the leak.

The field installation instrumented with thermistors and FBGS presented strong evidence that temperature changes around a pipeline can be indicative of a leakage event. The water temperature in a water network, even if left stagnant for a long duration, will soon be replaced with cooler or warmer (flowing) water, in which case a temperature differential can be observed at a leak location.

A leak manifests on a thermal record as a slope change. If the leak continues, a significant temperature differential with respect to the pre-leak baseline will develop rapidly.

The performance of a fibre optic cable attached to the pipeline, as well as a cable placed in the trench corner, have been investigated. It was found that FBGSs attached to the pipeline reacted strongly to water pressure fluctuations, especially closest to a pipe joint where the pipe is typically allowed to undergo more strain due to some flexibility at the coupling. The optimal cable location relative to the pipeline has been found to be separated from the pipeline itself, due to effects of constant pressure changes being transferred to the attached sensor element. A continuously welded un-jointed pipeline restrained in a trench along its entire length might not show the same magnitude of strain changes as was found in this research study. An increase in compaction of the backfill will further limit pipe movement and increase friction between the pipe and the backfill.

If water is flowing through a pipe the temperature in close proximity to the pipe is similar to the temperature of the water. Therefore, when using measurement instrumentation to detect leaks based on thermal changes alone, such instruments should not be placed in direct contact with the pipe, but further from it to avoid the area of thermal equilibrium immediately around the pipe. Tests suggest that the pipe trench invert or the trench corner may be a suitable location.

A leakage detection system comprising of fibre optic strain sensors sensitive to mechanical and thermal strain appears to be highly sensitive to detect leaks. Such a system can be mechanically isolated from the pipe to measure thermal strains (i.e. temperature) in close proximity to the pipe which might indicate a leak. However, bonding the sensors to the pipe will result in the sensors also registering mechanical strains caused by bending of the pipe due to a change in support (bedding) conditions upon wetting. Results suggest that such a system would be at least an order of magnitude more sensitive than a system comprising of sensors sensitive to thermal effects only.

The daily temperature fluctuation in the soil at the field installation of the leakage experiment is exaggerated by an increase in saturation near a leak location as saturated soil has a higher thermal conductivity. After the leak was closed, the temperature recovered rapidly to follow normal daily temperature variation, however with greater variation than unsaturated parts. Once the soil is saturated at the leak location, it takes a substantial time for the saturation zone to dissipate. Permanent deformation due to softening caused by a leak has also been noted as well as partial deformation recovery.

The objective of this research study was to determine whether both temperature and total strain could be used to detect buried water pipeline leaks. Even though the primary focus of this study was on temperature changes, a combination of both thermal and mechanical strain

changes can be used as an effective leakage detection method. The hypothesis described in the scope of this study (Section 1.4) was therefore proven to be correct.

5.2 Recommendations

It is recommended that more locations be identified where temperatures in and around water mains in the soil can be monitored. By having a greater data base of ground temperatures and temperatures in water mains, areas where a leak detection system based on measuring temperature differentials as described here would not work, can be identified.

Should a leak detection system be used which is sensitive to both thermal and mechanical strain, it is not necessary to separate the thermal and mechanical strains as a combination of both could be indicative of a leak. The combination of the thermal strain due to the heat flux caused by the leak and the mechanical strain due to the change in pipe support conditions provide a powerful leakage detection parameter. The effect of external loading such as traffic loading should be further investigated. The effect of high water tables or elevated soil saturation conditions have to be investigated. However, for most parts of Southern Africa it can be assumed that at typical buried pipeline installation depth the pipeline will be surrounded in an unsaturated ground.

The field installation was monitored continuously before, during and after a leak event was induced, thereby creating a continuous measurement setup. This setup enabled the collection of valuable data which can be used for further research in the field of leakage detection for buried pipelines. FBGS, as used in the leakage experiments, are not ideal to be used over a long measuring distances due to limited amounts of individual FBGS or measurement locations, which is limited to 50 FBGS if a 2nm spacing is used between 1500nm to 1600nm. This range would indicate a limited amount of strain that could be measured, but a wide temperature range, if pure thermal strain is considered. However, in terms of materials testing and behaviour, FBGS might be ideally suited to their inherent sensitivity.

The results obtained from this experiment should be followed up with further studies in which distributed fibre optic sensors instead of FBGS are investigated. A discrete system, such as with FBGS, is limited to a finite number of measurement locations, depending on the wavelength spacing of the FBGS and differential strain which is expected to occur. A distributed system is potentially suitable to monitor many kilometres of pipeline. However, the measuring sensitivity of such systems are substantially reduced compared to that of FBGSs.

Such a distributed fibre optic trial installation should be conducted on a live pipeline to indicate the effect operational pressure changes. Leaks should be induced along the trial pipeline to replicate a real leakage event, allowing the proposed leakage detection system efficiency to be determined.

If an FBGS pipeline monitoring setup would be specified for an infrastructure project, the following recommendations would have to be made regarding the sensor spacing, monitoring periods, sensor location relative to pipe and data acquisition rate. Depending on the diameter and length of the pipeline to be investigated, the sensors would have to spaced to at least contain one sensor or FBGS every pipe section for a jointed pipe or 5m to 10m apart. This value depends on the stiffness of the pipeline and compaction details, for a stiffer pipeline the sensors can be spaced further apart, compared to a more flexible pipeline, where bending would occur more localised. Ideally a continuous data record is required with strain and temperature measurements taken every few seconds and added to a smart data acquisition, which combines rainfall and other environmental factors, to alert the pipeline operators of excessive strains and temperature changes. As discussed previously the sensor location relative to the pipe depends on the hydraulic operating regime of the pipeline as well as the type of coupling or jointing method. If for example the pipeline has no joints, is continuously welded, has no offtakes or branches and is operated with a constant hydraulic operation for certain hours every day, a sensor cable attached to the pipe could be used as a monitoring tool. If however the pipeline has many offtakes, the pressure fluctuations in the pipeline will be seen as noise with an attached sensor cable, therefore a mechanically unbonded from the pipeline cable is preferred. All of the above factors will however have to be investigated in future studies. The thermistors used in this study were used for experimental purposes only to obtain a reference temperatures, but are impractical to be used over long distances, due to the amount of wires and an increase in resistance with increase in length of lead cables.

6. REFERENCES

American Water Works Association (AWWA). 2009. *Water Audits and Loss Control Programs - Manual of Water Supply Practices*, M36 (3rd Edition). [Online] AWWA. Available from: http://app.knovel.com/hotlink/toc/id:kpWALCPMW4/water-audits-loss-control/water-audits-loss-control [Accessed 31 January 2017].

AVX. 2017. AVX Product Catalogue. [Online] Available from: http://www.avx.com/products/thermistors/ntc-disc/ [Accessed 30 March 2017].

Barry-Macaulay, D. Bouazza, A. Singh, R.M. and Ranjith, P.G., 2013. Thermal conductivity of soils and rocks from the Melbourne (Australia) region. *Engineering Geology*, (164), pp.131-38.

Buttrick, D. and Van Schalwyk, A.,1998. Hazard and risk assessment for sinkhole formation on dolomite. Environmental Geology 36 (1–2), November 1998, Springer-Verlag, pp 170-178.

Conway, M., 2010. *Heat Transfer in a Buried Pipe* (Masters Dissertation, University of Reading).

Du Plessis, J.A. and Hoffman, J.J., 2015. Domestic water meter accuracy. *WIT Transactions on Ecology and the Environment*, *200*, pp.197-208.

EPA. 2010. Control and mitigation of drinking water losses in distribution systems. Washington: EPA Office of Ground Water and Drinking Water.

FBGS. 2017. SMW-01 strain sensor. [Online] Available from: http://www.fbgs.com/productsadv/be-en/5/detail/item/31/page/1/ [Accessed 15 March 2017].

Florides, G. and Kalogirou, S. 2007. Ground heat exchangers - A review of systems, models and applications. Renewable energy, 32(15), pp.2461-2478.

Frings, J. 2011. Enhanced Pipeline Monitoring with Fibre Optic Sensors. *6th Pipeline Technology Conference 2011. London. 12 March*, pp1-12.

Gumbo, B., Juizo, D. and Van der Zaag, P. 2003. Information is a prerequisite for water demand management: experiences from four cities in Southern Africa. *Physics and Chemistry of the Earth, Parts A/B/C*, *28*(20), pp.827-837.

Henrie, M., Carpenter, P. and Nicholas, R.E. 2016. *Pipeline Leak Detection Handbook*. 2nd edition Cambridge. Gulf Professional Publishing.

Hibbeler, R.C., 2013. Statics and mechanics of materials. Pearson Higher Ed.. pp. 85.

Inaudi, D. and Glisic, B., 2010. Long-Range Pipeline Monitoring by Distributed Fibre Optic Sensing. *Journal of Pressure Vessel Technology*, pp 265-74.

Jülich, F., Aulbach, L., Wilfert, A., Kratzer, P., Kuttler, R. and Roths, J., 2013. Gauge factors of fibre Bragg grating strain sensors in different types of optical fibres. *Measurement Science and Technology*, 24(9), p.094007.

Kreuzer, M., 2013. Strain Measurement with Fibre Bragg Grating Sensors. Darmstadt, Germany: HBM.

McCarthy, T. and Rubidge, B., 2005. The Story of Earth & Life: A Southern Africa Perspective on a 4.6-Billion-year Journey. Struik. pp. 118.

McKenzie, R.S. Siqalaba, Z.N. and Wegelin, W.A. 2012. The State of Non-Revenue Water in South Africa. Pretoria: Water Research Commission. (Report no. TT 522/12)

McKenzie, R.S. Lambert, A.O. Kock, J.E. and Mtshweni, W. 2002. BENCHLEAK - Benchmarking of Leakage for Water Suppliers in South Africa. Pretoria: SA Water Research Commission. (Report no. TT 159/01)

McKenzie, R.S. and Bhagwan, J.N. 2005. Leakage Management - Introduction to WRC Tools to Manage Non-Revenue Water. Pretoria: SA Water Research Commission.

McKenzie, R.S. 2001. PRESMAC - Pressure Management Program. Pretoria: SA Water Research Commission. (Report no. TT 152/01)

McKenzie, R.S. 1999. SANFLOW- Development of a standardised approach to evaluate burst and background losses in water distribution systems in South Africa. Pretoria: SA Water Research Commission. (Report no. TT 109/99)

McKenzie, R.S. and Lambert, A. E. 2002. ECONOLEAK – Economic Model for Leakage Management for Water Suppliers in South Africa. Pretoria: SA Water Research Commission. (Report no. TT 169/02)

Mishra, A. and Soni, A. 2011. Leakage Detection using Fibre Optics Distributed Temperature Sensing. 6th Pipeline Technology Conference. Hannover Messe. Germany. Pp. 1-12.

National Instruments. 2011. Products - Fibre optic sensing technology. Texas: USA. Available from: http://www.ni.com/white-paper/12953/en/ [Accessed 15 March 2017]

Oosthuizen, A.C. and Richardson, S. 2011. Sinkholes and subsidence in South Africa. Council of Geoscience (Report no. 2011-0010). Cape Town.

Parks, G.A. 1984. Surface and interfacial free energies of quartz. *Journal of Geophysical Research* 89(B6), pp 3997-4008.

Rajani, B. and Tesfamariam, S. 2004. Uncoupled axial, flexural, and circumferential pipe soil interaction analyses of partially supported jointed water mains. *Canadian geotechnical journal*, *41*(6), pp.997-1010.

Rao, Y.J., 1997. In-fibre Bragg grating sensors. *Measurement science and technology*, 8(4), p.355.

SABS, 1983. SABS 1200 LB: BEDDING (PIPES). Pretoria: South African Bureau of Standards.

SABS, 1989. SABS 1200 DB: EARTHWORKS (PIPE TRENCHES). Pretoria: South African Bureau of Standards.

SABS, 2008. SANS 1200-DP1: Earthworks for buried pipelines and prefabricated culverts. Pretoria: South African Bureau of Standards.

Schofield, A.N. 1980. Cambridge Geotechnical Centrifuge Operations. Geotechnique, 30(3), pp 227-268.

Soga, K., Mohamad, H. and Bennett, P.J., 2008. Distributed Fiber Optics Strain Measurements for Monitoring Geotechnical Structures. 6th International Conference on Case Histories in Geotechnical Engineering. 11-16 August 2008 Arlington. Available from: scholarsmine.mst.edu/cgi/viewcontent.cgi?article=2974&context=icchge [Online].

Sophocleous, M., 2010. Understanding and explaining surface tension and capillarity: an introduction to fundamental physics for water professionals. Hydrogeology journal, 18(4), pp.811-821.

Utilis Israel Ltd. 2017. Utilis. Israel. Available from: http://utiliscorp.com/#hp_slider [Accessed 4 April 2017].

Van Dijk, M., 2016. Pipeline Course 2016 – Presentation 6 slide 10. 7 July 2016. University of Pretoria. Available from: Pipeline Coursework [CD-OM]. Van Zyl, J.E. 2014a. Introduction to operation and maintenance of water distribution systems. Pretoria: SA Water Research Commission. (Report no. TT600-14)

Van Zyl, J.E. 2014b. Theoretical modeling of pressure and leakage in water distribution systems. Procedia Engineering, 89, pp.273-277.

Van Zyl, J.E. Alsaydalani, M.O.A. Clayton, C.R.I. Bird, T. and Dennis, A. 2013. Soil fluidisation outside leaks in water distribution pipes-preliminary observations. Proceedings of the Institution of Civil Engineers, 166(10), p.546.

Vorster, T.E., Klar, A., Soga, K. and Mair, R.J. 2005. Estimating the effects of tunneling on existing pipelines. *Journal of Geotechnical and Geo-environmental Engineering*, *131*(11), pp.1399-1410.

Wang, C., Olson, M., Doijkhand, N. and Singh, S., 2016, October. A novel DdTS technology based on fiber optics for early leak detection in pipelines. In Security Technology (ICCST), 2016 IEEE International Carnahan Conference on (pp. 1-8). IEEE.

Wegelin, W.A. and McKenzie, R.S. 2013. Metropolitan Municipality Non-Revenue / Water Loss Assessment. PEP: National Non-revenue Water Assessment. Department of Water Affairs. South Africa.

Wenzel, R.N. 1936. Resistance of solid surfaces to wetting by water. Industrial and engineering chemistry 28(8), pp 988-994.

World Health Organization (WHO). 2014. Water safety in distribution systems. World Health Organization.

Yokogawa . 2010. AQ8603: Optical Fiber Strain Analyzer. Available from: www.yokogawa.com. [Accessed 20 October 2017].

Zahoor, A. and Kanninen, M.F., 1981. A plastic fracture mechanics prediction of fracture instability in a circumferentially cracked pipe in bending—Part I: J-integral analysis. Journal of Pressure Vessel Technology, 103(4), pp.352-358.

Zou, L. and Landolsi, T. 2014. Pipeline leakage detection using fibre-optic distributed strain and temperature sensors. OZ Optics Ltd., Canada, Ottawa

APPENDIX A – CREATING FIBRE BRAGG GRATINGS

University of Johannesburg's Mr. Michael Grobler of the Photonics labs at the faculty of electronic and electrical engineering offered to make FBGS for experimental purposes, however their set-up was not yet optimised to produce FBGS with consistent quality. A photograph of their set-up with description is shown in Figure A-1 and Figure A-2 making of a fibre optic Bragg by exposing the photosensitive fibre optic cable to ultraviolet (UV) light interference pattern is shown in Figure A-2.

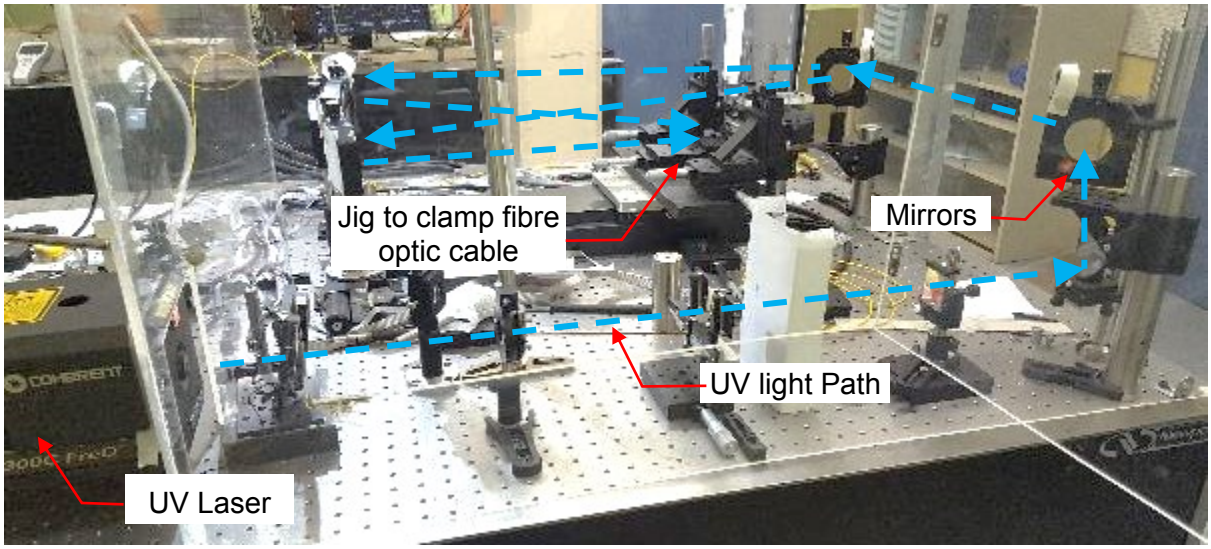

Figure A-1: University of Johannesburg FBGS setup

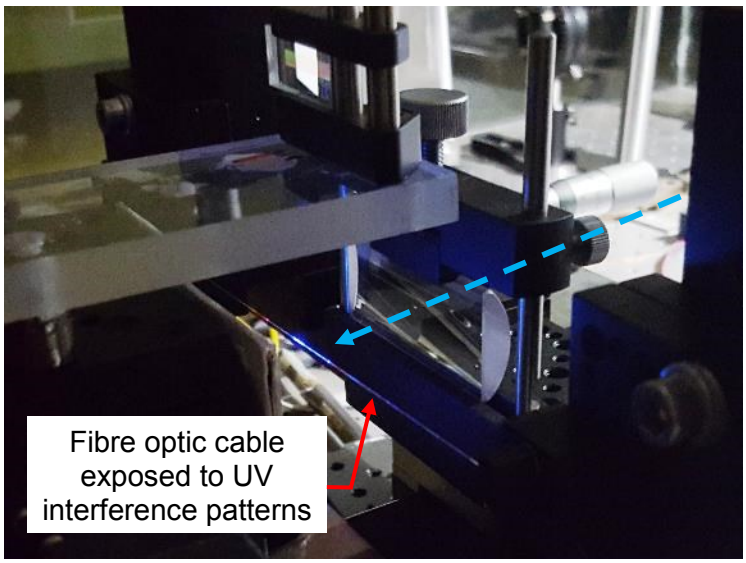

Figure A-2: Creating two-beam interference FBGS

The germanium doped fibre optic cable is fragile if unprotected and uncoated, therefore making it difficult to work with. Unfortunately no adequate coating solution was found, except for epoxying onto steel or any other material, which gave satisfactory results.

Industrial available fibre Bragg sensors are expensive due to quality assurance and the involved process of creating them. The germanium doped photosensitive fibre optic cable is one order of magnitude more expensive than ordinary telecommunication grade fibre optic cable.

APPENDIX B – PIPE STIFFNESS

Pipe stiffness changes due to the addition of collars at the leak tap-in point on the 100mm uPVC pipe was investigated. The collars were added to prevent failure of the pipe due to the hole in the main pipe and overburden weight. Figure B-1 pipe collar with linear variable displacement transformer (LVDT) and the full pipe length with LVDTs placed at 1m intervals over the 6m long pipe. The pipe was simply supported 0.1m from both ends and weights were hung at the centre (Figure B-2).

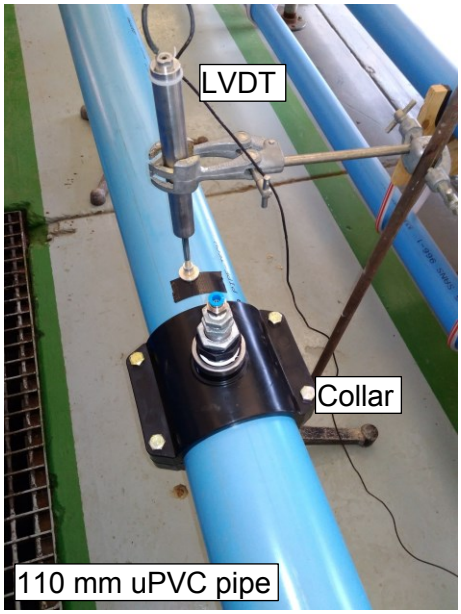

Figure B-1: Example of pipe collar added to tap-in point

Figure B-2: LVDT setup along pipe

The results indicate that adding one or two collar does not have a significant effect on its stiffness or resistance to bending compared to a pipe with no collars. The pipe collars in the graphs are indicated by a red vertical line the Figure B-3 indicating no collars, Figure B-4 indicating one collar and Figure B-5 indicating two collars.

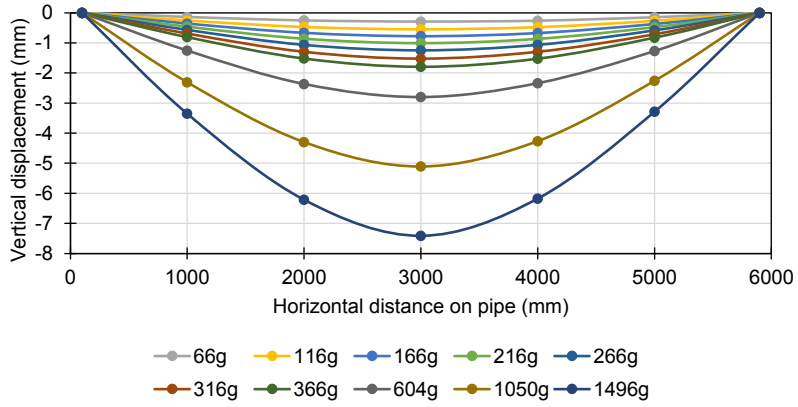

Figure B-3: No collar added on pipe

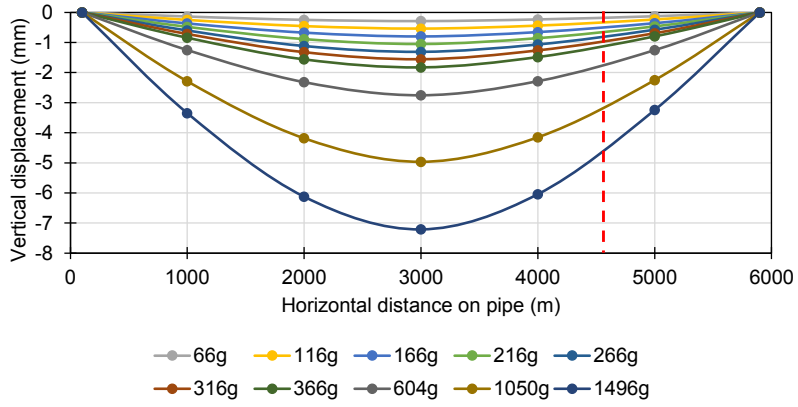

FigureB-4: One collar on pipe

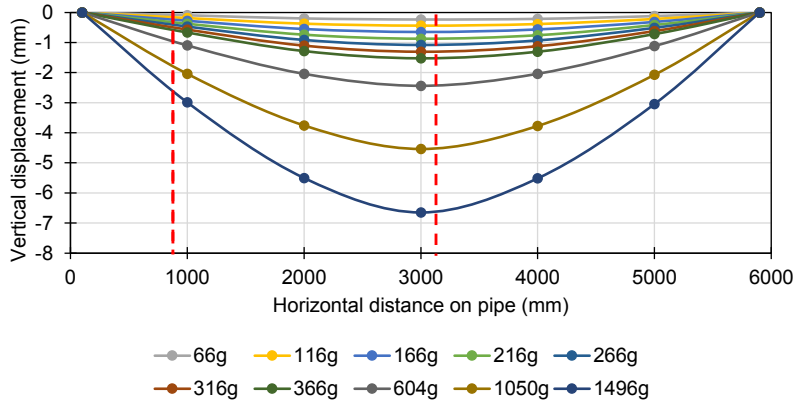

Figure B-5: Two collars on pipe

APPENDIX C – FBGS TEMPERATURE CALIBRATION

The temperature calibration was done by inserting a DTG FBGS, with a nominal wavelength of 1573.48 nm at 10 ºC, inside of a 4mm polyurethane pipe with low viscosity oil into a temperature controlled bath filled with a medium viscosity oil. The bath was first cooled down to 10 ºC to initiate the test, thereafter the bath was increase by 5 ºC increments to 15 ºC, 20 ºC and finally to 25 ºC. Thereafter the temperature was cycled down to 10 ºC as shown in Figure C-1 below.

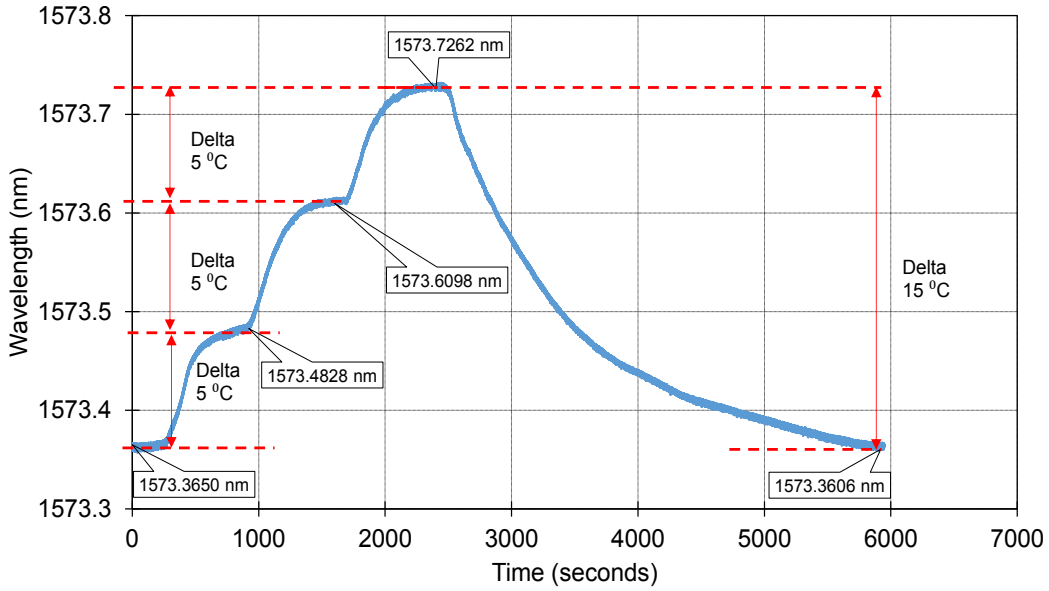

Figure C-1: FBGS temperature calibration

The results obtained from the test indicated an average change of 0.02408 nanometre per degrees Celsius. The FBGS placed within a 4 mm PU pipe is similar to the setup used on the field installation.

APPENDIX D – PRESSURE TRANSDUCER CALIBRATION

A 7 bar (70 m) pressure transducer (PT) was calibrated by using a pressurised water supply with a pressure control valve and a bladder system. The PT was left at atmospheric conditions initially indicating close to 3.92mA as base or 0bar reading. The pressure was increased incrementally by 10m of pressure up to the maximum system value of 64m, as shown in Figure D-1. The pressure in the system could not be sustained therefore the gradient in the peak value. Thereafter the pressure was decreased in 10bar increments up to its base value of 0m. The calibration data implies that the values obtained by using the pressure transducer during testing are reliable.

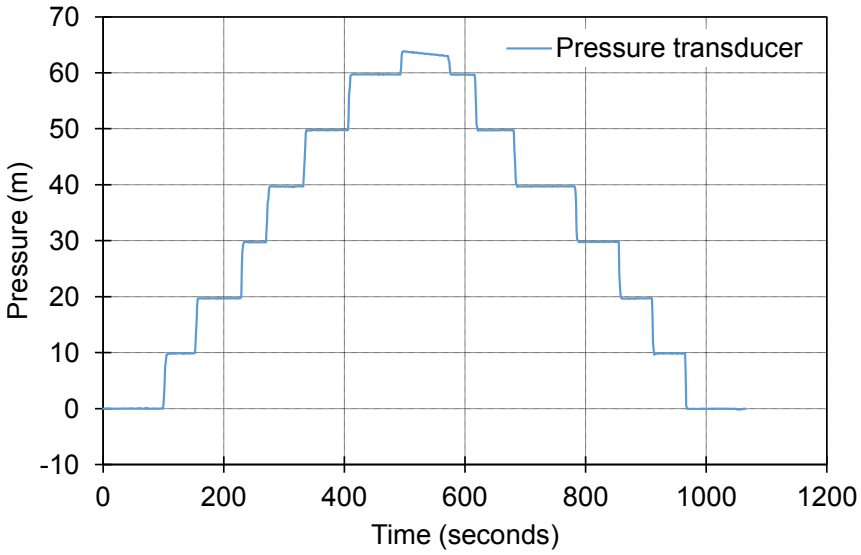

Figure D-1: Pressure transducer calibration curve